Linear Viscoelastic Behaviour and Relaxation Phenomena of Immiscible Blends: The Application of Creep

Vahid Shaayegan

A Thesis

in

The Department

Of

Mechanical and Industrial Engineering

Presented in Partial Fulfillment of the Requirements
for the Degree of Master of Applied Science (Mechanical Engineering) at
Concordia University
Montreal, Quebec, Canada

January 2010

Your file Votre référence
ISBN: 978-0-494-67105-4
Our file Notre référence
ISBN: 978-0-494-67105-4

ABSTRACT

Linear Viscoelastic Behaviour and Relaxation Phenomena of Immiscible Blends: Application of Creep

Small-amplitude oscillatory shear (SAOS) and incomplete creep/recovery experiments were employed to characterize the rheological behaviour of immiscible blends of polypropylene (PP) with dispersed droplets of polystyrene (PS) at different concentrations of minor phase and compatibilization state. While the linear viscoelastic properties of polymers in the melt state contain valuable information, the plateau and terminal zones of some polymers, especially polymers with very long relaxation time processes, are not accessible with common rheological methods. Furthermore, the interface relaxation phenomena in immiscible blends occur at longer times compared with pure components. A combination of the measurements from dynamic experiments and creep measurements was used to broaden the window of the linear viscoelastic behaviour of neat components as well as the blends. A new experimental creep protocol for immiscible blends was proposed based on Boltzmann Superposition Principle to minimize the morphological modification when sheared. The SAOS results were compared with those obtained from creep/recovery tests and supported by means of morphological investigations and the application of the Palierne model for immiscible blends. The effect of blend composition and compatibilizer, here styrene–ethylene/butylene–styrene (SEBS), on the relaxation spectrum of the blends was studied. The interfacial tension between phases was also determined using the Palierne model. It was found that the proposed creep method measures the linear viscoelastic behavior of

the blends and well characterizes their long time behaviour. An extended composite retardation spectrum was constructed by combining the short-time information from SAOS tests with the long-time data from creep/recovery experiments. The obtained spectrum was then used to re-calculate a composite relaxation spectrum as well as other viscoelastic material functions. It was found that the extended composite relaxation spectra predicted the long time relaxation mechanisms and relaxation spectrum portions which are out of the validity limits of the SAOS experiments, and were not seen by the application of dynamic tests only.

To my Parents

Acknowledgment

First of all, I would like to express my deepest gratitude to Dr. Paula Wood-Adams, my supervisor, for her outstanding, great supervision, every day consultation and discussion and her supports.

I extend my thanks to Dr. Demarquette and her research group, especially Dr. Adriana M.C. Souza for supplying the materials, samples and their academic supports and guidance.

My very special thanks go to Mr. A.H. Maani, for his constant support for SEM, image analyses and modeling, helps, and his beautiful discussions which really helped me for a better understanding.

A sincere word of thanks goes to Dr. H. Tabatabaei for his help and discussions.

I am particularly grateful to Yury, who friendly advised me during my research. I would like to thank Heng for training; and all my colleagues at Dr. Wood-Adams' research group who helped me at different stages of this research: Ramin, Sina, Hany, Niusha, Nithya, Emam, and Gavin.

I wish to recognize the strong role of my parents in the completion of this work, for giving me the encouragement, hope and supports despite the long distance between us.

Table of contents

Nomenclature

Latin symbols:

Ca	capillary number
d_p	droplet diameter (μm)
G	relaxation modulus (Pa)
G_e	equilibrium modulus (Pa)
G'	storage modulus (Pa)
G''	loss modulus (Pa)
G^*	complex modulus (Pa)
G_m^*	matrix complex modulus (Pa)
G_i^*	droplet complex modulus (Pa)
H	relaxation spectrum (Pa)
h	gap distance between parallel plates in rheometer (mm)
J	creep compliance (Pa^{-1})
J_g	glassy comliance (Pa^{-1})
J^*	complex compliance (Pa^{-1})
J'	storage compliance (Pa^{-1})
$J^{"}$	loss compliance (Pa^{-1})
K	viscosity ratio
L	retardation spectrum (Pa^{-1})
M_n	number average molecular weight (kg/mol)
M_w	weight average molecular weight (kg/mol)
R	droplet radius (μm)
R (t)	recoverable compliance (Pa^{-1})
$\bar{R}_v$	volume average radius (μm)
$\bar{R}_n$	number average radius (μm)
t	time (s)
T	temperature (°C)
T_g	glass transition temperature (°C)
T_m	melting point (°C)
w	weight fraction

Greek symbols:

α	interfacial tension (mN/m)
γ	strain
$\dot{\gamma}$	strain rate (s^{-1})
δ	loss angle
η	(steady state) shear viscosity (Pa.s)
η^*	complex viscosity (Pa.s)
η_0	zero-shear viscosity (Pa.s)
η'	real component of complex viscosity (Pa.s)

η''	imaginary component of complex viscosity (Pa.s)
η_m	matrix viscosity (Pa.s)
η_i	droplet viscosity (Pa.s)
λ	relaxation time (sec)
λ_D	shape relaxation time (sec)
λ_β	terminal relaxation time (sec)
β_d^*	surface dilatation modulus (Pa^{-1})
β_s^*	surface shear modulud (Pa^{-1})
μ	micron
σ	shear stress (Pa)
$\dot{\sigma}$	shear stress rate (Pa/s)
τ	retardation time (sec)
ϕ	volume fraction
ω	frequency (rad/s)

Abbreviations:

BSP	Boltzmann superposition principle
HDPE	high density polyethylene
LVE	linear viscoelastic
MFI	melt flow index
NLREG	nonlinear regularization
PA	polyamide
PE	polyethylene
PMMA	polymethyl methacrylate
PP	polypropylene
PS	polystyrene
SAOS	small-amplitude oscillatory shear
SEBS	styrene-ethylene/buthylene-styrene
SEM	scanning electron microscope
STD	standard deviation

Chapter 1. Introduction

1.1. Viscoelasticity

Polymers are viscoelastic materials at all temperatures, i.e. they behave both elastically and viscously. In fact, if a weight is applying stress on a polymeric specimen, the strain increases with time due to the rearrangement of molecular chains. When the applied stress is removed, it takes a certain time for chains to recover fully and attempt to return to their former configuration. These phenomena happen due to the length of the chains and represent the typical behaviour of polymers which are classified as viscoelastic materials. Viscoelastic materials are elastic as they recover and viscous as they creep.[1]

1.2. Rheology as a Tool to Study the Behaviour of Polymer Melts

Complex fluids such as polymer melts do not follow Hooke's law in elastic behaviour. In addition, their stress-deformation rate relationship is different from Newtonian fluids; hence they do not follow Newton's law of viscosity. Rheology is the study of the flow behaviour and deformation of fluids (such as polymer melt) under applied stresses.[2,3]

1.3. Linear Viscoelactic Limit

The linear viscoelastic region is a range of deformation magnitude in which the stress and strain are related by linear differential equations[3]. This means that the deformation (strain) is small enough that the molecule's departure from their equilibrium state is negligible, so the behaviour is similar to an unstrained material.[4] In the linear viscoelastic

region, all material functions are independent of the applied stress or the applied strain. Linear viscoelastic behaviour may be observed under small deformations, very slow deformation (even if it is large), or the short time portion of high rate deformations. The behaviour of a polymer melt becomes nonlinear if the strain or strain rate exceeds polymer's critical level.[3] For large, rapid deformation, none of the principles governing linear viscoelastic region are valid.

Small-amplitude oscillatory shear and creep tests are the most common experiments used to analyze linear viscoelastic behaviour of polymers.[4]

1.3.1. Small-Amplitude Oscillatory Shear (SAOS)

Small-amplitude oscillatory shear is one of the most important rheological experiments in which the time-dependent shear rate is periodic. At low strain amplitudes in the linear viscoelastic region, the produced shear stress is also sinusoidal. The shear strain (γ) and shear stress (σ) in this flow can be written as:

$$\gamma(t) = \gamma_0 \sin \omega t \tag{1}$$

$$-\sigma = \sigma_0 \sin(\omega t + \delta) \tag{2}$$

$$= \sigma_0 (\sin \omega t \cos \delta + \sin \delta \cos \omega t) \tag{3}$$

$$= (\sigma_0 \cos \delta) \sin \omega t + (\sigma_0 \sin \delta) \cos \omega t \tag{4}$$

where ω is the frequency in (rad/s), γ_0 is the strain amplitude, δ is the phase difference between the strain wave and stress response. This equation is valid only in the linear viscoestic region[3].

The latter contains a part proportional to $\sin \omega t$, in phase with imposed strain, and a part proportional to $\cos \omega t$, in phase with imposed strain rate. We can relate the first with the elastic part of the response and the second with the viscous part.

The shear stress in Newtonian fluids is expressed as:

$$\sigma = - \mu \dot{\gamma} \tag{5}$$

in which μ is Newtonian shear viscosity, and $\dot{\gamma}$ represent the strain rate.

In addition, Hooke's law can generally be written as:

$$\sigma = - G \gamma \tag{6}$$

where G is the elastic modulus.

Comparing Equations 4, 5 and 6, it is clear that the stress response in SAOS includes an elastic part (proportional to strain) and a viscous part (proportional to strain rate) which make it a suitable test to study viscoelastic materials. Based on this property, the storage modulus and loss modulus which are in turn a measure of elasticity and viscosity of polymers can be defined as follows:[3]

$$G'(\omega) = \frac{\sigma_0}{\gamma_0} \cos \delta \tag{7}$$

$$G''(\omega) = \frac{\sigma_0}{\gamma_0} \sin \delta \tag{8}$$

As expected, G'=0 for a Newtonian fluid. Similarly, G''=0 for a fully elastic solid. For viscoelastic materials like polymers, $G'$and $G''$are both nonzero and a function of frequency. Other material functions for SAOS are summarized in Table 1.1. [3]

Table 1.1: Material functions for SAOS [3]

Complex modulus magnitude	$\lvert G^* \rvert = \sqrt{G'^2 + G''^2}$
Loss tangent	$\tan\delta = \frac{G''}{G'}$
Dynamic viscosity	$\eta' = \frac{G''}{\omega}$
Out-of-phase component of η^*	$\eta'' = \frac{G'}{\omega}$
Complex viscosity magnitude	$\lvert \eta^* \rvert = \sqrt{\eta'^2 + \eta''^2}$
Complex compliance magnitude	$\lvert J^* \rvert = \frac{1}{\lvert G^* \rvert}$
Storage compliance	$J' = \frac{1/G'}{1+tan^2\delta}$
Loss compliance	$J'' = \frac{1/G''}{1+(tan^2\delta)^{-1}}$

1.3.2. Shear Creep

The transient shear experiment in which the flow is driven under a constant stress is called creep. The fluid is subjected to constant stress and the time-dependent deformation is measured.

The creep compliance J(t), the material function which relates the measured sample deformation to the applied stress, is defined as:

$$J(t) = -\frac{\gamma(t)}{\sigma_0} \tag{9}$$

Accordingly, the creep compliance can be plotted versus experiment time as in Figure 1.1. After a certain time, the change in strain with time becomes linear showing that the flow reaches steady state. If the applied stress is removed at any time bigger than zero, the elastic portion of the polymer springs back and the whole creep-recovery curve can be shown as Figure 1.1.

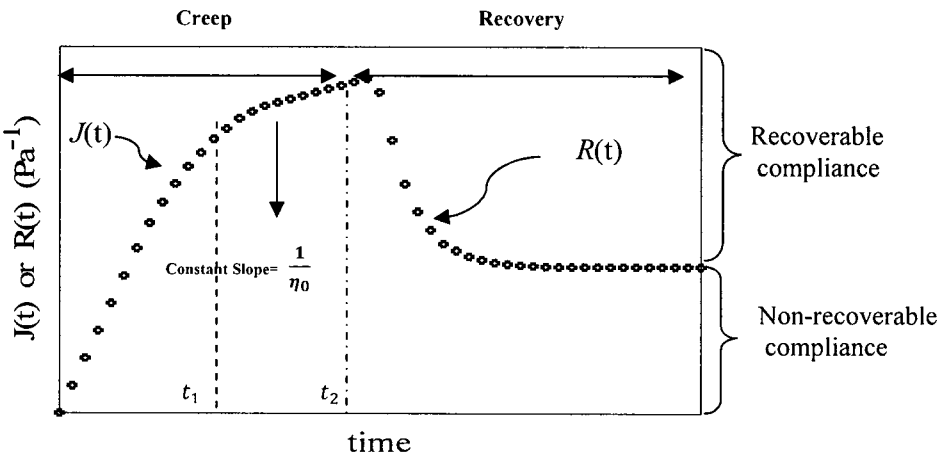

Figure 1.1: Creep curve followed by recovery.
After t_1 seconds the curve reaches steady state. At t_2 seconds the constant stress is removed.

If the creep test is performed in the linear viscoelastic limit, the inverse of the constant slope in the steady state region is equal to the zero shear viscosity or η_0 . For this, the stress must be small enough to keep the strain in the linear regime until reaching steady-state[4]. In linear viscoelastic region, all material functions are independent from the applied stress; therefore creep test can be used to define the limits for nonlinearity of polymeric systems. [1,3]

1.4. Relaxation and Retardation Spectra

Viscoelasticity results in a different response to shear cessation [shear rate ($\dot{\gamma}$) = 0] in Newtonian and Non-Newtonian fluids. Newtonian fluids relax immediately when the flow is stopped, yet Non-Newtonian fluids relax over a certain amount of time. If the flow (at constant $\dot{\gamma}$, i.e. in steady shear state) stops, the stress relaxes over a certain time; hence a characteristic time is defined for Non-Newtonian fluids called the relaxation time λ. The relaxation time can be considered to be the memory time for the fluid.

If a sample at rest is subjected to a constant, large strain rate for a small time ζ (step-strain experiment), then the stress relates to strain as:

$$\sigma(t)= \int_{t_0-\zeta}^{t_0} G(t-t')\,(\dot{\gamma})\,dt' \qquad (10)$$

where t_0 is the time at which the strain is completed. Solving the integral, if t_0 is shifted to 0 and for longer times compared with ζ, the Equation is re-written as:

$$\sigma(t)= \gamma\, G(t) \qquad (11)$$

and $G(t)$ is called the relaxation modulus.[3,4,5]

The term modulus, which is the ratio of stress to the corresponding strain, is generally defined as $\frac{\sigma}{\gamma}$ for a perfectly elastic solid. $G(t)$ represents the equivalent time-dependent property in viscoelastic materials.[3,5]

1.4.1. Modeling of Viscoelastic Materials, Maxwell element, Voigt element

Viscoelastic systems can be modeled by a spring combined with a dashpot, corresponding to the material's elasticity ($G_i = {}^{1}/_{J_i}$) and viscosity (η_i) respectively. [2,5]

If the spring and dashpot are combined in series, the Maxwell model is found. The relaxation time of this element is defined as $\lambda_i = \eta_i/G_i$, the time required for stress to relax. Here, the relaxation modulus is written as:

$$G(t) = G_i e^{-t/\lambda_i} \tag{12}$$

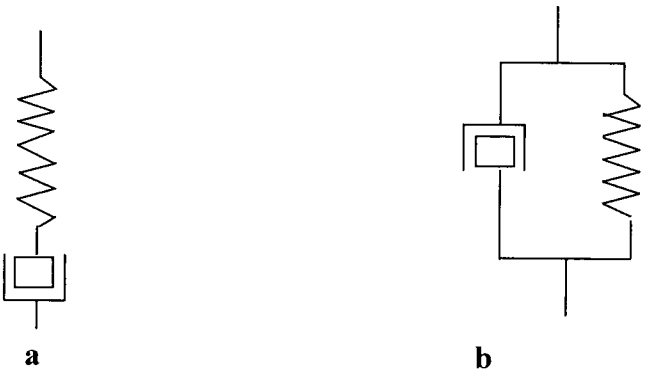

Figure 1.2: a) Maxwell element b) Voigt element

If the spring and dashpot are joined in parallel, a Voigt element is defined and $\tau_i = \eta_i/G_i$ is called the retardation time which is the time required for the spring to return to its equilibrium length while retarded by the dashpot.[5]

The compliance exhibited by the Voigt element is:

$$J(t)= J_i\ (1\text{-}e^{-t/\lambda_i}) \tag{13}$$

The Maxwell model describes stress relaxation after step strain, while Voigt describes creep.

If a group of Maxwell elements are combined in parallel, then a discrete relaxation time spectrum is generated in which each λ_i is related to a G_i . Forces (stresses) are additive in a parallel arrangement, hence $G(t)$ is the summation of all elements in the Maxwell model[5]. For n parallel elements in the Maxwell model:

$$G(t) = \sum_{i=1}^{n} G_i\ e^{-t/\lambda_i} \tag{14}$$

If n goes to infinity, i.e. an infinite number of Maxwell elements in parallel, it results to a continuous relaxation spectrum and the Equation (14) can be re-written as:[4,5]

$$G(t)= G_e + \int_{-\infty}^{\infty} H\ e^{-t/\lambda}\ d\ \ln\lambda \tag{15}$$

It is common to plot the continuous relaxation spectrum as $H^*\ d\ ln\lambda$ vs. logarithmic time scale, as the time scale range of important relaxation mechanisms is broad.[4,5] The term H contributes to the modulus associated with relaxation times between $\ln\lambda$ and $\ln\lambda + d\ \ln\lambda$ and is a measure of the magnitude of the relaxation mechanisms with relaxation times between $\ln\lambda$ and $\ln\lambda + d\ \ln\lambda$.[5] Each peak in the relaxation spectrum refers

to the concentration of relaxation mechanisms in that time, measured by their contribution to the relaxation modulus.

G_e , called the equilibrium modulus, is introduced for viscoelastic solids or cross-linked elastomers in which one of the relaxation times is infinite. For viscoelastic liquids $G_e = 0$.[4,5] In viscoelastic liquids such as uncross-linked polymers, H approaches zero at enough long times as steady-state flow is reached, called the terminal zone.

Similarly, a group of Voigt elements joined in series makes a discrete retardation time spectrum, in which every τ_i relates to a compliance magnitude J_i.[5] In a series arrangement, strains are additive, so the viscoelastic function J(t) turns into:

$$J(t) = \sum_{i=1}^{n} J_i \, (1 - e^{-t/\tau_i}) \tag{16}$$

Again, a continuous retardation spectrum is considered for an infinite number of Voigt elements.

$$J(t) = J_g + \int_{-\infty}^{\infty} L(1 - e^{-t/\tau}) \, d \ln \tau + t/\eta_0 \tag{17}$$

The term t/η_0 is added to reflect the steady state flow, like the case of uncross-linked polymers. Also, J_g represents any possible discrete contribution with τ equal to zero.[5] Glassy compliance $J_g \approx 0$ for the polymer melts. L is plotted against time on double logarithmic axes and vanishes whenever the uncross-linked polymer reaches steady-state. The maxima show the concentration of retardation processes, measured by their contribution to compliance. While H shows the contribution to the modulus, L shows the

contribution of compliance. The relaxation and retardation functions are interrelated through Equations (18) and (19):[5]

$$H = \frac{L}{\left[J_g - \int_{-\infty}^{\infty} \frac{L(u)}{1 - u/\tau} d\ln u - \frac{\tau}{\eta_0}\right]^2 + \pi^2 L^2} \tag{18}$$

$$L = \frac{H}{\left[G_e - \int_{-\infty}^{\infty} \frac{H(u)}{\tau/u - 1} d\ln u\right]^2 + \pi^2 H^2} \tag{19}$$

In general, in the linear viscoelastic regime, short-time mechanisms are more accurately obtained from SAOS tests, while long-time processes are accurately obtained from creep measurements.

In theory, any linear viscoelastic function can be obtained from another. As viscoelastic results are not measureable over all frequencies (or time) and there are imprecisions, no one experiment contains complete information and we need to extract the results from different viscoelastic material functions and combine them to extend the viscoelastic window.[6] Once H and L are obtained, other material functions can be readily calculated. Equations (20) to (26) show the relation between the spectrum functions and some linear viscoelastic material functions.[5]

$$G' = G_e + \int_{-\infty}^{\infty} \left[\frac{H\omega^2\tau^2}{1+\omega^2\tau^2}\right] d\ln\tau \tag{20}$$

$$G'' = \int_{-\infty}^{\infty} \frac{H\omega\tau}{1+\omega^2\tau^2} d\ln\tau \tag{21}$$

$$J'(\omega) = \int_{-\infty}^{+\infty} L(\tau) \frac{1}{1+\omega^2\tau^2} d\ln\tau \tag{22}$$

$$J''(\omega) = \frac{1}{\omega\eta_0} + \int_{-\infty}^{+\infty} L(\tau) \frac{\omega\tau}{1+\omega^2\tau^2} d\ln\tau \tag{23}$$

$$G'(\omega)=\frac{J'(\omega)}{J'(\omega)^2+J''(\omega)^2} \tag{24}$$

$$G''(\omega)=\frac{J''(\omega)}{J'(\omega)^2+J''(\omega)^2} \tag{25}$$

$$\eta_0 = \int_{-\infty}^{\infty} H\,\tau\, d\ln\tau \tag{26}$$

Therefore, by having a full window of relaxation (or retardation) spectrum, all other material functions such as the relaxation modulus, the creep compliance, storage and loss modulus would be obtained, i.e. the linear behaviour is entirely specified.

The main problem is that experimental data are noisy regarding the environmental imposed factors or instrument's accuracy, and after this, some experiments might be incomplete. Considering operator errors, it is very difficult to obtain perfect experimental data.

1.5. Research Objective

The main goal of this project is to evaluate the applicability of using creep measurements for immiscible blends of polypropylene/polystyrene in the limit of linear viscoelastic regime (LVE). For this aim, two problems must be overcome:

a) Determination of appropriate stress to keep the immiscible blends in the LVE region

b) Minimizing the morphological modifications during the creep measurements

Having established the creep method, the following objectives will be pursued:

a) The feasibility of combining the creep measurements with the SAOS information to extend the linear viscoelastic experimental window over broad frequencies for the blends

b) Calculating the linear relaxation spectrum and other material functions over broader frequencies than that of using only the SAOS experiments

c) Analysing the linear relaxation behaviour of the blends

Chapter 2. Literature Review

2.1. Methods of Determination of Relaxation Spectrum

As mentioned in Section 1.4., the LVE material functions can be calculated from relaxation and retardation spectra; therefore, the spectra characterize the behaviour of the polymer melts. On the other hand, there are no direct experiments to obtain the spectra, and they must be calculated from measured material functions.[7] It has been shown by numerous researchers that the determination of the relaxation spectrum from SAOS data is an ill-posed problem as the problem relates to an integral equation of the first kind.[7,8] Honerkamp and Weese pointed out the shortcomings of the application of the linear regression method and suggested that the Tikhonov regularization method was better.[8] Honerkamp suggested that in addition to regularization method, the maximum entropy method is also useful.[9] Elster *et al.* used the program FTIKREG to calculate the relaxation and retardation spectra using Tikhonov regularization.[10] They also modified the maximum entropy method and found it a very reliable method to determine the relaxation spectrum.[11] Honerkamp *et al.* studied different methods of determination of the regularization parameter used in Tikhonov regularization.[12] In 1993, Honerkamp *et al.* demonstrated that although Tikhonov regularization is useful to calculate the spectra over the regions corresponding to the experimental data, it is not accurate for long relaxation times (Figure 2.1).[7]

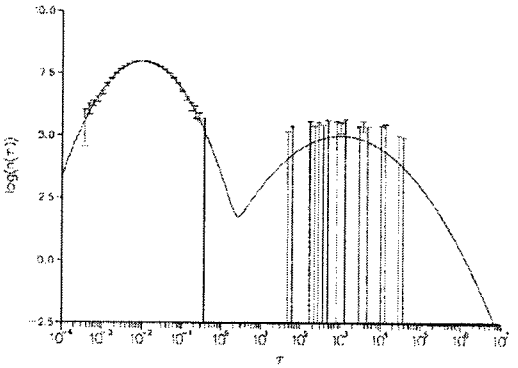

Figure 2.1: Relaxation spectrum using Tikhonov regularization method[7] (the curve is the actual spectrum and the symbols are from Thekhonov regularization)

This limitation of Tikhonov regularization method is due to the breath of important relaxation times. Honerkamp *et al.* applied a nonlinear regularization method to overcome these shortcomings by solving for $\log H$ instead of H as shown below:

$$G' = \int_{-\infty}^{\infty} \frac{\omega^2\tau^2}{1+\omega^2\tau^2}\ 10^{\log H} d\ln\tau \tag{27}$$

$$G'' = \int_{-\infty}^{\infty} \frac{\omega\tau}{1+\omega^2\tau^2}\ 10^{\log H}\, d\ln\tau \tag{28}$$

Figure 2.2 shows the results for the relaxation spectrum calculated using the nonlinear regularization method for the part shown in Figure 2.1. It is obvious that this method improved the estimation of the spectrum.[7]

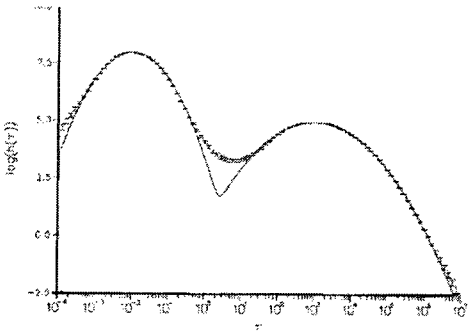

Figure 2.2: Relaxation spectrum calculated using non-linear regularization[7] (the curve is the actual spectrum and the symbols are from non-linear regularization)

A program was developed by Weese to perform the numerical calculation of nonlinear regularization (NLREG) which is widely used.[7] This software receives the angular frequency, ω (rad/s), $G'$and G''(in Pa), or time (in seconds) and the creep compliance J (in Pa^{-1}) ,and estimates the relaxation and retardation spectra based on the parameters such as λ_{max} and λ_{min} defined by the user and the regularization parameter which is determined either automatically by the software or manually by the users. Hansen estimated relaxation spectrum by using Bayesian analysis from dynamic results.[13]

2.2. Range of Validity of Spectrum in NLREG

As a quick estimation, it was believed that the dynamic moduli covering a frequency range of $\omega_{min} < \omega < \omega_{max}$ can predict a relaxation spectrum over a time range of $(\omega_{max})^{-1} < \tau < (\omega_{min})^{-1}$. Davis *et al.* showed that in fact the relaxation spectrum is accurate over a narrower time range than this.[14] They proved that the correct interval is shorter than the reciprocal frequencies by 1.36 decades and modified the range of the validity of the relaxation spectrum as:[14]

$$(e^{\pi/2})\omega_{max}{}^{-1} < \omega < (e^{-\pi/2})\omega_{min}{}^{-1} \qquad (29)$$

2.3. Linear Viscoelastic Properties of Polymers with Long Relaxation Times

Linear viscoelastic properties of molten polymers provide valuable information about structure, especially in the plateau or terminal zones.[15] Some polymer melts such as high density polyethylene, or highly branched molecules have a very broad relaxation spectrum which is not accessible with dynamic measurements (SAOS), because they take a very long time and as the melt measurements are performed at elevated temperatures, it may result in material degradation. Also, the zero-shear viscosity, which is very sensitive to molecular weight, is obtainable in the limit of almost zero frequencies (very long times).[4] Again, with materials with very long relaxation times, dynamic measurements are not suitable to investigate the viscoelastic behaviour at long times (or very low frequencies) since the stress is too small to be measured precisely and the experiment takes too long.[4] SAOS results are generally precise only for shorter experiment times. Certain relaxation phenomena in immiscible blends happen at relatively long times. Therefore, using only SAOS measurements to characterize their behaviour can result in incomplete information.

It is apparent that the creep experiment is readily useful to probe the long time behaviour of polymer melts. In creep experiments, low enough stresses are required to keep the sample within the linear viscoelastic limits. However, to reach steady-state and zero-shear viscosity, a large strain in needed that may take the sample into nonlinear region.[4] Furthermore, it should be taken into account that the level of applied stress should be large enough to have accurate, noise-free results with reasonable resolution from the instrument which in turn may take the sample into the nonlinear regime.

In addition, creep experiments are not accurate at very short times, because it takes time for the stress to reach the set point at the start of the experiment. While the creep test is not accurate at very short times, SAOS data are accurate at short times; therefore SAOS data can be combined with the creep data to make a complete spectrum.[15,16,17]

Eckestein *et al.* used creep data to expand the experimental window of dynamic G'' of a high-molecular-weight polypropylene.[17] They constructed the L (retardation spectrum) from the creep compliance using NLREG and calculated $J'(\omega)$ and $J''(\omega)$ from L. Finally, they converted the dynamic compliances to the corresponding $G'(\omega)$ and $G''(\omega)$. They found a broad overlap between dynamic moduli calculated from L and those obtained from directs SAOS experiment. They then used the dynamic moduli as a medium to combine the data.

Meissner used a combination of an incomplete creep test followed by recovery to characterize melts with high molecular weights, having long relaxation and retardation times. Using the Boltzmann superposition principle, the recovery data were used to calculate the strains for complete creep while keeping the maximum strain within the linear viscoelastic regime.[18]

According to the Boltzmann superposition principle, in the linear viscoelastic regime, the stress responses to successive deformations are additive.

$$\sigma(t)= \int_{-\infty}^{t} G(t-t')\, d\gamma(t')= \int_{-\infty}^{t} G(t-t')\dot{\gamma}\,(t')\, d(t') \qquad (30)$$

Similarly, the strain responses to successive stresses are additive:

$$\gamma(t)= -\int_{-\infty}^{t} J(t-t')\dot{\sigma}(t')dt' \qquad (31)$$

If a creep experiment is performed under a constant stress σ_o for t_1 seconds such that steady shear is not reached, and then the recovery is monitored, the experiment is called incomplete creep followed by recovery. Based on the definition of linear viscoelastic creep compliance, the creep compliance between $t= 0$ to $t= t_1$ is defined as:

$$\gamma(t)= J(t)\,\sigma_o \qquad 0 < t < t_1 \qquad (32)$$

The recovery portion that begins at $t = t_1$ can be considered as a second creep experiment performed under the constant stress ($-\sigma_o$). Then $\gamma(t)$ at times longer than t_1 is calculated by Equation (33).

$$\gamma(t)= J(t)\,\sigma_o + J(t-t_1)\,(-\sigma_o)= \sigma_o[J(t)- J(t-t_1)] \qquad t > t_1 \qquad (33)$$

Re-arranging Equation (33), the creep compliance for the times great than t_1 is obtained in terms of shear strain measured during the recovery part.

$$J(t)= \gamma(t)/\sigma_o + J(t-t_1) \qquad t > t_1 \qquad (34)$$

where $J(t-t_1)$ is measured during the initial creep period.[15]

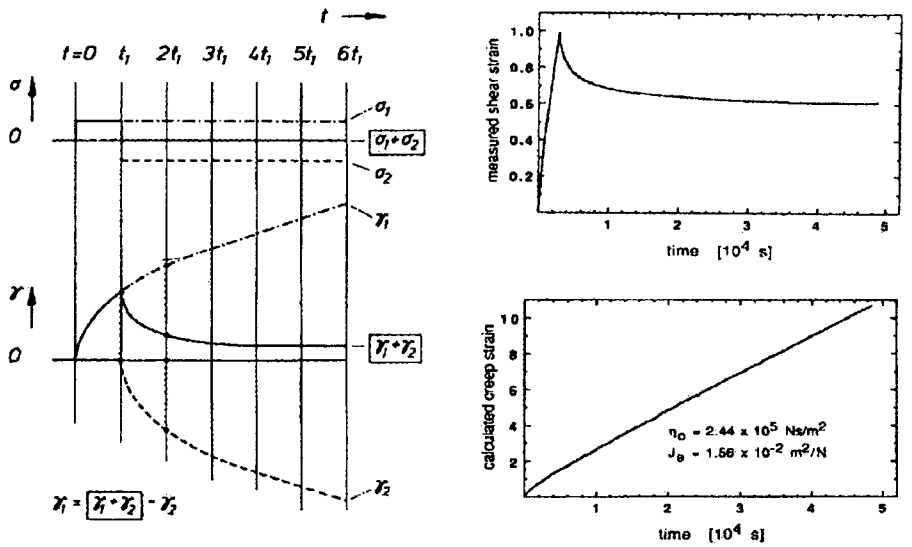

Figure 2.3: Extension of creep strain using recovery strains (Boltzmann Superposition Principle)[18]

Kraft *et al.*also employed the incomplete creep experiment followed by recovery.[16] In their work, a discrete retardation spectrum from re-constructed creep compliance was calculated using Kascha and Schwarzl method.[19,20] In the next step, they calculated the complex compliance (J^*) from the complex modulus (G^*) and converted it to a continuous retardation spectrum using the regularization method. A combined spectrum was obtained by adding the retardation spectra from dynamic and steady measurements. They re-calculated J^* from the combined spectrum and converted it to G^*. Comparing the re-calculated results with G' and G'' measured in SAOS, showed that the combined spectrum extended the information to lower frequencies. The combined weighted relaxation spectrum in this way covers a broad time ranges which are not accessible with only SAOS experiments.[16] The importance of small-amplitude oscillatory shear test is to extend the ranges to higher frequencies (or shorter relaxation times).[16] Also, the

overlapping range of two spectra is a cross-check to insure minimal error in the entire procedure.

He *et al.* established a new method to combine the data set from dynamic and steady experiments. They argued that the discrete spectrum is not precise as it was obtained from an empirical equation having determined by constants without physical significance.[15] Instead, they converted the creep experiment results, $J(t)$, to a continuous retardation spectrum using the NLREG technique. Figure 2.4 shows the composite retardation spectrum, which consists of a short time part from the complex modulus and a long time portion obtained from the creep test.[15]

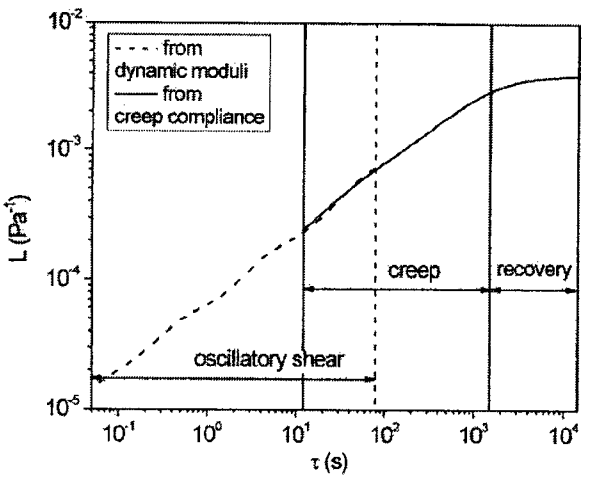

Figure2.4: Composite retardation spectrum obtained by combining short time part of L from SAOS and long time part of L from creep tests[15]

With this method, He *et al.* extended the experimental SAOS data with the creep test making it possible to reach the terminal zone of a branched polypropylene with a very long relaxation time.[15]

In the aforementioned methods, the challenge was to find a material function having information from both sets of data. Storage and loss modulus are integrals over all times, i.e. over all relaxation mechanisms. In addition, when two spectra from two experiments overlap, all other material functions obtained by the integration of two spectra overlap.[15] He *el al.* argued that the inverse statement is not necessarily true, i.e. the overlapping of two material functions from two experiments does not indicate that the two corresponding spectra overlap.

2.4. Blends

2.4.1. Introduction

New materials produced by polymer blending have become increasingly important for providing high performance alternatives to pure polymers. Blending makes it possible to combine the properties of both components and take advantage of having them in one product. In addition economical interests play an important role in development of multi-phase polymeric blends.[21,22] As the use of blends has increased, characterization of their rheological behaviour has become very important.

The overall properties of an immiscible blend are not only dependent on the components themselves, but also on the morphology of the blend which in turn is influenced by different parameters such as the blend composition,[23,24] viscosity ratio of the components,[25,26] method of blending, compatibilizers[27] as well as the interfacial tension. The multi-phase structure changes the rheological properties of the substance;

hence polymeric blends show complex flow behaviour due to the relation between their morphology and rheology.[22]

To study the morphology change during shearing, different methods have been attempted. In most studies, the morphological modifications have been correlated with the observed rheological properties and the flow conditions after steady state. In direct observation methods, scientists have used optical microscopy or light scattering methods, both of which are limited by the transparency of the sample. Indirect methods of investigating the morphology include cessation of flow (after reaching steady-state) and then analyzing the morphology via optical devices or quenching the sample and examining the microstructure using electron microscopy.[21]

In a method used by Martin *et al*, the morphology of the sample is captured by freezing the sample under constant stress between parallel plates.[21] Using this method, the *in situ* morphology was kept, avoiding any break-up of highly deformed droplets due to relaxation of the sample and interfacial tension. In this method, there was no morphological change after quenching as the viscosity of matrix and droplets increases rapidly.

Morphological changes including droplet deformation, coalescence and break up occur under the applied shear stress during most rheological investigations. These micro-structural changes are the result of a competition between viscous forces, due to applied stress/deformation, tending to change the morphology, and interfacial forces that tend to retain the morphology.[28]

The capillary number governs the deformation of an isolated droplet in flow, which is defined as:

$$Ca = \frac{hydrodynamic\ stress}{interfacial\ stress} = \frac{\eta_m\ \dot{\gamma}\ d_p}{2\alpha} \tag{35}$$

Where η_m is the matrix viscosity, $\dot{\gamma}$ is the shear rate, d_p the droplet diameter, and α is the interfacial tension.[21,29] The capillary number is the ratio between viscous forces ($\dot{\gamma}\eta$) attempting to break the droplets and the interfacial forces ($^{\alpha}/_{R}$) that try to retain the morphology.

The dispersed phase retains its equilibrium shape if the Ca is smaller than a critical value. On the other hand, we have deformation and break-up of the drops if the capillary number exceeds the critical value for that system.[28,30,31] To investigate the coalescence phenomenon, the applied stress must be below the stress required for break-up of the dispersed phase. The critical capillary number depends upon the viscosity ratio, the ratio of the viscosity of the droplets to that of the continuous phase. Break-up occurs only at viscosity ratios less than 4.[30]

2.4.2. Linear Viscoelastic Behaviour of Immiscible Blends

Most studies have revealed that small amplitude oscillatory shear (SAOS) flow at small enough strain amplitudes does not change the morphology of blends, i.e. the deformations are in the linear viscoelastic regime.[22,32,33,34]

SAOS investigations on blends showed that they exhibit a pronounced elasticity at low frequencies, i.e. very long relaxation time processes.[32,33,35,36,37,38]. This means that the

behaviour of immiscible blends is governed by the interface at low frequencies. This phenomenon is related to the interfacial tension. It is illustrated in Figure 2.5, showing that the storage modulus $G'$of a two-phase blend is higher than those of the neat components at lower frequencies.

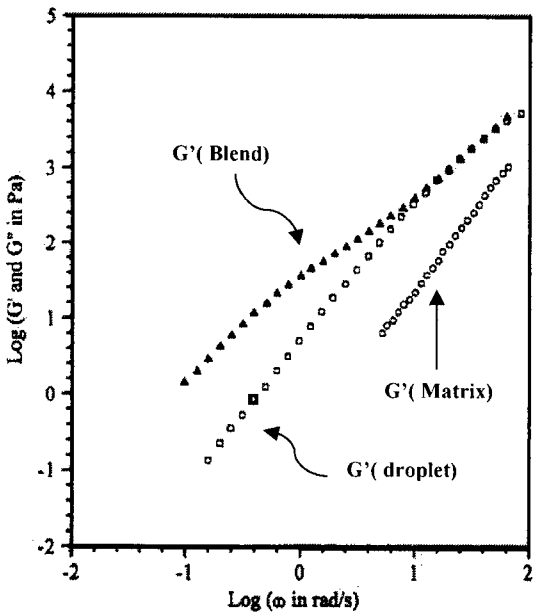

Figure 2.5: Dynamic moduli of a two phase polymer blend in comparison with those of its components[32]

(This figure was modified from the original in reference No. 33)

2.4.2.1. Emulsion Model (*Palierne* Model)

Different researchers have modeled the linear viscoelastic behaviour of immiscible blends.[39,40,41,42,43]

One of the most useful models to predict the rheology of polymer blends in SAOS was proposed by Palierene.[42,44] Graebling *et al.* expressed an equation for the complex shear modulus assuming that the interfacial tension between the matrix and dispersed phase is

independent of local shear and variation of interfacial area. Also, they considered that the droplet deformation is small, and in the linear viscoelastic regime. The Palierne model is given below:

$$G^*(\omega) = G^*_m(\omega)\frac{1+3\sum \varphi_i\ H_i(\omega)}{1-2\sum \varphi_i\ H_i(\omega)} \tag{36}$$

where:

$$H_i(\omega) = \frac{\left\{4\left(\frac{\alpha}{R_i}\right)[2G_m^*(\omega) + 5G_i^*(\omega)] + [G_i^*(\omega) - G_m^*(\omega)][16G_m^*(\omega) + 19G_i^*(\omega)]\right\}}{\{40\left(\frac{\alpha}{R_i}\right)[G_m^*(\omega) + G_i^*(\omega)] + [2G_i^*(\omega) + 3G_m^*(\omega)][16G_m^*(\omega) + 19G_i^*(\omega)]\}}$$

Here, $G_i^*(\omega)$ is the complex modulus of the droplet, α is the interfacial tension, φ_i is the volume fraction of dispersed phase of radius R_i, $G_m^*(\omega)$ is the complex modulus of matrix and $G^*(\omega)$ is that of the emulsion at frequency ω. With the simplification that all the droplets of the dispersed phases have the same radius of R and both phases are described by the single relaxation time Maxwell model, this model can be used to explore the behaviour of polymer blends:

$$G_m^*(\omega) = \frac{i\omega\eta_m}{1+i\omega\lambda_m} \tag{37}$$

$$G_i^*(\omega) = \frac{i\omega\eta_i}{1+i\omega\lambda_i} \tag{38}$$

where η_m, λ_m and $G_m = \frac{\eta_m}{\lambda_m}$ are viscosity, relaxation time, and matrix modulus respectively; η_i, λ_i and $G_i = \frac{\eta_i}{\lambda_i}$ belongs to those of dispersed phase.[32]

For such a system, the Palierne model predicts the G'versus frequency curves shown in Figure 2.6.

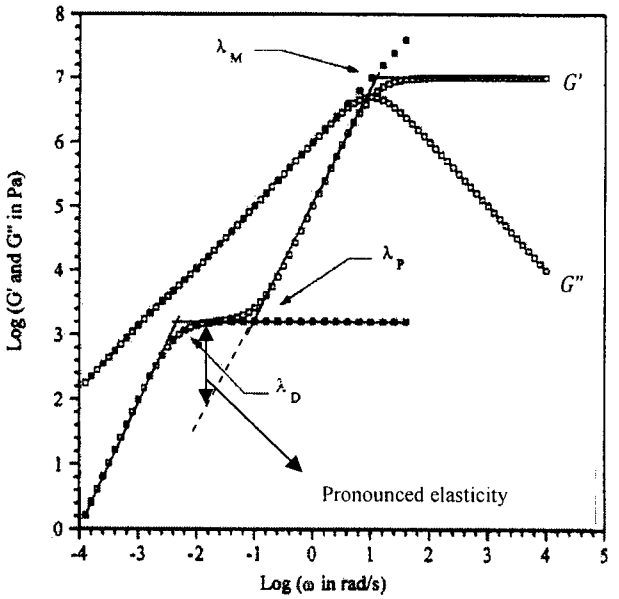

Figure 2.6: Dynamic moduli vs. Frequency for a blend of two viscoelastic component. R=1μm, α=10 mN/m , φ= 0.2, η_m=η_i=10^6 Pa.s, λ_m=λ_i= 0.1 s [32]

Graebling et al pointed out four frequency zones and three characteristic relaxation times as follows:[32]

- a plateau zone for G'(G'=G) at frequencies above $1/\lambda_M$
- $G' \propto \omega^2$, and $G^{"} \propto \omega$ in the range of $[1/\lambda_P , 1/\lambda_M]$,
- a *secondary plateau* for G'(G'=Gp) in the frequency range of $[1/\lambda_D, 1/\lambda_P]$
- a *terminal zone* of the emulsion at frequencies lower than $1/\lambda_D$.

Here, λ_M is the mean relaxation time of the phases which is generally in the order of the relaxation time of the matrix (λ_m), λ_D is related to the shape relaxation of the droplets, and is the longest relaxation time of the emulsion considered in this model. The interfacial tension is directly related to the secondary plateau in G'.[32] The secondary plateau (and the longer relaxation time) shows the direct contribution of geometric relaxation of the droplets to the storage modulus of the blend. It is worth noting that the

secondary plateau can be observed for real blends only when the relaxation times are well separated. ($\lambda_D >> \lambda_P >> \lambda_m$)

Considering some assumptions and simplifications, Graebling *et al.* described λ_D, Gp (secondary plateau modulus),G_∞ (high frequency plateau modulus), G', λ_M and λ_P from the Palierne model [Equation (36)] as below:

$$\lambda_D = \frac{R\,\eta_m}{4\alpha}\frac{(19K+16)(2K+3-2\varphi(K-1))}{10(K+1)-2\varphi(5K+2)} \tag{39}$$

$$G_P = 20\frac{\alpha}{R}\varphi\frac{1}{(2K+3-2\varphi(K-1))^2} \tag{40}$$

$$G_\infty = G_m\frac{2K+3+3\varphi(K-1)}{2K+3-2\varphi(K-1)} \tag{41}$$

$$G' = \omega^2\eta_m\lambda_m\left[\frac{3(1-\varphi)(1-x)}{2K+3-2\varphi(K-1)} + \frac{(2K+3+3\varphi(K-1))(2K+3x-2\varphi(K-x))}{(2K+3-2\varphi(K-1))^2}\right] \tag{42}$$

The particular frequencies at which $G' = G_\infty$ defines the λ_M as:

$$\lambda_M{}^2 = \frac{\eta_m\lambda_m}{G_\infty}\left[\frac{3(1-\varphi)(1-x)}{2K+3-2\varphi(K-1)} + \frac{(2K+3+3\varphi(K-1))(2K+3x-2\varphi(K-x))}{(2K+3-2\varphi(K-1))^2}\right] \tag{43}$$

and λ_P when $G' = G_P$:

$$\lambda_P{}^2 = \frac{\eta_m\lambda_m}{G_P}\left[\frac{3(1-\varphi)(1-x)}{2K+3-2\varphi(K-1)} + \frac{(2K+3+3\varphi(K-1))(2K+3x-2\varphi(K-x))}{(2K+3-2\varphi(K-1))^2}\right] \tag{44}$$

In the above Equations, K= η_i / η_m is the viscosity ratio and $\chi = \lambda_i/\lambda_m$. By using these equations one can easily see the effects of each viscoelastic parameter. Equations 39 to

44 can be used to examine whether or not a secondary plateau exists, i.e. if the shape relaxation of droplets is even visible in the experimental window. The Palierne Model is based on the assumption that the inclusions are spherical in equilibrium. Since the additional relaxation is due to the perturbation of the droplet shape during SAOS test, a higher droplet concentration results in a more pronounced elasticity at lower frequencies.[22]

From Equation (39) we see that λ_D is proportional to (R/α), showing that particle size has the inverse effect of interfacial tension on the relaxation time of the droplets.[32] When interfacial tension increases, at a constant size of the droplets, the driving force of the interface to return to its equilibrium shape is higher and the droplets relax sooner.

2.4.2.2. Application of Viscoelastic Models in Determination of Interfacial Tension and Droplet Size

The *Palierne Model* can be used to calculate the complex modulus of the emulsion if the distribution of droplet sizes in the blend is known. By replacing the *summation of* H_i *terms over the distribution* by the volume average particle radius ($\bar{R}_v$), Graebling *et al.* showed that the interfacial tension, α, can be obtained from viscoelastic data, providing the secondary plateau for $G'(\omega)$ exists and the droplet polydispersity, ($\frac{\bar{R}_v}{\bar{R}_n}$), does not exceed a value of about 2.[45,46,47]

$$\bar{R}_v = \frac{\sum \varphi_i R_i}{\varphi} \tag{45}$$

$$\bar{R}_n = \frac{\sum n_i R_i}{\sum n_i} \tag{46}$$

$\bar{R}_n$ stands for number-average radius, φ_i is volume fraction of droplets, R_i is radius of droplet i, $n_i$is the number of droplets of radius R_i, and $\varphi = \sum \varphi_i$ is the total volume fraction of the dispersed phase. After replacing the summation, Equation (36) becomes:

$$G^* = G_m^* \frac{40\left(\frac{\alpha}{\bar{R}_v}\right)[G_m^*+G_i^*]+[2G_i^*+3G_m^*][16G_m^*+19G_i^*]+3\varphi[4\left(\frac{\alpha}{\bar{R}_v}\right)[2G_m^*+5G_i^*]+[G_i^*-G_m^*][16G_m^*+19G_i^*]}{40\left(\frac{\alpha}{\bar{R}_v}\right)[G_m^*+G_i^*]+[2G_i^*+3G_m^*][16G_m^*+19G_i^*]-2\varphi[4\left(\frac{\alpha}{\bar{R}_v}\right)[2G_m^*+5G_i^*]+[G_i^*-G_m^*][16G_m^*+19G_i^*]} \quad (47)$$

By fitting G', the value of $\frac{\alpha}{R}$ is readily calculated, which in turn leads to the values of volumetric mean radius if the interfacial tension is known or the interfacial tension if the volumetric mean radius is known.

Gramespacher *et al.* suggested that the position of the maximum in the weighted relaxation spectrum relates to the relaxation time of the droplets.[22,48] Following this idea, Vinckier *et al.* used Equation (39), and the fact that the maximum of each spectrum is related to the interfacial relaxation time in the blend, they calculated the mean volumetric radius of the droplets.

Vinckier *et al.* proposed using a relaxation spectrum of the interface to find the relaxation time of the droplets. They obtained an interfacial relaxation spectrum by subtracting the contribution of the components from the blend relaxation spectrum, assuming that the component contributions are cumulative when weighted by their volume fractions[22].

$$H_{blend} = \varphi_m(H_m) + \varphi_d(H_d) + H_{interface} \quad (48)$$

Figure 2.7 shows several examples of interfacial relaxation spectra from their work.

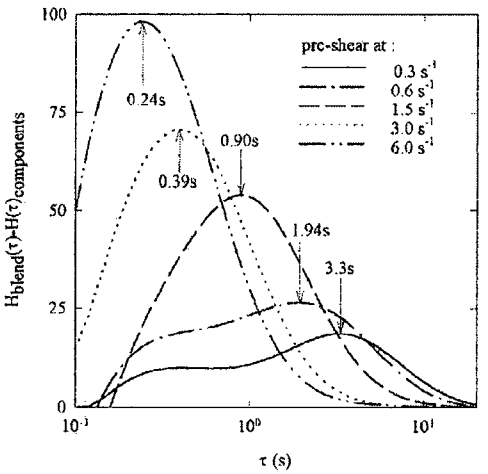

Figure 2.7: Interfacial relaxation spectra at different pre-shear histories for the blends of 30%Polyisobutene in Polydimethylsiloxane[22]

In these spectra, the magnitude of the peak is related to the amount of interfacial area, while the time the peak is determined by droplet size. In these experiments, they used different pre-shear treatments that change droplet size. The higher the pre-shear rate, the finer the dispersed phase and so there is larger area of interface.

The relaxation spectrum of a blend is composed of the relaxation spectra of component plus an extra peak from which the interfacial tension can be inferred. Gramespacher and Meissner calculated the extra relaxation time (τ_1), which is due to the relaxation of the interface, in the discrete relaxation spectrum of a blend as follow:[35,48]

$$\tau_1 = \tau_0\left(1+\varphi\frac{5(19K+16)}{4(K+1)(2K+3)}\right) \tag{49}$$

$$\tau_0 = \frac{\eta_m R}{\alpha}\frac{(19K+16)(2K+3)}{40(K+1)} \tag{50}$$

Where η_m is matrix Newtonian viscosity, K is viscosity ratio, while R and φ are the average radius and volume fraction of dispersed phase respectively.

Macaubas *et al.* examined a blend system of polypropylene and polystyrene (90/10) in which the difference between storage modules of the matrix and dispersed phase was not large enough to distinguish any secondary plateau, i.e. a system in which *Palierne* model cannot be applied to infer the interfacial tension.[35]

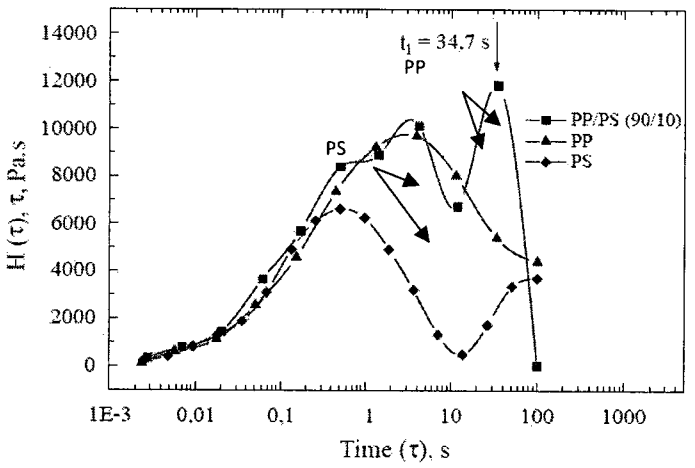

Figure 2.8: Weighted relaxation spectrum for blend PP/PS (90/10) and pure components[35]

Three relaxation peaks were observed in their blend relaxation spectrum, two of which are related to the blend components and the third one is correlated to the relaxation of the interface between components.[35,49] The peaks concerning the blend components occur at the same times as the ones of the pure phases.[35] By using Equation (49) and substituting the interfacial relaxation time obtained from the weighted relaxation spectrum above, they obtained the to the value of interfacial tension about 6.25 mN/m at 200° C.

In the case of compatibilized blends, a fourth peak, related to an even a longer relaxation mechanism may also be observed, this will be explained later.

2.4.3. Interfacial Tension and the Effect of Compatibilizer

The overall properties of polymer blends are affected by the morphology. In turn, the morphology of polymer blends is totally dependent to the compatibility of the components. As the polymers are mostly immiscible, this produces a coarse morphology with weak adhesion between matrix and droplets resulting in poor mechanical properties.[35,50] In this regards, compatibilizers are added to the blend to improve the compatibility between the components and control the morphology.[50,51,52]

Compatibilizers, usually copolymers, are added to inhibit coalescence. These additives lower the interfacial tensions, and so the interfacial restoring stresses, and facilitate the break-up phenomenon.[53,54,55,56,57]Overall, compatibilization is divided into two groups, physical compatibilization at which the compatibilizer is added before blending, and reactive compatibilization in which the compatibilizer is generated by interfacial reactions during blending.[58] Because of the macro-molecular nature of the compatibilizers, some behaviour is typical. Firstly, low diffusivity of the compatibilizars due to their high molecular weight results in some non-equilibrium phenomena, such as entrapment of the compatibilizer in micelles. Entanglement between compatibilizer molecules and bulk is likely.[58] Matos *et al.* suggested while the molecular weight of the compatibilizer is not critical, its chemistry has a crucial role in its efficiency.[59] Willis *et al.* argued that the effect of interface modification on morphology might be greater than that of composition or viscosity ratio.[27]

Figure 2.9 shows the interfacial tension between polypropylene and polystyrene in a blend of PP/PS (90/10) as a function of the amount of compatibilizer added to PS.[35] It can

be seen that the interfacial tension between components, and consequently the average radius of polystyrene droplets dispersed in polypropylene matrix, decreases as the compatibilizer concentration increases, following the emulsion curve.

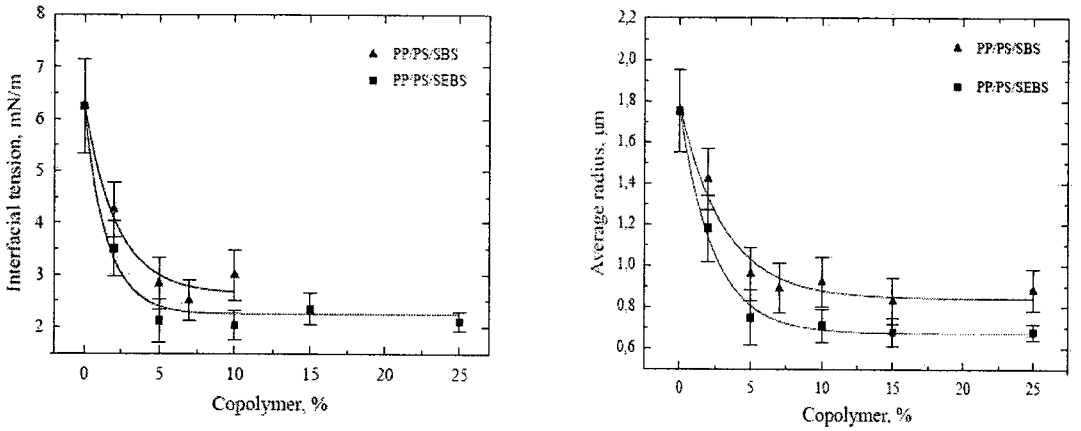

(a) (b)

Figure 2.9: a) Interfacial tension and b) droplet average radius as a function of compatibilizer concentration in a blend of PP/PS (90/10)[35]

There is a critical compatibilizer content after which the droplet size reached a constant value.[54,59,60,61] The reduction in dispersed phase size is due to both the suppression of coalescence as well as the reduction of interfacial tension[60].

Huitric *et al.* added up to 2% polyethylene-graft-maleic anhydride to a blend of low-density polyethylene and 30% polyamide and observed the morphological changes show below. [53]

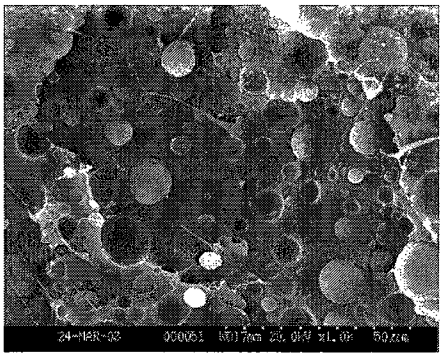

$\varphi_c = 0\%$

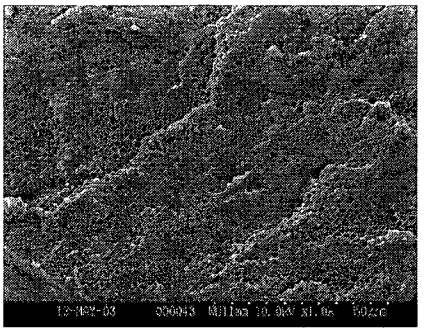

$\varphi_c = 2\%$

Figure 2.10: Effect of compatibilizer on morphology[53]

As discussed before, immiscible blends show a higher elasticity at low frequencies, related to the shape relaxation of dispersed phase (the third peak in the weighted relaxation spectrum). There are two forces acting in the relaxation mechanism of the interface, shearing forces (proportional to $\eta\dot{\gamma}$) that tends to deform the droplets and cohesive forces (proportional to $\frac{\alpha}{R}$) which try to keep the droplets in the equilibrium (spherical) shape. This results to a characteristic shape relaxation time of dispersed phase.[62] Once compatibilized, the interfacial tension between the phases, and so the retraction forces in the interface, decreases which results in longer times for the interface to relax.[49]

In compatibilized blends with block copolymers, a forth relaxation peak is sometimes reported which occurs at even longer times, attributed to the relaxation of Marangoni stresses tangential to the interface of the matrix and droplets.[55] Marangoni stresses are introduced because of a gradient in the interfacial tension, due to a gradient in the concentration of the compatibilizer at interface. This additional relaxation time occurs at very low frequencies (or long times) and it may superpose with the shape relaxation of

the droplet (at too high concentration of compatibilizer); therefore it may not be seen experimentally.[55]

Jacobs *et al.* assumed that the surface dilatation modulus, β_d^* (ω), and the surface shear modulus, β_s^* (ω), in the *Palierne* general model, are purely elastic, so they set them as a non-zero constants called β_{10} and β_{20} respectively to find shape relaxation time (λ_D) and the terminal relaxation time (λ_β).[63] Wang *et al.* modified the latter and calculated the additional relaxation time as follow:[55,64]

$$\lambda_D = \frac{B}{2}\left[1-(1-4\frac{A}{B})^{0.5}\right] \tag{51}$$

$$\lambda_\beta = \frac{B}{2}\left[1+(1-4\frac{A}{B})^{0.5}\right] \tag{52}$$

$$A = \frac{\bar{R}_v\eta_m}{4\,\alpha}\,\frac{(19K+16)[2K+3-2\varphi(K-1)]}{10(K+1)+\frac{\beta_{20}}{\alpha}(13K+12)-2\varphi((5K+2)+\frac{\beta_{20}}{2\alpha}(13K+8))} \tag{53}$$

$$B = \frac{\bar{R}_v\eta_m}{8\,\beta_{20}}\,\frac{10(K+1)+\frac{\beta_{20}}{\alpha}(13K+12)-2\varphi((5K+2)+\frac{\beta_{20}}{2\alpha}(13K+8))}{1-\varphi} \tag{54}$$

R_v is volume average radius, η_m the viscosity of the matrix, φ volume fraction of droplets, K viscosity ratio, and α is interfacial tension.[55]

Yee *et al.* followed this model to characterize compatibilized blends of PMMA/PS (90/10) and (95/05) shown in Figure 2.11.[55] While the first one is related to the superposition of the components, the second and third ones corresponds to λ_D and λ_β respectively.[55]

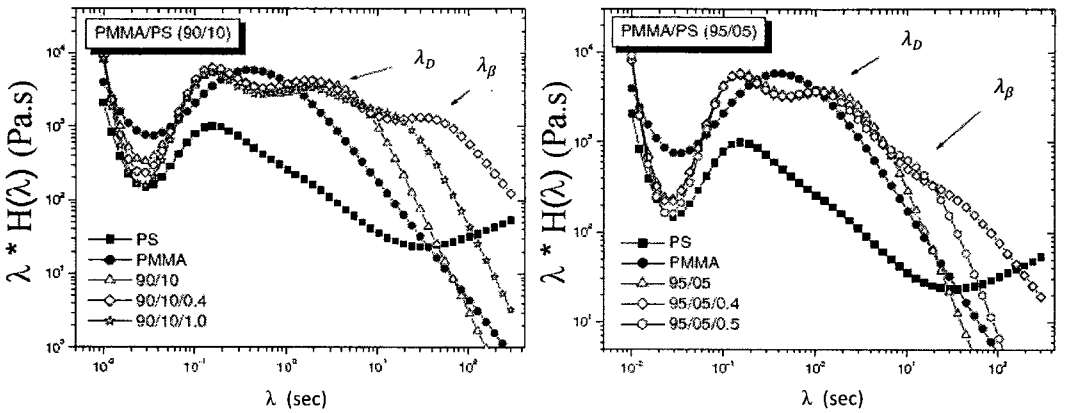

Figure 2.11: The presence of λ_F and λ_β in the weighted relaxation spectra of the blends of PMMA/PS [55]

(This figure was modified from the original in reference No. 53)

Similar phenomenon was reported with other compatibilized blend systems.[50,62] Reimann *et al.* also observed the forth peak related to the terminal relaxation of blends of PMMA/PS compatibilized by diblock copolymers.[50,62] They concluded that the presence of the additional relaxation time depends upon a sufficient deformability of the drops as well as entanglement interactions between the compatibilizer and the matrix. Hemelrijck *et al.* argued that the terminal relaxation time speeds up as the amount of compatibilizer increases; hence it is possible that shape and terminal processes merge and show a single relaxation time.[65] In the case of uncompatibilized blends, $\beta_{20} \rightarrow 0$, and Equation (51) is the same as Palierne's Model.

2.4.4. Rheology and Morphological Investigations under Steady State Shear Flow

The deformation of uncompatibilized droplets in blends depends on capillary number, *Ca*, and viscosity ratio, K= $\frac{\eta_i}{\eta_m}$, in which η_i and η_m are the viscosity of the droplets and matrix respectively.[58] If *Ca* number exceeds a critical value, beak-up happens which can be the breakage of an extended drop into two drops or a highly extended one into several droplets. Grace concluded that the minimum critical capillary number happens at viscosity ratios 0.1< K< 1, i.e. breakup is very effective at this range, and almost impossible for K>4.[22,30]

On the other hand, we have collisions of droplets due to applied flow, or even Van der Waals attractions, which cause coalescence. Besides facilitating break-up, compatibilzers inhibit coalescence in two ways: firstly, when two drops approach each other, the compatibilizer is drained out from the gap between drops, due to the flow between two approaching drops, producing a gradient in compatibilizaer concentration (and consequently in interfacial tension) which in turn cause a tangential stress, called Marangoni stress, which immobilizes the interface and postpones the drainage of the film.[66] Velankar *et al.* discussed and simulated the effect of copolymer concentration gradient due to drop deformation and Marangoni stresses intensively.[67] The second mechanism, suggested by Sundararaj *et al.*[68], is that the suppression of coalescence is due to the compression of the compatibilizer block, resulting in a repulsive force when droplets approach. They said that the suppression of coalescence is due to stabilizing the interface, not the reduction of interfacial tension.[57,58]

There are two mechanisms for coalescence. At lower stresses, it occurs by droplet-droplet collisions at different flow paths while the droplets are spherical. By increasing the stress, as the droplets become ellipsoid or even fibril, the coalescence is only possible at the same flow path and is controlled by head-to-tail collisions. At higher stresses, the increase of droplet size is less pronounced; because the interfacial tension cannot balance the viscous flow and break-up occurs.[21]

Indeed, morphological changes occur at high stresses or high strain rates under steady state conditions. Figure 2.12 shows the evolution of morphology during a creep experiment done by Martin *et al.*[21] Comparing with the morphology of the reference sample, there is no significant deformation in drops at lower stresses and small strains, yet the coalescence was observed if the flow was continued to a larger strain. At higher stresses, spherical droplets reshape to ellipsoids and orient to the flow direction.

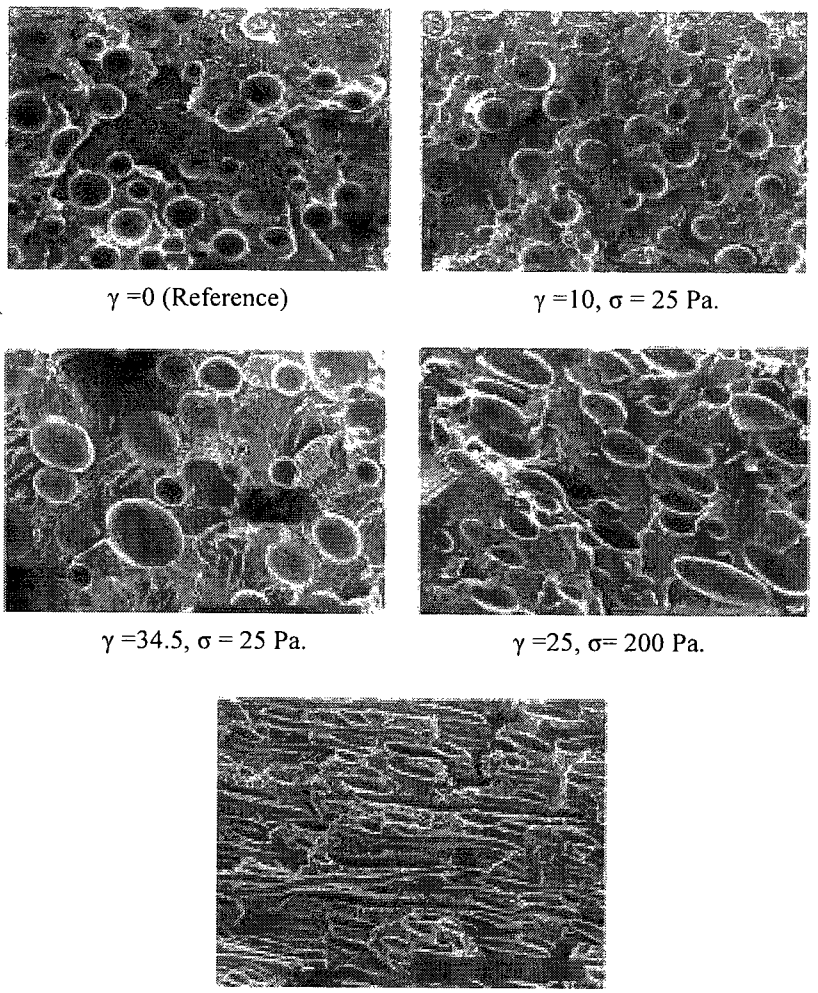

Figure 2.12: Morphology evolution, blends PS/HDPE at different stresses and deformations in creep test[21]

Figure 2.13 shows the complex viscosity changes and the variation of droplet size in start up and creep tests done by Huitric *et al* on blends of polyethylene and polyamide. At small shear rates, the viscosity overshoot at small strains (small shear rates) is related to droplet deformations. The progressive decrease in the complex viscosity is due to the coalescence and the increase in droplet size; whereas at larger strains it reaches an equilibrium value.[53] Due to the size increase of the droplets at the beginning of the

experiments, the capillary number reaches its critical value and the size of droplets becomes comparable with break-up limits; hence the morphology becomes coalescence/break-up controlled and the curves level off. In higher strain rates, morphological evolution was govern by break-up/coalescence from the beginning, so the behaviour is more complex.[53]

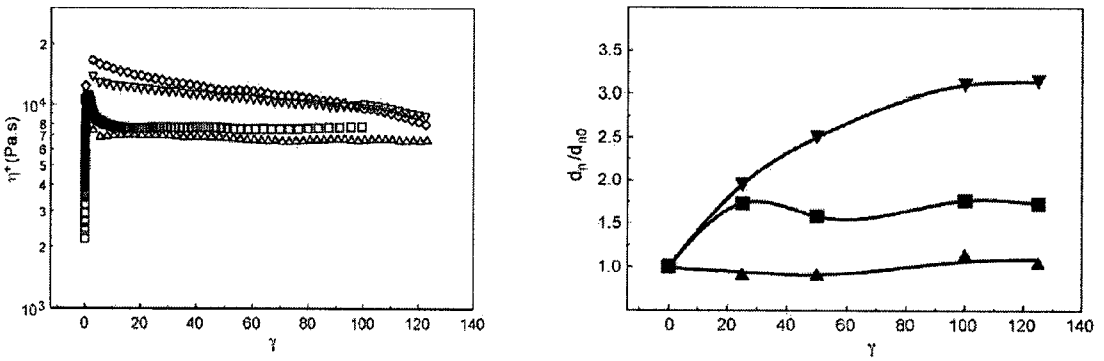

Figure 2.13: a) Complex viscosity changes due to strain [◊ (0.025 S^{-1}), ∇ (0.05 S^{-1}) , Δ(0.35S^{-1}), □(2000 Pa)]
b) the variation of droplet size versus strain [▼(0.05s^{-1}) , ▲(0.35 s^{-1}), ■ (2000 Pa)] [53]

Iza *et al.* discussed that once compatibilized, the blend will be more resistant to the flow, meaning that it would be less shear thinning.[51] Under steady-state flow experiment, they showed that the Cox-Merz rule [$\eta(\dot{\gamma}) \approx \eta^*(\omega = \dot{\gamma})$ in which $\eta^*(\omega)$ is dynamic viscosity and $\eta^*(\dot{\gamma})$ is the steady-state viscosity] is in a good agreement for blends of PS/HDPE and the one compatibilized with 1% of Kraton in low and intermediate shear rates between 0.1 and 1 s^{-1}. They concluded that the morphology was not changed significantly in this range. At higher shear rates, the morphology will change significantly, and Cox-Merz rule is not fulfilled. They also concluded that the effect of

compatibilizer is mainly observed at low shear rates (in steady-state shear) and low frequencies (in dynamic measurements).

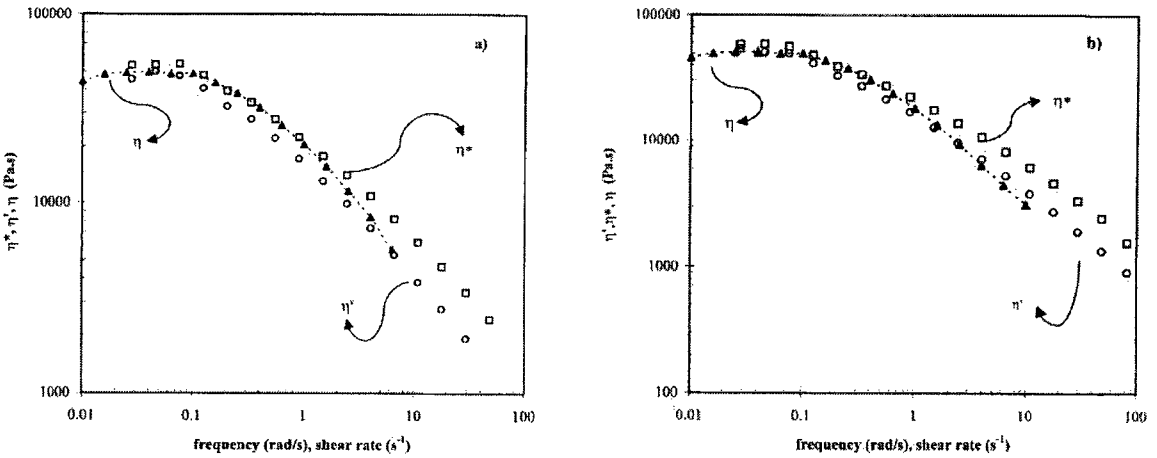

Figure 2.14: Cox-Merz rule at low shear rates and corresponding frequencies

a) PS/HDPE blend b) PS/HDPE blend with 1%of Kraton[51]

The equilibrium droplet size is the result of continuous breakup and coalescence. As the concentration of droplets increases, the coalescence increases, and $d_n$increases linearly with concentration of dispersed phase.[69] Lyu *et al.* studied blends PS/HDPE under steady-state shearing and concluded that the coalescence at higher shear rates is slower and that the coalescence rate is faster at higher volume fraction of dispersed phase.[70] Vinckier *et al.* presheared blends of polydimethylsiloxane/polyisobutene at high rates to produce a fine morphology, and then suddenly stepped down the shear rate to induce coalescence. They reported that with all other parameters being fixed, the time scale for coalescence is inversely proportional to the square of the droplet fraction in blend.[71]

Chapter 3: Materials and Experimental Methods

3.1. Material Preparation

3.1.1. Materials

Two pure polymers as well as four blends of pure components at different concentrations, uncompatibilized and compatibilized were employed to fulfill the aim of this research. The pure polymers used in this project were a polypropylene and polystyrene. The properties of these materials are summarized in Table 3.1.

Table 3.1.: Material properties

Name	M_n (g/mol)	Mw (g/mol)	MFI (g/10min)	Commercial name	Supplier	Type
Polypropylene (PP)	97000	340000	8	HM6100	Quattor	Homopolymer
Polystyrene (PS)	not available	not available	4	158K	BASF	Homopolymer
styrene–ethylene/butylene–styrene (SEBS)	79000	79000	not available	G1652	Kraton	Block co-polymer

The blends were prepared in an extruder, Rheomix PTW-16, coupled to a torque rheometer ThermoHaake PolyLab 900, with four heating zones, all set at 200° C and 100 rpm. A commercial block copolymer styrene-ethylene/butylene-styrene (SEBS), a thermoplastic elastomer, was used to compatibilize the blends of polypropylene/polystyrene at different compositions. The blends used in this research

are: PP/PS(90/10), PP/PS(90/10)+SEBS, PP/PS(70/30) and PP/PS(70/30)+SEBS. The compatibilizer was added at 10wt% with respect to the dispersed phase (PS). The experiment temperature was chosen 200 ° C because it is sufficiently above the melting point of PP (matrix), and in addition, it is not too high to cause thermal degradation which will be discussed in Section 3.2.1.1. All blend preparation was performed by Dr. Demarquette's research group at the University of Sao Paulo, Sao Paulo, Brazil.

3.1.2. Compression Moulding

The pure components and the blends in the shape of pellets were compression moulded into discs using a Carver Laboratory Hydraulic Press, equipped with hot plates. As bubbles and liquid drops may form in polystyrene during moulding[21], a cycle of press-release was employed to make the blend samples. The pellets of blends were put in the moulds and kept at 200° C for about 8 minutes to melt, while the force (on a 22×22 cm^2 mould plate) was gradually increased up to 1 metric ton. Then the force was increased up to 5 tons and held for 2 minutes before the pressure was released. The last step was repeated three times. A similar method was used by Martin *et al.*[21] At the end, the mould was cooled down using water circulation. The neat components were moulded with the same cycles used for the blends as it is essential that the pure components have the same thermo-mechanical history as the blends for further comparison and analyses.

3.1.3. Drying

All PS samples as well as the blends were dried under vacuum before each experiment for 15 hours and 30 minutes at 110° C, well above the T_g of PS. For this purpose, a VWR Economy Vacuum Oven, model 1400E was used, which provides a vacuum up to 30 inch.*Hg* was used. Time sweeps after different drying times were done to rheologically optimize the drying duration.

3.2. Rheological Measurements

The Rheometer MCR500 (Anton Paar US) with parallel plate geometry of 25mm diameter, using US200 software, was used to perform dynamic and creep tests. The minimum and maximum applicable torque is within the range of 0.25 and 200 μNm, while the torque resolution and accuracy are 0.002 and a max of 0.2 (0.5 %) μNm.

This stress-control rheometer is equipped with a nitrogen circulation system which provides an inert atmosphere in the hot chamber, protecting the sample from degradation and any chemical changes in the polymer.

Sample loading requires a careful attention to ensure correctness and reproducibility of the results. The loaded samples should be alike as possible, and also all pollutants, bubbles and other defects should be minimized. To load the sample, at first the temperature was set to heat up the chamber to the desired temperature above the melting point of the sample. Meanwhile, the nitrogen circulation was applied to protect the sample from degradation. Reaching the exact temperature, the "zero gap" operation was done to calibrate the measuring system before each experiment. Next, the plates were set to their maximum distance, the hot chamber was opened and the sample was quickly

loaded. During loading, gentle radial strokes with a spatula helped the removal of captured bubbles between the sample and plates. During loading, the temperature falls, therefore it is necessary to wait for thermal equilibrium and then the upper plate is brought down to the specified gap. After this step, trimming is done to remove excess material. Again, time is taken to let the temperature reach equilibrium and sample loading is complete.

Trimming plays a crucial role to obtain accurate results. To reduce the edge effects, the best rim shape is semi-spherical, shown in Figure 3.1.

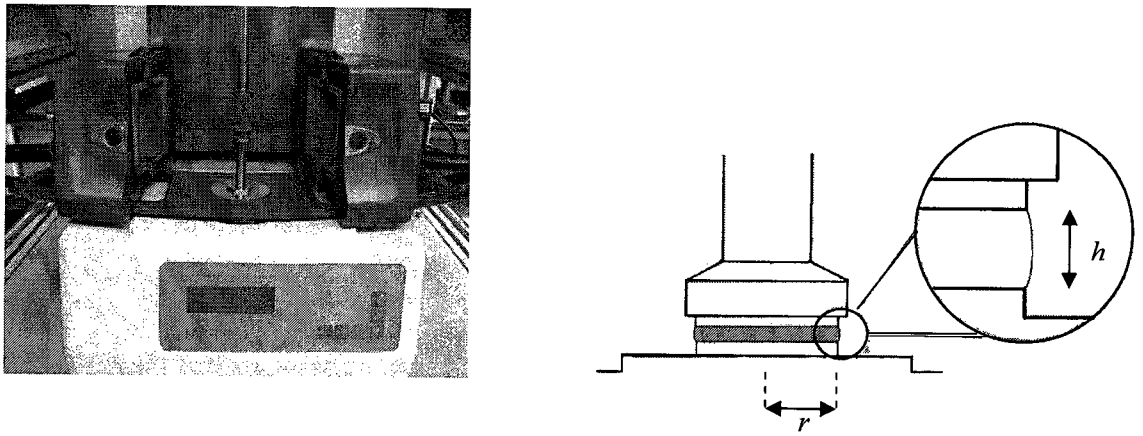

Figure 3.1: Parallel plate measuring system in rheometer MCR500 and the sample rim shape

The optimum gap between the parallel plates is dependent on the material (viscosity) and the nature of the experiment being done. For the sample to feel a pure shear (drag flow) and unidirectional flow, it is favourable that the plate curvature, θ, tends to zero; hence the gap distance over the radius, $\frac{h}{r}$, should be minimum which calls for smaller h. Also, for low viscosity melts a small gap would be used, preventing the material from being pulled out. On the other hand, to study some materials like blends, the overall

(macroscopic) properties are of interest, and one needs as many as droplets to be sheared to yield precise data. In this regard, very small gap distances may interfere with the results especially when the droplets are big. In addition, with very high viscosity melts, it is difficult or impossible to reach small gaps.

There are two major geometries to perform measurements with a rotational rheometer, cone-plate and parallel plates. In the cone-plate geometry, the shear rate is constant which makes it a suitable geometry to investigate the changes with shear rate, whereas in a plate-plate geometry there is a shear rate gradient, i.e. a minimum in the center and a maximum at r =R. In a cone-plate geometry, when the melt viscosity is too high, it is difficult to reach the gap (as the gap in the center should be ideally near zero), producing too high normal forces. Again, measurements on blends with big drops do not yield exact data using cone-plate geometry. In this work, plate-plate geometry was used to avoid these problems. A gap of 1 mm in this geometry is large enough to reduce wall effects and its interference with morphology.[21]

Before running each experiment, this is recommended to pre-heat the samples for a certain time.[18,21] This is crucial with blends as thermal morphology changes has been reported by many authors.[21,60,72] A pre-heat at the operating temperature for 10 min was established in this study before each experiment.

3.2.1. Dynamic Measurements (Small-amplitude Oscillatory Shear Tests)

Dynamic measurement, i.e. small-amplitude oscillatory shear test, is maybe the most efficient method to obtain precise data of rheological behaviour of polymers in the linear

viscoelastic limit. In this regard, time sweep, strain sweep, and frequency sweep tests were employed to obtain storage modulus, loss modulus, and complex viscosity which were used to construct relaxation and retardation spectra over shorter time scales.

3.2.1.1. Time Sweep, Determination of Material Stability

The measurement of linear viscoelastic properties of polymers calls for long time (broad frequency) investigations. Thermal degradation and chemical changes in the structure of polymers may occur at elevated temperatures even if stabilizers are added to polymer and the atmosphere is protected by nitrogen.[21] Thermal stability of samples was verified by means of time sweep test to ensure that the obtained data were stable over the time.[15,18] In this regard, the SAOS response in terms of complex viscosity and/or storage modulus was measured for the estimated experiment time at the experiment temperature for a constant frequency of 1 rad/s.[15,21]

The storage modulus is more sensitive to chemical changes than complex viscosity, therefore the thermal stability of the all samples were examined by means of time sweeps of the normalized storage modulus. I used the complex viscosity changes to show the effect of drying as this would be easier for the readers to understand its effect on polymer properties. Figure 3.2 shows the results of time sweeps of relative complex viscosity, normalized over the complex viscosity at the first point, performed on PS to determine the optimum drying time. The *just-moulded* PS shows dramatic changes at the beginning of the test. By increasing the drying time up to 15 hours and 30 minutes, the variation in viscosity reaches its minimum. By drying for longer times, again dramatic changes were observed due to the start of thermal degradation.

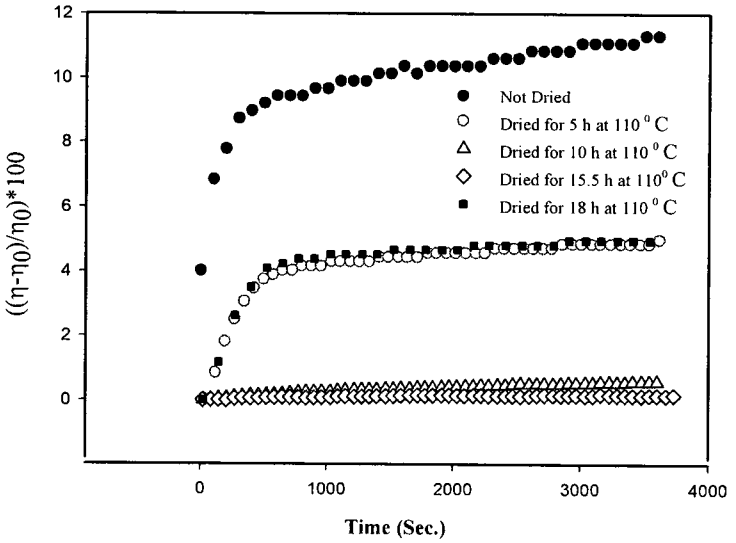

Figure 3.2: Time sweep of PS at 200° C at different drying periods

Furthermore, as mentioned in previous section, some volatiles were produced during sample moulding affecting the rheology.[18] Figure 3.3 shows the difference in complex viscosity of PS, before and after drying.

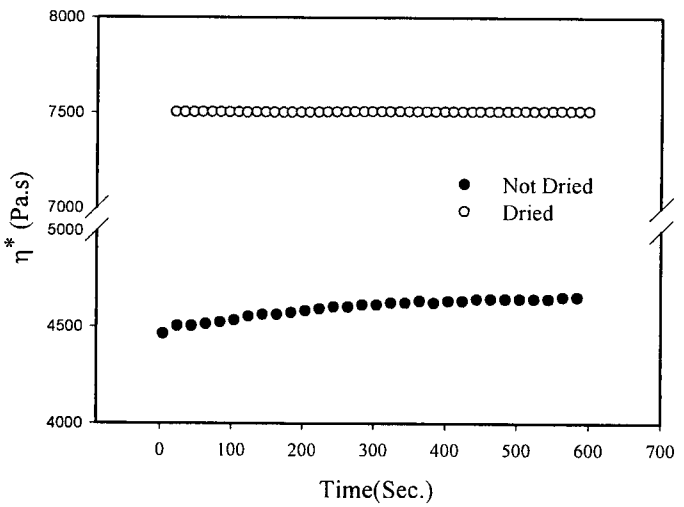

Figure 3.3: Time sweep of PS at ω= 1 ($^{rad}/_{sec}$) and 200° C

The thermal stability of all samples were examined by means of time sweeps of the normalized storage modulus, performed at constant frequency of 1 (rad/s) and strain magnitude of 5%, for the prospective experimental time at 200° C. Figure 3.4 shows the results of the time sweeps of the PP and PS.

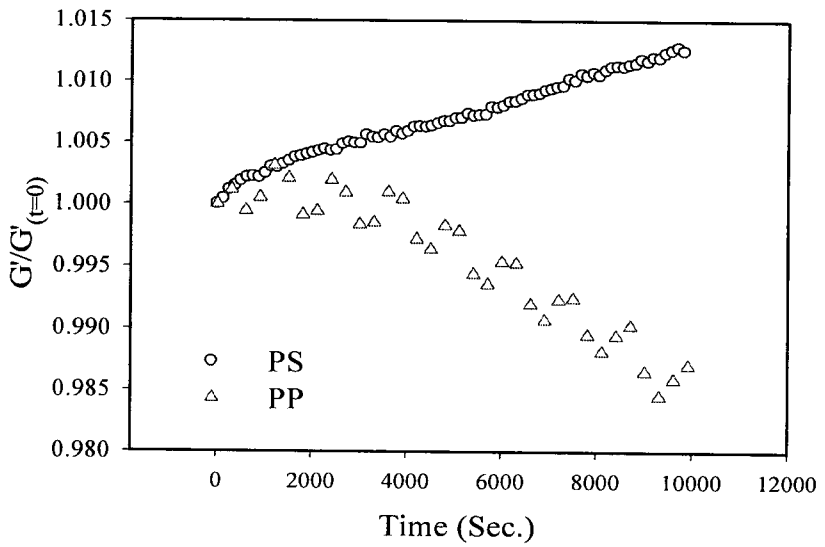

Figure 3.4: Thermal stability of neat components at 200° C for 3 hours

The changes in storage modulus over three hours for PP and PS are less than 3% and 2 % respectively, indicating that the influence of chemical changes on the rheology of the neat polymers is negligible. There are opposite trends of variation in the PP and PS properties over the time sweep. As mentioned before, PS contains some volatiles even after drying. The escape of the remaining water during shearing increases the storage modulus. In PP, there is a very small drop in the storage modulus due to a small amount of chain scission.

Figure 3.5 shows the results of thermal stability tests of blends, carried out at constant angular frequency of 1 rad/s and strain magnitude of 5%, at 200° C. The change in normalized storage modulus was less than 5 percent for the longest time sweep, indicating that the material was sufficiently stable in all experimental times. In the case of compatibilized PP/PS(90/10), the small variation in the normalized storage modulus is due to some probable thermal noises (variations), happened during the time sweep, which was experimentally negligible.

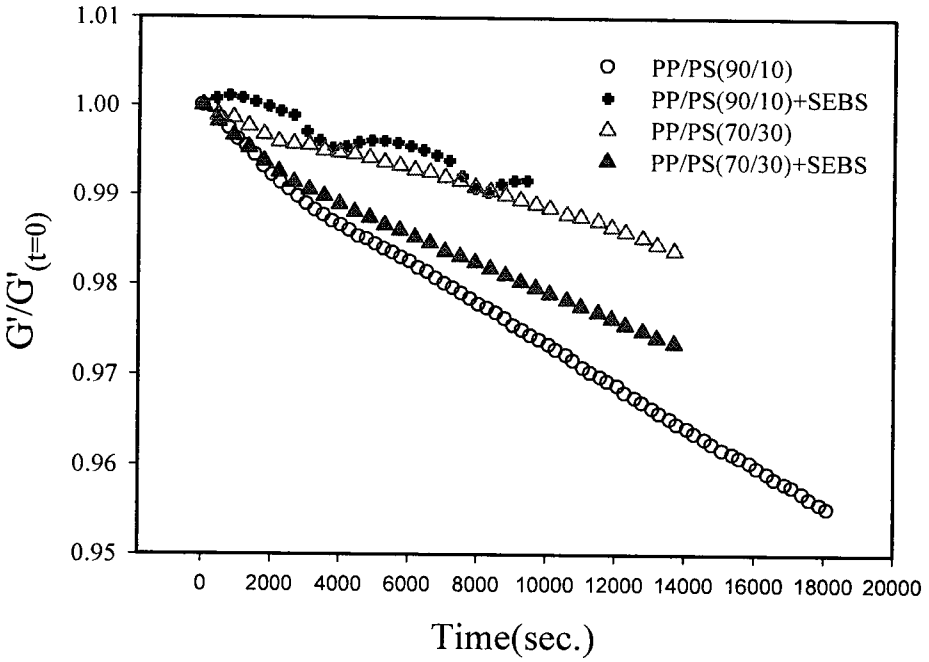

Figure 3.5: Time sweep of normalized storage modulus for compatibilized and non-compatibilized immiscible blends of PP/PS at 200° C

3.2.1.2. Strain Sweep, Determination of LVE Limits

To make sure that SAOS experiments were carried out in LVE regime, strain sweep test were performed to define the magnitude of the strain to be used in experiments over the whole frequency range. In theory, higher strains can be applied at lower frequencies, meaning that the strain magnitude which keeps the material in LVE at higher frequencies would be good enough at lower frequencies. On the other hand, high enough strain (or stress) leads to more accurate data; hence strain sweeps of complex viscosity were done at four frequencies, 100, 10, 1, 0.1 (rad/s.). If the material property is independent of applied strain at the fixed frequency, the applied strain amplitude is in the LVE region. For these reasons, several strain sweeps of storage modulus were performed at different frequencies and the strain amplitude at each frequency decade was assigned. The results of strain sweeps experiments are shown in Figure 3.6.

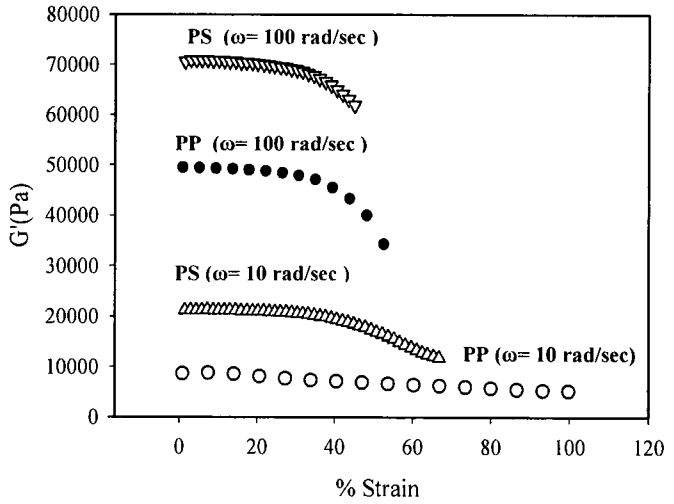

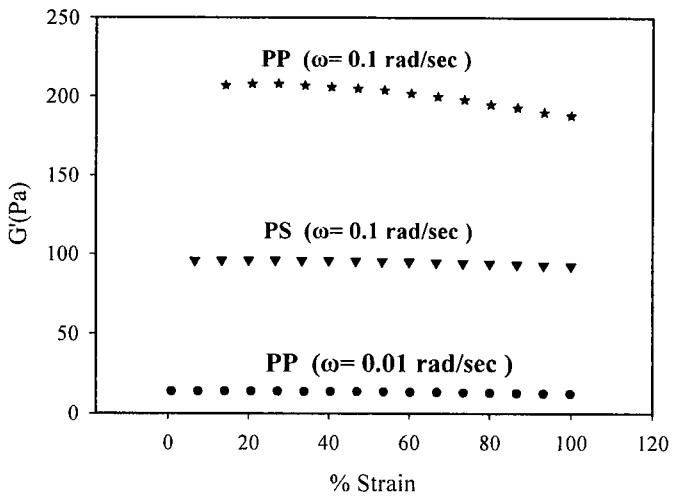

Figure 3.6: Strain sweep of storage modulus of PP and PS at 200° C

To yield precise data, all frequency sweeps were done over four decades and the strain magnitude used in each decade is summarized in Table 3.2.

Table 3.2: Determination of LVE limits for γ used in frequency sweep on pure components at 200° C

Sample	γ magnitude to keep the sample in LVE regime at each frequency decade			
	%γ (100-10 rad/s)	%γ (10-1 rad/s)	% (1-0.1 rad/s)	%γ (0.1-0.01 rad/s)
PP	4	4	4	4
PS	4	4	4	4

More care had to be taken as with the blends, as compared to the pure components, since there might be morphological modifications. Figures 3.7 and 3.8 show the strain sweep results for the blends used in this study. Table 3.3 summarises the strain magnitude used over each decade of frequency.

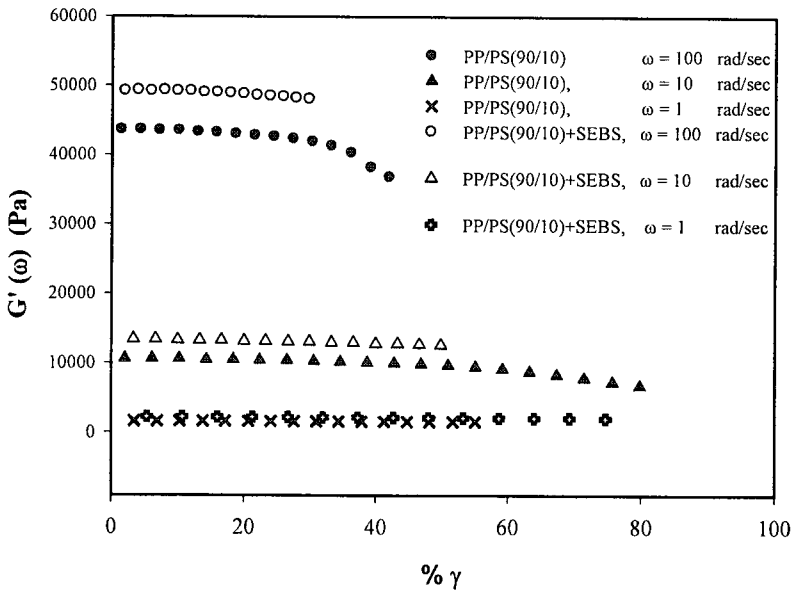

Figure 3.7: Strain sweep of storage modulus of immiscible blends of PP/PS (90/10), compatibilized and uncompatibilized , at 200° C

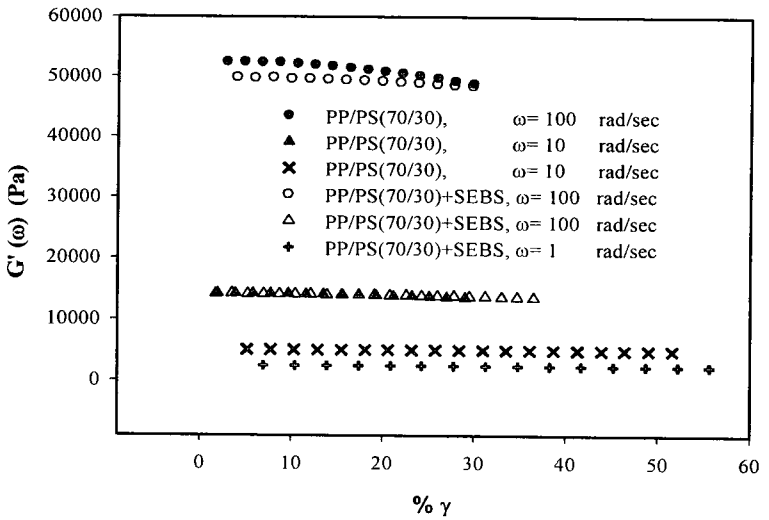

Figure 3.8: Strain sweep of storage modulus of immiscible blends of PP/PS (70/30), compatibilized and non-compatibilized , at 200° C

Table 3.3: Determination of LVE limits for γ used in frequency sweep for blends of PP/PS at 200° C

Blend	γ magnitude to keep the sample in LVE regime at each frequency decade			
	%γ (100-10 rad/s)	%γ (10-1 rad/s)	% (1-0.1 rad/s)	%γ (0.1-0.01 rad/s)
PP/PS(90/10)	2	2	2	2
PP/PS(90/10)+SEBS	3	3	4	4
PP/PS(70/30)	3	3	4	4
PP/PS(70/30)+SEBS	4	4	4	4

3.2.1.3. Frequency Sweep, Determination of LVE Properties of Polymer

Dynamic measurements were performed over four decades of frequency. Frequency sweep tests were carried out at 200° C within the limits defined by previous strain sweeps and the polymer thermal stability. To examine the reproducibility of each experiment, three identical experiments were done at the same testing condition with different samples for each pure material. A standard deviation from average of less than 5% was considered as acceptable for reproducibility. With blends, in which sample-to-sample variation due to morphology is essential, averaging the results of at least five different samples was done.

3.2.2. Steady Measurements (Creep and Creep-recovery Tests)

3.2.2.1. Linear Viscoelastic Response during Creep Test

To have LVE response in a creep test, preliminary creep tests were performed at different stress levels. The behaviour of the polymer is in linear viscoelastic regime if the material function, the creep compliance, is independent of the applied stress. Hence, different creep tests were carried out at different stress levels, and the material behaviour was determined to be linear if all $J(t)$ at different stresses were superposing.

With pure polymers, each creep test at a certain stress level was done on a different sample, and the obtained creep compliance of each sample was compared with other trials. In blends, due to the sample-to-sample morphology variation, the aforementioned method was applied on *the same sample* to determine linear viscoelastic region, and then repeated three times on different samples. (will be discussed in Section 4.2.2.1)

Finally, an optimum stress level was found for each creep experiment on each material. This optimum stress should be small enough to keep the sample in LVE regime, and large enough to yield precise results in the limit of torque resolution.[15]

3.2.2.2. Creep and Creep/recovery of Pure Components

After determination of the appropriate stress level, both creep test only and creep test followed by recovery were performed to find creep the compliance, $J(t)$, within the LVE regime. A creep test followed by recovery was employed in which the creep portion was then re-constructed from recovery information using the Boltzmann superposition principle described in Section 2.3.

3.2.2.3. Establishment of Creep Method for Blends

Because of significant sample-to-sample morphology variation, an experimental protocol was developed for blends in this research. This variation in morphology leads to different values of creep compliance, making it impossible to verify linearity with the usual method. Therefore, the LVE regime was determined on the *same sample*. In this regard, the first creep test was carried out, for the pre-determined creep time, on one sample followed with recovery. As soon as the recovery curve levelled off, implying that the blend system is fully relaxed, another creep experiment was started driven at a higher stress for the same creep time as the first one. This is worth noting that an interval of 15 minutes of rest was considered between two successive creep tests. This procedure was continued at different stresses and an optimum stress level was determined. The results were verified on three samples. At this stage, this is probable that the last deformation

took the sample to nonlinear region. Having determined the stress magnitude for a certain creep time, *increasing creep time* was employed to see the effect of creep time and find out whether or not the very last deformation kept the sample in LVE limit. For this, a creep experiment was performed at the determined stress level and defined time, say t_1, on one sample followed by recovery. When fully relaxed, another creep was run at the same stress magnitude, for longer time $t_2 > t_1$, on the same sample. If both creep compliances superposed, the stress magnitude and creep time, t_1, was established. Finally, five creep experiments were carried out on five samples at established creep parameters. The results and graphs are shown in Section 4.2.2.

3.3. Morphology Analysis

Morphology analyses were done for following purposes:

1- To determine the level of droplet polydispersity

2- To find out the volume average diameter ($\bar{R}_v$) to be used in emulsion models and the determination of relaxation times

3- To examine morphological changes during shearing

In this regard, the samples were quenched *in situ* using liquid nitrogen to ensure that the morphology was captured unchanged, and the droplets were prevented from recoiling from their extended, deformed shape.[53] The cooling rate using liquid nitrogen was about 4.25 $°C/s$ as shown in Figure 3.9. The droplet relaxation processes would be negligible at such high cooling rates.

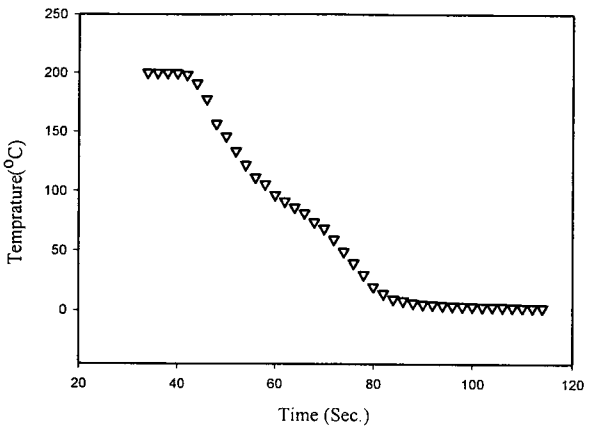

Figure 3.9: Quench rate with liquid nitrogen

As there might be some morphological evolutions/modification due to sample loading, pre-heating[21,60,72], and gap setting in the rheometer, three samples of each experiment were quenched after loading the sample to the rheometer and pre-heating, without shearing. Then, the heating system was turned off, the chamber was opened quickly and the sample was quenched by flashing liquid nitrogen on the sample, while it was between parallel plates. These morphologies were used as a reference to ensure that any change in morphology seen after the experiments is just due to shear. For the morphology evolution studies due to shear, three samples of each type were quenched at the end of the creep experiment, using liquid nitrogen while the sample was still under the applied stress.

After saving the morphology, the samples were broken in liquid nitrogen.[21,53] To see the morphological changes, the samples should be analysed in the flow direction; therefore the samples were broken on a plane whose normal is in the radial direction. Furthermore, in parallel plate geometry, the shear rate is changing from a minimum at the center to a maximum at the edge, meaning that the morphology would vary in the radial

direction. To optimize this effect, the samples were freeze fractured at 3/4 distance of the disk radius from the center.[21] To accent the morphology, fractured blends were etched for 10 hours in cyclohexane which dissolves the PS phase. The developed surfaces were sputtered-coated with a thin layer of gold/palladium alloy and observed with a scanning electron microscope (SEM), model JSM-840. Image analyses were done by SigmaPlot software to determine the polydispersity and volume average radius of the droplets.

3.4. Determination of Relaxation and Retardation Spectra, NLREG Method

The storage and loss moduli, from frequency sweep tests, as well as creep compliance, from creep tests, were converted to relaxation and corresponding retardation spectra using the nonlinear regularization software (NLREG).[7] The NLREG program estimates the relaxation spectrum, and corresponding retardation spectrum, based on the defined mode, minimum and maximum time of relaxation spectrum, and the regularization parameter.

Chapter 4. Results and Discussion

4.1. Pure Polymers

4.1.1. Dynamic Measurements

4.1.1.1. Dynamic Moduli

Three frequency sweeps were carried out on three different PP and PS samples, and the standard deviation was less than 2% for PP and less than 3% for PS. Figure 4.1 illustrates the average complex viscosity, storage and loss moduli vs. frequency over four decades for the pure components at 200° C.

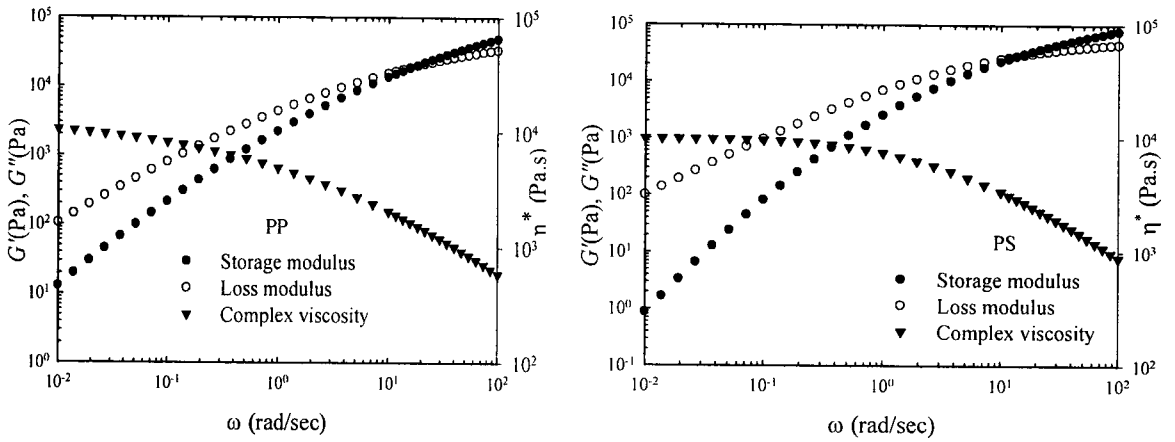

Figure 4.1: Average dynamic moduli and complex viscosity (of three frequency experiments) at 200° C

a) Pure PP b) Pure PS

4.1.1.2. Relaxation and Retardation Spectra from SAOS

The weighted relaxation spectrum and corresponding retardation spectrum were calculated using NLREG software. Figure 4.2 shows the relaxation and retardation spectra for PP. In the relaxation spectrum, one relaxation peak was observed at 2.54 seconds, relating to the time most of the polymer chains relax. To determine the limits over which the spectra are valid, Davies and Anderssen's method[14], shown with vertical lines in Figure 4.2, was employed. In accord to the frequency range in this experiment, minimum and maximum limits of the validity of the spectra were calculated 0.048 and 20.8 seconds respectively.

$$t_{min} = \frac{e^{\pi/2}}{\omega_{max}} = \frac{4.81}{100} = 0.048 \text{ (Sec.)}$$

$$t_{min} = \frac{e^{-\pi/2}}{\omega_{min}} = \frac{0.208}{0.01} = 20.8 \text{ (Sec.)}$$

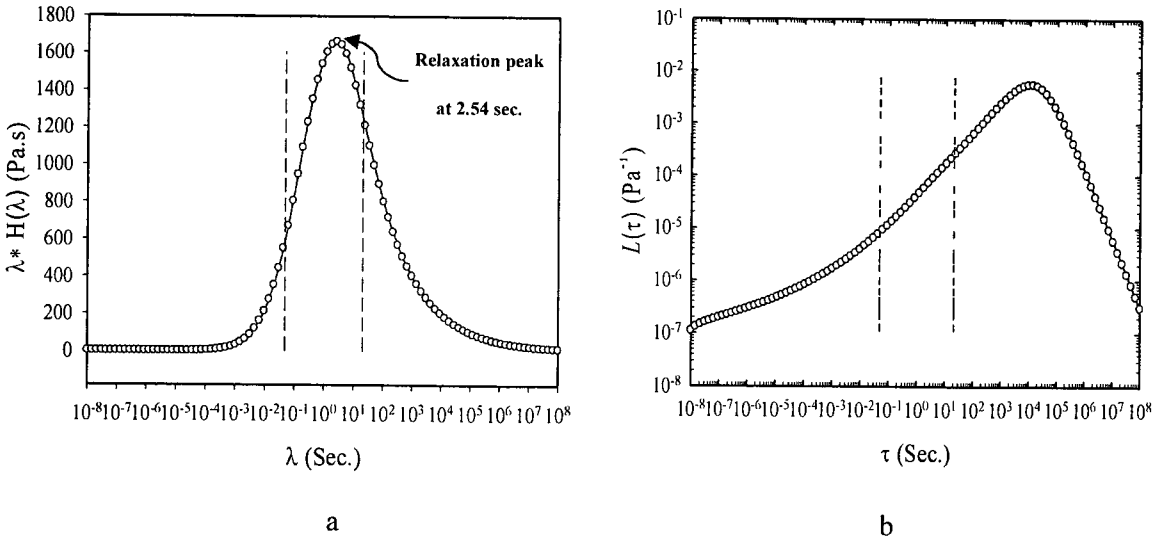

Figure 4.2: a) Weighted relaxation spectrum for neat PP b) Retardation spectrum for neat PP

(Vertical lines show the limits over which the spectra are valid, Temperature = 200° C)

Similarly, the weighted relaxation spectrum of PS obtained with a relaxation peak at 0.53 second is shown in Figure 4.3.

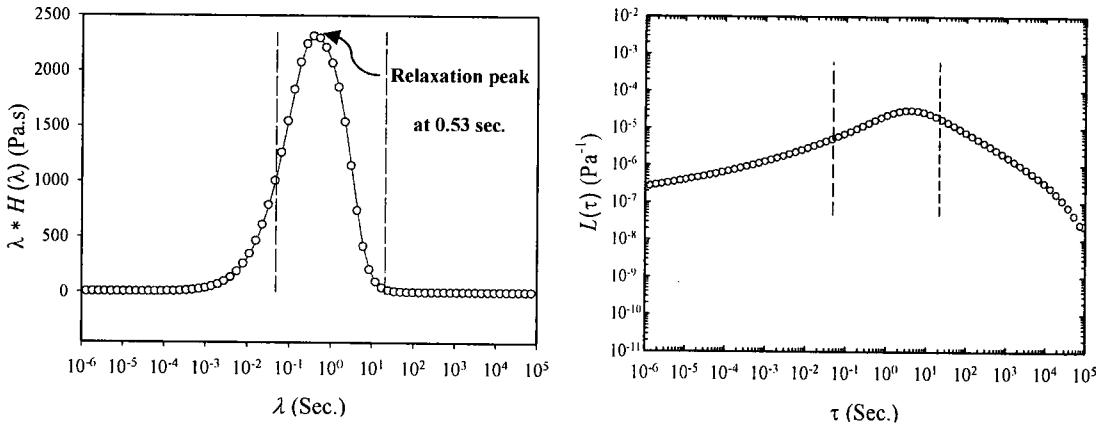

Figure 4.3: a) Weighted relaxation spectrum for neat PS b) Retardation spectrum for neat PS

(Vertical lines show the limits over which the spectra are valid, Temperature = 200° C)

As shown in Figure 4.3, the PS relaxation spectrum gives a peak at 0.53 second, which is too fast to be detected by a creep test.

4.1.2. Steady Measurements

4.1.2.1. Creep/Recovery Experiments

To perform creep tests, preliminary experiments were done to determine the stress level at which the polymer behaviour was linear. For this, compliances corresponding to different stresses should be independent from applied stress. In this regard, four creep tests were carried out on each of four different PP samples at 40, 50, 60 and 100 Pa for 120 seconds and the resulting creep compliances were compared. The creep compliances

superpose up to 120 seconds except for the experiment at 100 Pa that did not superpose at times longer than 100 seconds, demonstrating the nonlinear behaviour of the polymer at experiment times longer than 100 seconds ran at the stress level of 100 Pa. For creep/recovery experiments, a stress magnitude of 50 Pa was chosen for this polymer.

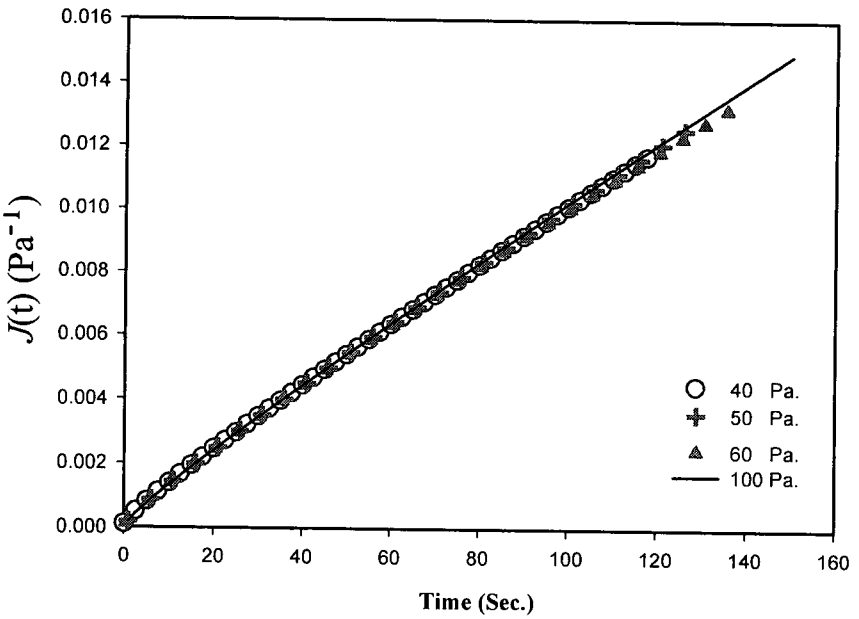

Figure 4.4: Determination of LVE regime in creep test for PP at 200° C

As discussed before, the stress level should be low enough to keep the sample in the linear viscoelastic regime, and high enough to yield precise data. In creep, the amount of deformation depends on the time of shearing; possibly taking the sample into the nonlinear region at long shearing times. Therefore, a method previously used by He *et al.*[15] is employed here which is incomplete creep test followed by recovery. In this method, the creep experiment is stopped before reaching steady state and the strain is recalculated from recovery information, using the *Boltzmann Superposition Principle* [4,5,15,16,18] (also see Section 2.3). Hence, the strain was kept in

the linear viscoelastic limit, yet the creep information for a longer creep experiment was obtained. To find the onset of steady-state in creep, the strain rate vs. time curve at the creeping stress can be plotted.

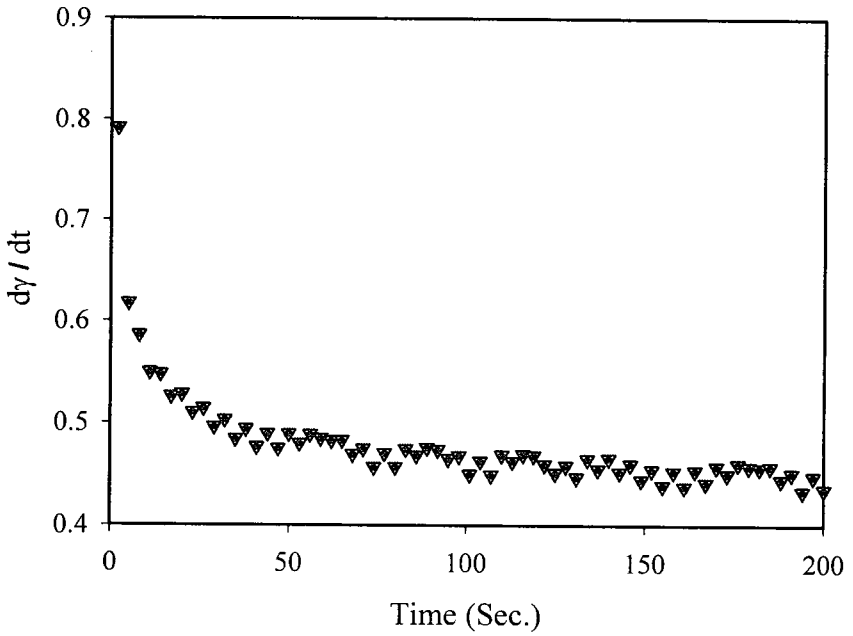

Figure 4.5: Strain rate vs. time for pure PP in the creep test performed at 50 Pa at 200° C

Three creep/recovery experiments were carried out at 50 Pa on three different PP samples. The creep portion was performed for 120 seconds, well before the onset of steady state, while the recovery portion lasted 3700 seconds. The standard deviation was about 2%. The average values of creep and re-constructed strain as well as the creep compliance vs. time for PP sample are shown in Figure 4.6.

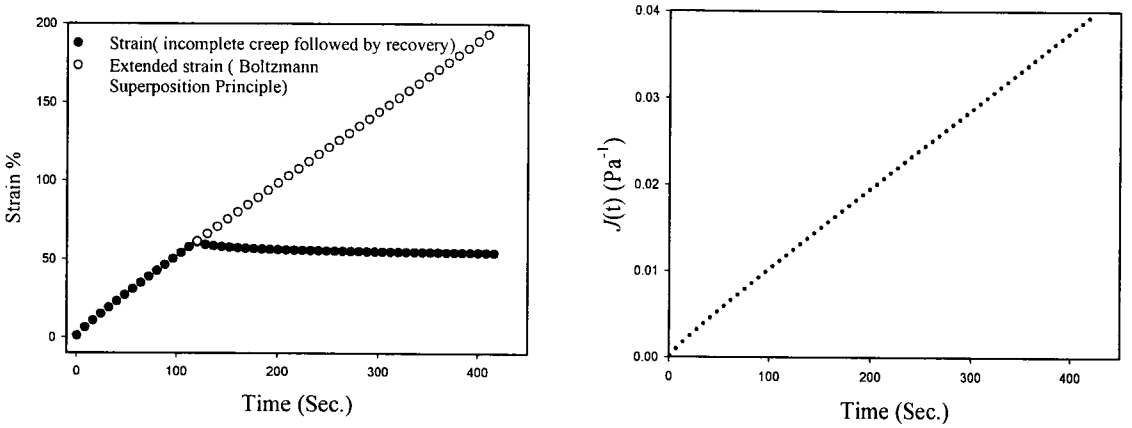

Figure 4.6: a) Creep/ recovery strain and re-calculated strain from recovery information for the PP at 200° C
b) Creep compliance extended from recovery data for the PP

All the aforementioned procedures were also followed with the PS samples. A stress magnitude of 60 Pa was chosen to run creep experiments in the linear viscoelastic region for 50 seconds, well before reaching the steady state, and the experiment was followed by a 4000 second recovery. Five creep/recovery experiments were performed on five different samples and the average values were considered as the overall behaviour of PS samples. Figures 4.7 and 4.8 show the results of LVE determination in creep experiments, determination of the onset of creep steady-state portion, the application of *Boltzmann Superposition Principle* as well as the creep compliance vs. time for PS samples.

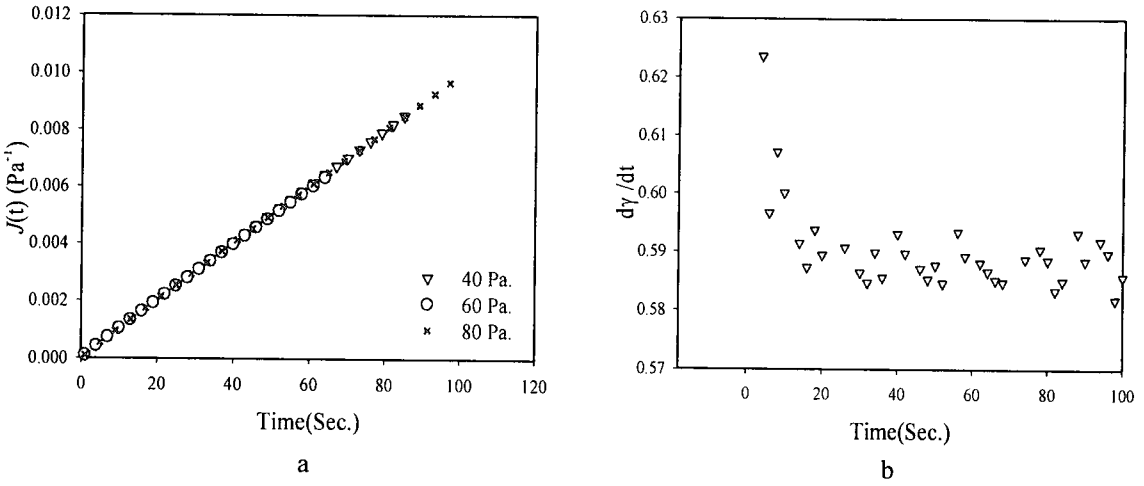

Figure 4.7: a) Determination of LVE regime in creep test for PS at 200° C b) Strain rate vs. time for pure PS in the creep test performed at 60 Pa at 200° C

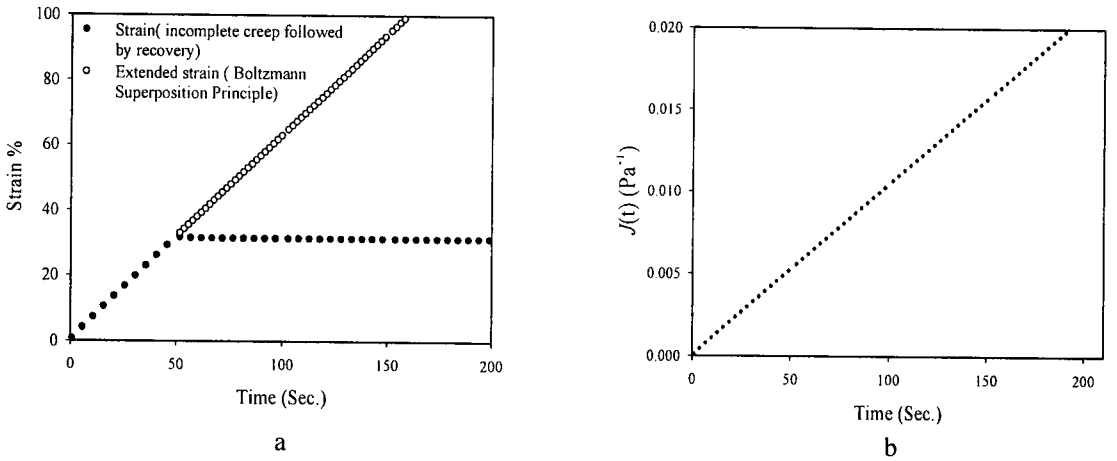

Figure 4.8: a) Creep/recovery strain and recalculated strain from recovery information for PS at 200° C b) Creep compliance extended from recovery data for PS

4.1.2.2. Relaxation and Retardation Spectra from Creep Experiments

The creep compliance obtained from the experiments was then converted to the continuous retardation and corresponding relaxation spectra, using NLREG software. Figure 4.9 illustrates the weighted relaxation spectrum obtained from the creep experiment and compares with that from the SAOS results. It can be seen than the spectra superpose each other at intermediate times, as expected. The SAOS experiments are more accurate at shorter times, while creep tests result in precise data at longer times; therefore, the relaxation spectrum obtained from creep experiment loses accuracy at shorter times and the weighted relaxation spectrum from creep is more reliable after the maximum validity limit of the SAOS.

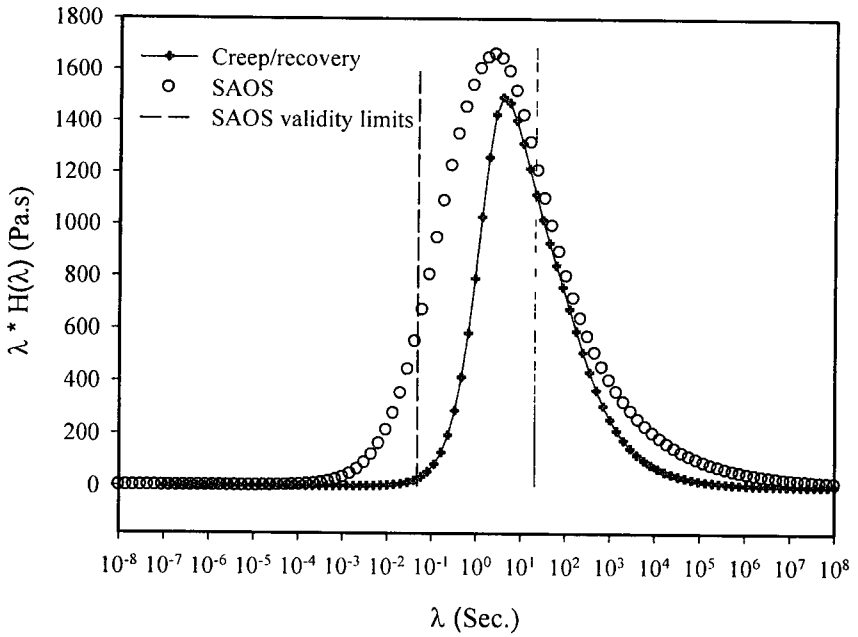

Figure 4.9: Comparison between weighted relaxation spectra for PP obtained from creep/recovery and SAOS tests

To further elaborate, and to demonstrate the long time precision of the creep method in finding the relaxation peak, SAOS as well as incomplete creep followed by recovery were performed on a copolymer of ethylene and octane-1, POP3, which shows a relaxation peak at relatively longer times. Three frequency sweep test were carried out on three different samples with a standard deviation of average less than 1 % at 170° C. The creep experiment was run at 40 Pa for 170 seconds, followed by 3500 seconds recovery. The results of recovery were used to extend the creep compliance using *Boltzmann Super Position Principle*. Finally, the dynamic moduli as well as creep compliance were converted to corresponding relaxation spectra using the NLREG program. Figure 4.10 compares the two relaxation spectra obtained from SAOS and creep/recovery experiments. The SAOS prediction of peak position was 10.7 seconds, while the creep test predicted the relaxation peak at 11.9 seconds. In conclusion, creep experiments are useful to analyze the relaxation behaviour of polymers provided the relaxation mechanisms happen at relatively long times.

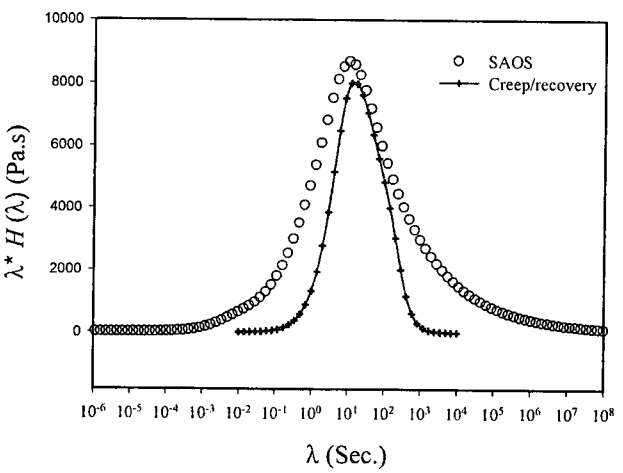

Figure 4.10: Comparison between weighted relaxation spectra for POP3 obtained from creep/recovery and SAOS tests

4.1.3. Combination of Dynamic and Steady Results, Composite Spectrum

As discussed in Section 1.4.1, in the linear viscoelastic regime, short-time mechanisms are more accurately obtained from the SAOS experiments, while long-time processes are more detailed by creep measurements.[5] If one combines the information of both sets, SAOS and creep results, the whole window of polymer behaviour would be accessible.[15,18] He *et al.* extended the experimental window of SAOS test with additional creep test to reach terminal zone of a branched polypropylene with very long relaxation times to determine the zero-shear viscosity.[15] The same method was employed in this work to construct an extended retardation spectrum of PP. In Figure 4.11, the retardation spectrum obtained from SAOS overlaps with that obtained from creep/recovery tests for a considerable time interval. Taking into consideration the valid time range of the SAOS data[14] and the smooth change of the two spectra, a composite retardation spectrum was created (Figure 4.12) whose short-time portion was made of the SAOS information and long-time part was from the creep/recovery information. To combine two retardation spectra, the short-time data from the SAOS experiment were taken up to the point at which both sets of data superpose. Then, the rest of the data were taken from the creep measurements to make the long-time portion of the composite retardation spectrum. One may alternatively combine two retardation spectra from the point of the upper validity time limit of SAOS in the same manner.

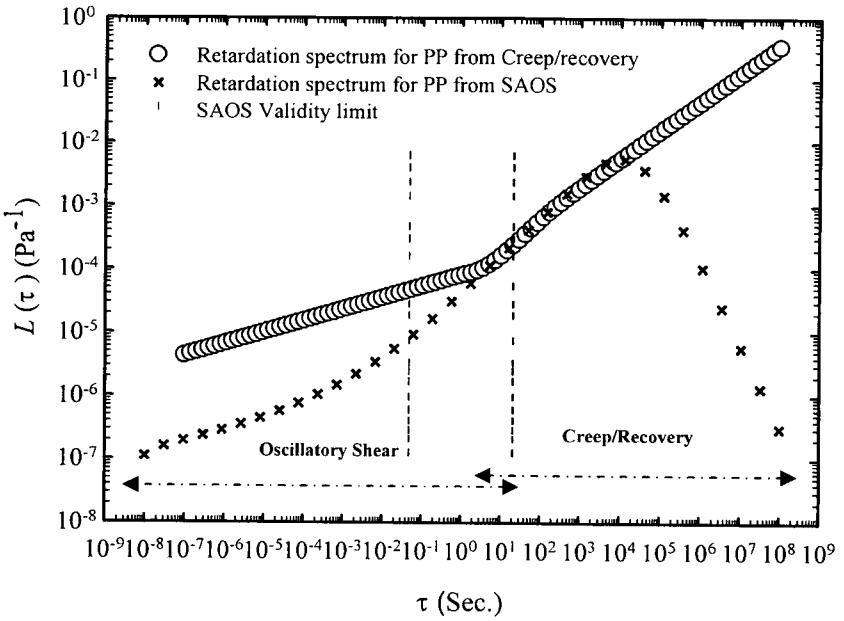

Figure 4.11: Retardation spectra obtained from SAOS and Creep/recovery experiments for PP at 200° C

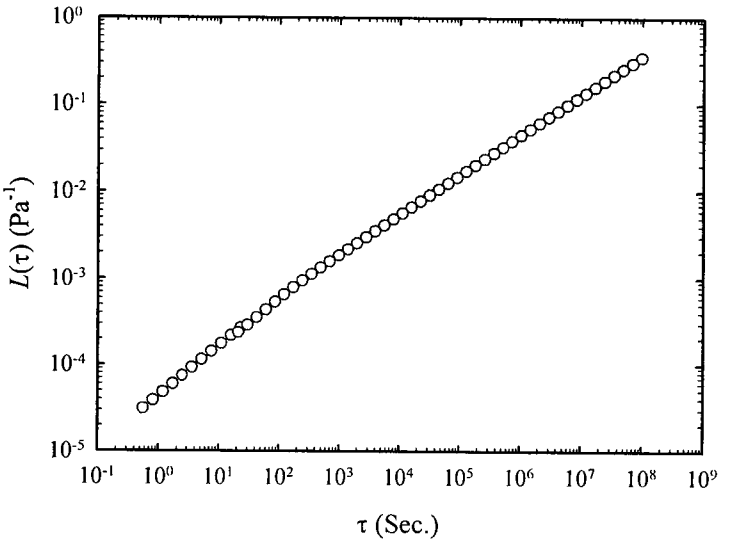

Figure 4.12: Composite retardation spectrum constructed from SAOS data in low frequencies and creep/recovery data at high frequencies for PP at 200° C

The extended retardation spectrum can then be used to calculate other material functions for PP.[5,6,15] Figure 4.13 shows the re-calculation of dynamic moduli for the PP using the obtained composite spectrum.

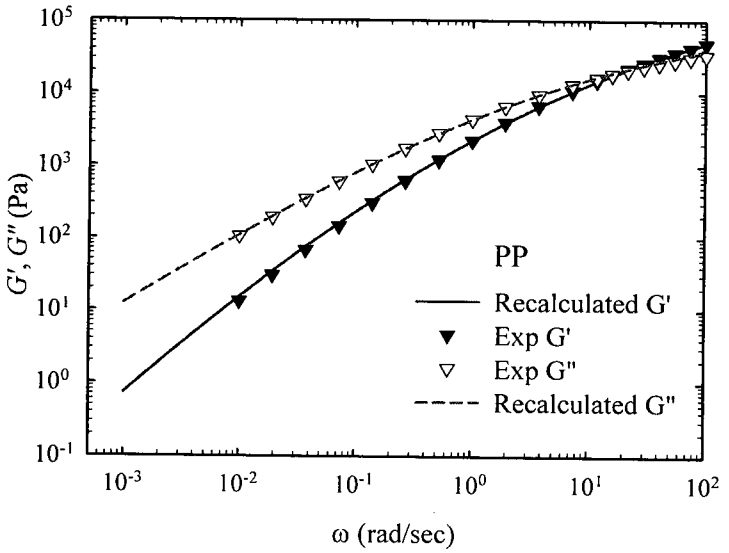

Figure 4.13: Re-calculation of storage and loss moduli from composite spectrum for PP

Since the relaxation processes of the PS occurred at very short times, the retardation spectrum obtained from creep/recovery experiments on PS did not provide any additional information; therefore a composite retardation spectrum for PS is of no use.

4.2. Blends

Morphology and morphological changes during rheological measurements of blends make it more challenging than in the case of the neat components. Care should be taken to keep the blend in LVE region all through the experiments, and avoid morphological modifications. SAOS experiments do not affect the morphology at small enough

strains[22,32,33,34], while steady shearing would cause morphological changes at high stress or long-time deformations[21,31,51,53,70].

The other issue while working with blends is the variation in properties from one sample to another arising from the fact that the morphology of prepared samples is not exactly the same. In other words, samples moulded from the same batch of pellets might have different morphology; therefore the following parameters must be taken into account when dynamic and steady-shear measurements are being compared:

a) the magnitude of the stress

b) creep time or strain magnitude

c) significant sample-to-sample variation

4.2.1. Dynamic Measurements

Having determined the appropriate strain magnitude for each decade of frequency (Table 3.3), frequency sweep tests were performed on at least five different samples of each blend, and the average values of the measured properties were considered to represent the average LVE dynamic behaviour of each blend. Figure 4.14 shows how the SAOS results of the PP/PS(70/30) blend vary from one sample to another.

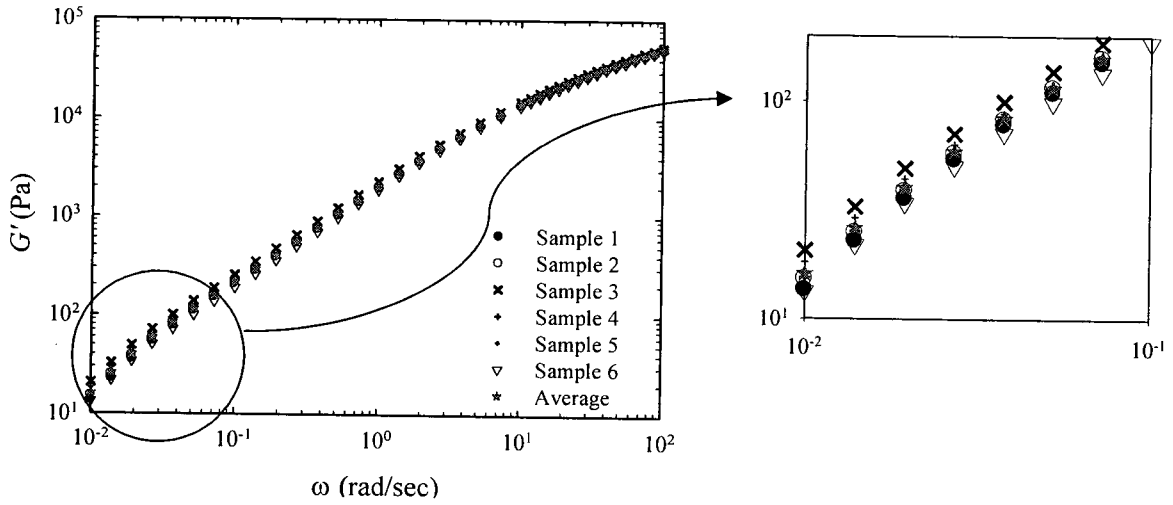

Figure 4.14: Frequency sweep of storage modulus of blend PP/PS(70/30) at 200° C

The standard deviation varies with concentration and compatibilization. Figure 4.15 shows the percentage of standard deviation of the storage modulus for the blends. It can be seen that the sample-to-sample variation is higher in the blends with higher concentration of dispersed phase, since the morphological differences in these blends are more accented.

Also, the effect of the compatibilizer in stabilizing the interface is clearly seen by comparing the percentage of standard deviation of the blends of PP/PS(90/10) and PP/PS(70/30)+SEBS. The standard deviation of the compatibilized blend with higher concentration of droplets is less than that of the uncompatibilized blends with lower percentage of droplets. This is because the addition of the compatibilizer stabilizes the interface between the matrix and drops, resulting in less morphological variations.

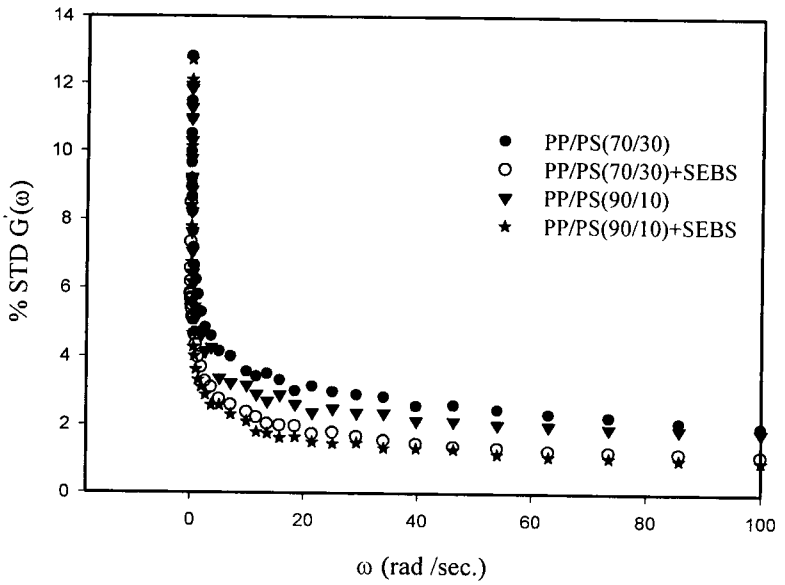

Figure 4.15: Percentage of the standard deviation of the storage modulus for blends

Care should be taken that the properties of neat components of a blend can be compared with those of the blend when the pure component has undergone the same thermo-mechanical history as the blend underwent during blending process. This point is very important as polymers show totally different behaviour under different thermo-mechanical histories. PP demonstrates a lower elasticity, showing itself with lower values of storage modulus, when it undergoes thermo-mechanical processes of blending. The reason is due to the breakage that happens in molecular chains of polypropylene, resulting in less molecular weight, less viscosity and elasticity. On the other hand, some polymers may show higher elasticity after thermo-mechanical steps due to the cross linking of the chains.

Figure 4.16 shows the storage moduli vs. frequency curves of the immiscible blends of PP/PS at different concentrations, compatibilized and non-compatibilized, compared with the pure components.

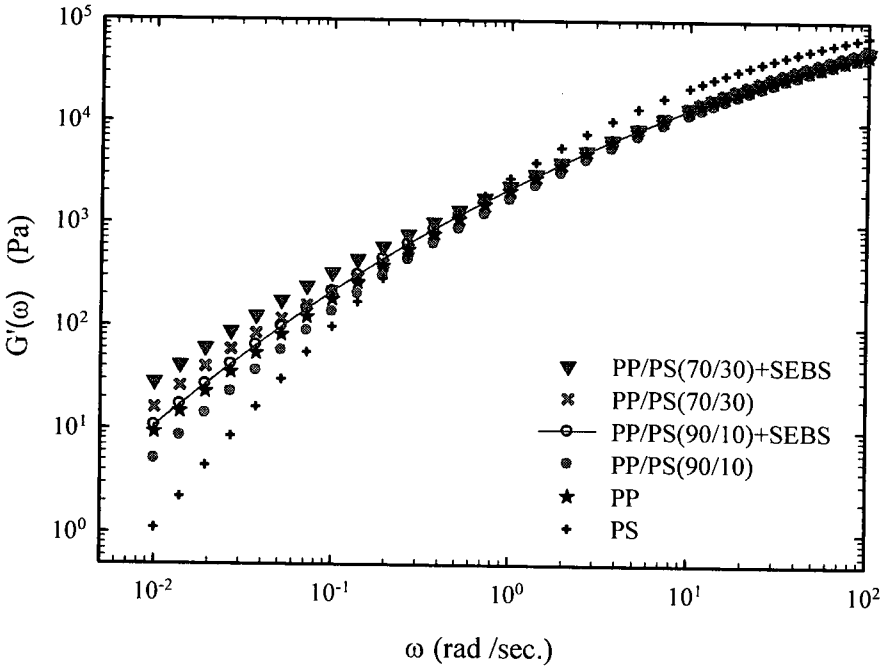

Figure 4.16: Frequency sweep of storage modulus of blends at different concentrations, compatibilized and non-compatibilized, with respect to neat components

The pronounced elasticity at low frequencies, which is a well-known behaviour of immiscible blends due to the long-time relaxation mechanisms[32,35,55], clearly shows itself by an increase in storage modulus for the compatibilized PP/PS(90/10), and the compatibilized and uncompatibilized PP/PS(70/30). In the binary systems, the behaviour of the storage modulus at low frequency implies another relaxation mechanism which is directly related to the interfacial tension, which tends to keep the shape of droplets by elastic forces of the order of $\frac{\alpha}{R}$, opposing the viscous forces of the matrix. The new

mechanism of energy storage in the blended systems is in fact originated from the imposed deformation to the spherical droplets. The deformed droplets tend to reduce the interfacial energy by minimizing the interfacial area or in other words, minimizing the entropy of the system. Compared to the chain relaxation mechanism of the neat component molecules, this mode of relaxation, which is called form (or shape) relaxation mechanism, occurs over a relatively longer period and hence the low frequency data are influenced by the interfacial relaxation phenomenon. Therefore there is a higher G' at low frequencies due to the geometrical relaxation of droplets at longer times when slightly sheared. This can also be explained using Figure 2.6. The first plateau at higher frequencies is related to the time needed for the chains of the matrix to relax and retaining their equilibrium recoil conformations. Once reaching the time for the matrix to relax, λ_M seconds, the matrix relaxes. After long time enough, the interface relaxes at λ_D and the pronounced elasticity is seen.

A negative deviation in elasticity was observed in the PP/PS(90/10) as compared to the pure PP which most likely is due to some mistakes in the blending procedure such as using different grades of pure components or other mixing steps. The storage modulus of the PP/PS(90/10) should be above that of the PP or at least above the simple mixing rule curve. The mixing rule simply predicts the storage modulus of the blend by adding the storage moduli of the neat components that are weighted by their concentrations. Because of this, most of the discussion will be focused on the other three blends.

The effect of droplet concentration and compatibilizer on the storage modulus can be readily inferred from Figure 4.16. The increase in the concentration of second phase results in a higher elasticity at low frequencies. It can be seen that the blend with higher

volume fraction, i.e. PP/PS (70/30) and PP/PS (70/30) + SEBS show higher G' as compared to PP/PS (90/10) and PP/PS (90/10)+SEBS respectively. This can be explained by the fact that the higher concentration of the second phase results in higher number of droplets as well as larger droplet size and so larger interfacial area. Therefore the relaxation process of the droplets becomes longer and causes more elasticity.[32,55,73]

In addition, for each set of blends with the same composition, the compatibilized blend again shows higher storage modulus. The direct effect of the presence of the compatibilizer is a reduction in droplet size leading to the higher number of the droplets and more interfacial area; hence there is a higher elasticity. This can be predicted by Palierne model. Based on Equation (40), the plateau modulus is proportional to the inverse of the radius of the droplets, i.e. $G_p \alpha \frac{\alpha}{R}$ at the constant composition. It is worth noting that the interfacial tension is a property of the interface which is chemically determined; hence it does not depend on the concentration of the blend. Compatibilizers change the chemistry of interface and reduce its tension.

Finally, the increased elasticity is not very evident in the case of the compatibilized PP/PS (90/10). This is due to the low concentration of the PS which imposes less elasticity to the blend and only a shoulder is seen.[32,73]

Figure 4.17 shows the frequency sweep of the complex viscosity for the blends at different concentrations and compatibilization state with respect to the matrix at 200° C.

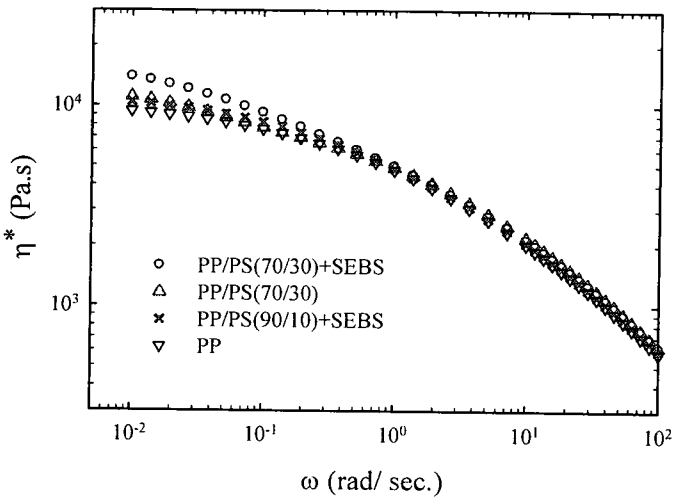

Figure 4.17: Frequency sweep of complex viscosity of blends at different concentrations, compatibilized and non-compatibilized, with respect to the matrix at 200° C

The zero shear viscosity of emulsions is found to be always above that of the matrix.[32] Yee *et al.* showed that the zero shear viscosity increases by adding copolymers to the blends of PMMA/PS and it increases as the concentration of compatibilizer increases.[55] When the copolymer is added to the blend, it gives better adhesion between the pure components due to compatibilizing effect, resulting in higher viscosities.[49] Also, the actual interface between the components increases when the droplets' size decreases, leading to more resistance to viscous flow and consequently higher viscosity.

Furthermore, it can be seen that the viscosity increases with the concentration of the second phase. Bigger droplets with higher concentration of dispersed phase introduce larger area of interface between the components; therefore the interfacial tension increases and produces more resistance against the viscose flows which increases the viscosity.

4.2.2. Steady Measurements in Blends

4.2.2.1. Establishment of Creep Method in Blends

As discussed before, the creep test may take the sample to the nonlinear regime of viscoelasticity. Therefore, several preliminary tests should be done to make sure that the stresses as well as the deformation time are small enough to keep the sample in the linear viscoelastic regime and the material function is independent of the applied stress. On the other hand, morphological modifications are inevitable while shearing blends; hence a minimum stress, large enough to yield accurate results while small enough to prevent morphological changes and passing nonlinear limit, and an appropriate shearing time should be assigned for steady experiments. In addition, sample-to-sample morphology variation, also mentioned in Section 4.2.1, produces some variation from average values and makes it impossible to determine the appropriate stress and shearing time for blends. Figure 4.18 shows the results of eight creep tests, each done on a different sample, at a stress of 5 Pa for 100 seconds on the PP/PS(90/10).

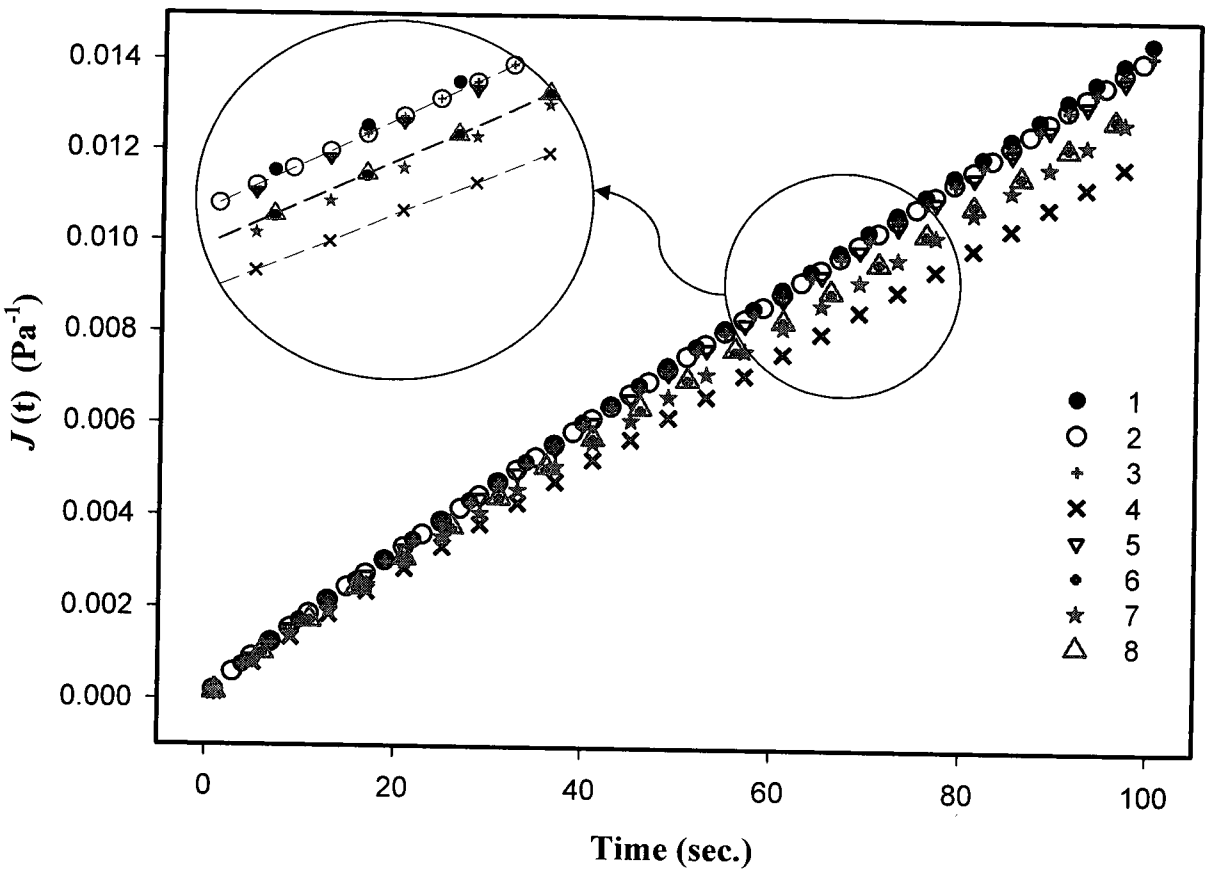

Figure 4.18: Creep compliance vs. time, at the stress of 5 Pa for 100 (sec.) on the PP/PS(90/10) at 200° C

Obviously, the compliance function varies significantly from one sample to another one. The probable reasons for such behaviour are:

1- Exceeding the limits of linearity

2- Morphology modifications such as coalescence and break-up which eventually changed the properties of the blend

3- Sample-to-sample variation of morphology

The stress in these creep experiments was carefully chosen to be small and applied for a short enough time to avoid entering nonlinear regime. Also the fact that the results are organizing into different clusters reinforces the idea that this variation is not related to nonlinear behaviour. To ensure that this behaviour is not related to nonlinearity, the sample-to-sample variable was removed and determination of linear viscoelastic regime was performed on *the same sample,* i.e. the first creep experiment was carried out on one sample, following another creep test run on the same sample at different stress while the appropriate relaxation time was allocated between two successive tests. This procedure was then repeated on different samples.

Figure 4.19 shows the results of successive creep experiments on *the same sample* for uncompatibilized PP/PS(90/10).

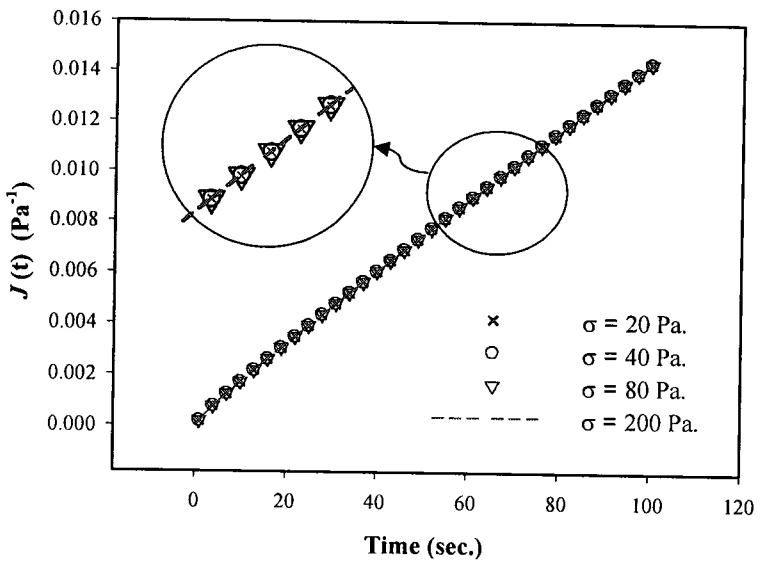

Figure 4.19: Successive creep experiments on *the same sample* for 100 (sec.), PP/PS(90/10) at 200° C (Specimen 1)

Clearly, by omitting the sample-to-sample variations, the creep compliance at different stresses superpose, indicating that the previous variation in properties was due to the variation of morphology in different samples. Furthermore, this *on the same sample* approach is the only possible method to determine the appropriate stress for creep experiments. These results were verified with two more PP/PS(90/10) samples as shown in Figure 4.20.

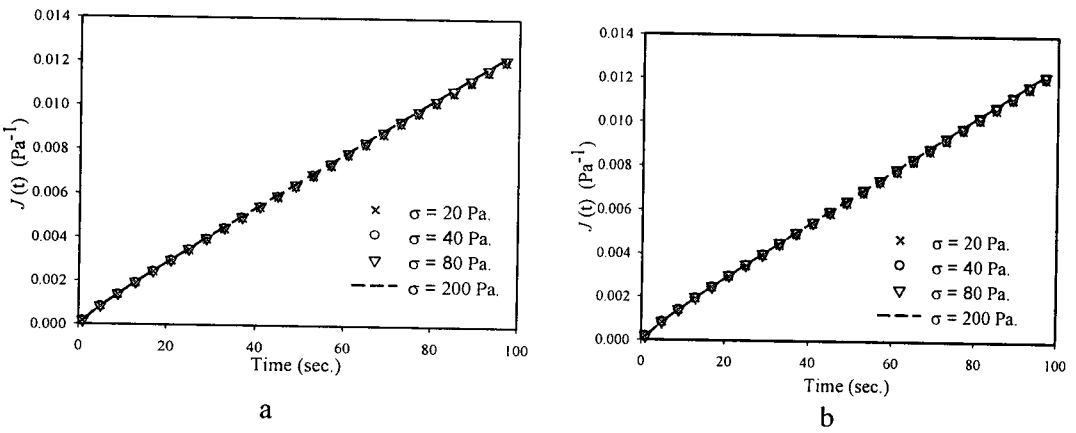

Figure 4.20: Successive creep experiments on *the same sample* for 100 (sec.) at 200° C
a) PP/PS(90/10), Specimen 2 b) PP/PS(90/10), Specimen 3

To examine the effect of higher magnitudes of stress, the same method was employed again. Figure 4.21 shows the results of five creep tests done for 100 seconds on one sample of PP/PS (90/10). As before, an appropriate relaxation time was allotted between each creep experiment.

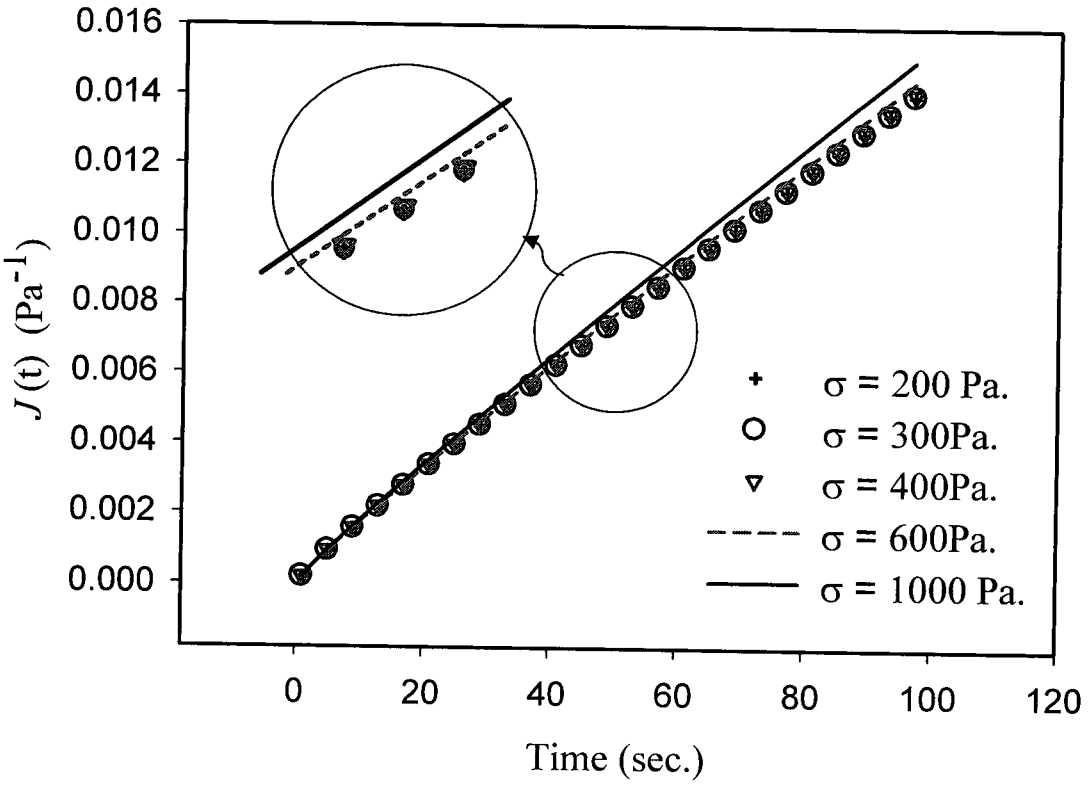

Figure 4.21: Successive creep experiments on *the same sample* for 100 (sec.) at 200° C
Sample: PP/PS(90/10)

From the results we can say that stresses up to 400 Pa kept the sample in the linear viscoelastic limit, whereas the sample was taken into nonlinear regime at a stress of 600 Pa and above. When entering the nonlinear region, the viscosity of polymers usually decreases leading to higher values of strain (at constant applied stress) and consequently higher values of creep compliance as shown in Figure 4.21.

The amount of morphological modification is not only dependent on the stress magnitude, but also is a function of shearing time; therefore the effect of the time of deformation must be examined once the magnitude of the stress is chosen for the creep experiment. Figure 4.22 shows the results of six successive creep experiments ran at 40

Pa for different shearing time on *the same sample*. To make sure that the experiment time keeps the blend in the linear viscoelastic zone, the creep compliance in the longer experiment must superpose with that of a shorter experiment.

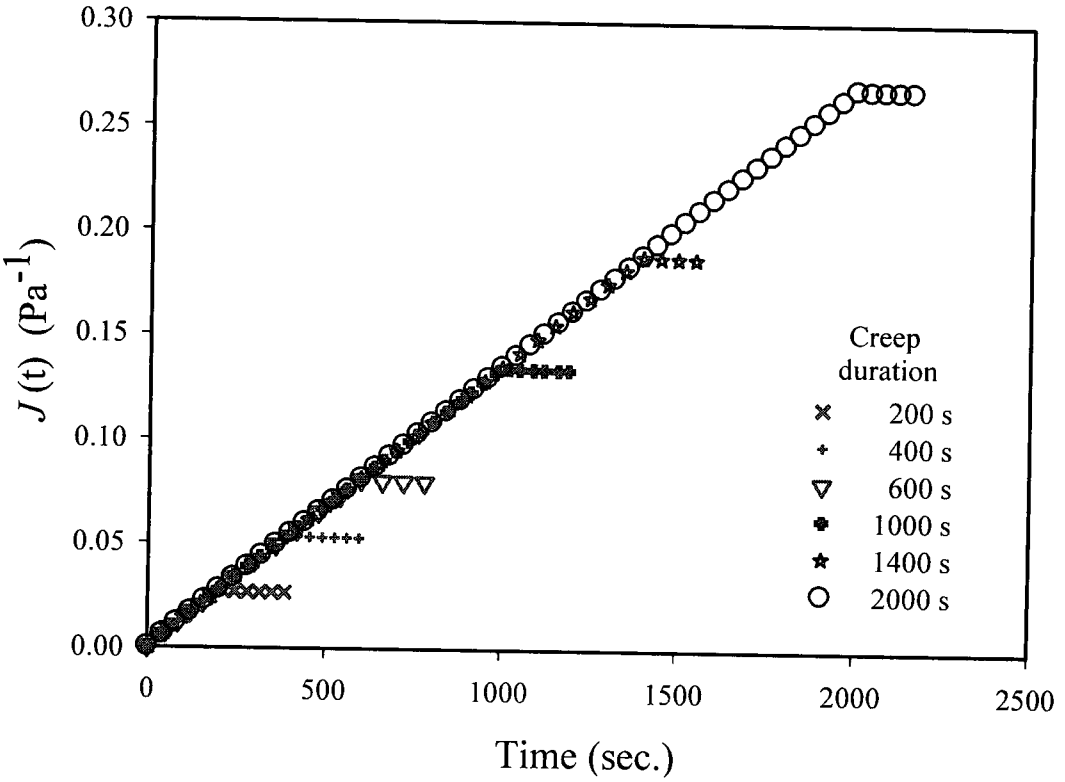

Figure 4.22: Creep compliance vs. time for different creep duration, successive creep experiments on *the same sample,* σ =40 (Pa) at 200° C, Sample: PP/PS (90/10)

Although the creep compliances in different creep experiments (and different experiment times) superpose, there is a certain morphology (and so property) modification as we will see later; hence the application of incomplete creep experiment followed by recovery and re-construction of creep compliance from recovery information will minimize this effect.

Eventually, after the selection of the creep stress and deformation time regarding the linear viscoelastic limits, five incomplete creep experiments followed by recovery were carried out on five different samples and the average values were taken to represent the overall behaviour of the blend.

4.2.2.2. Creep/Recovery Experiments in Blends

Preliminary tests were carried out to find out the limits of linear viscoelastic behaviour for the different blends. Figure 4.23 shows the results of the creep experiment on *the same sample* for three PP/PS(90/10) + SEBS samples ran at different stresses for 3000 seconds. It can be seen that the percentage of the difference between the two creep experiments for samples 1 and 2 which were tested at relatively low stresses was within 1.5 %, while it increases up to 2.5 % for sample 3 which was tested at higher stresses. A stress of 30 Pa was assigned for the further creep experiments on the compatibilized PP/PS(90/10) blends.

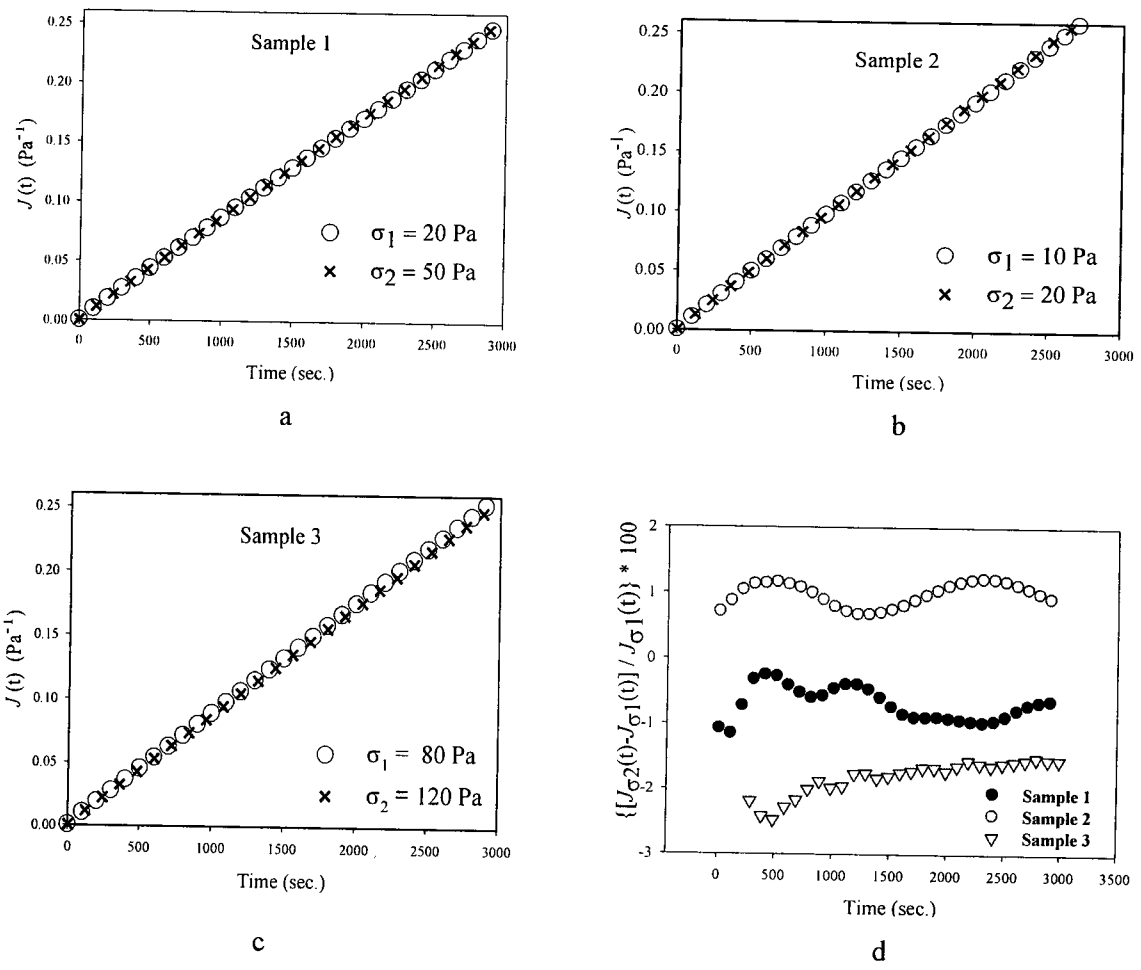

Figure 4.23: Successive creep experiments on *the same sample* for 3000 seconds, PP/PS(90/10)+SEBS at 200° C a) Specimen 1, two stress levels of 20 and 50 Pa, b) Specimen 2, two stress levels of 10 and 20 Pa, c) Specimen 3, two stress levels of 80 and 120 Pa, d) % variation of creep compliance in each experiment

The same experiments were repeated using incomplete creep followed by recovery and it was found that the best superposition, in creep compliances of successive creep experiments on *the same sample* was obtained when the incomplete creep test was performed for 200 seconds followed by recovery for 2800 seconds. A difference of 0.5 % between two successive creep experiments occurred in this case. This difference was reasonable in experimental errors as it can be attributed to viscosity changes already seen

in the time-sweep tests. In addition, the variation in the values of creep compliance was smoother as shown in Figure 4.23(d). Figure 4.24 and 4.25 show the results of the creep/recovery experiments.

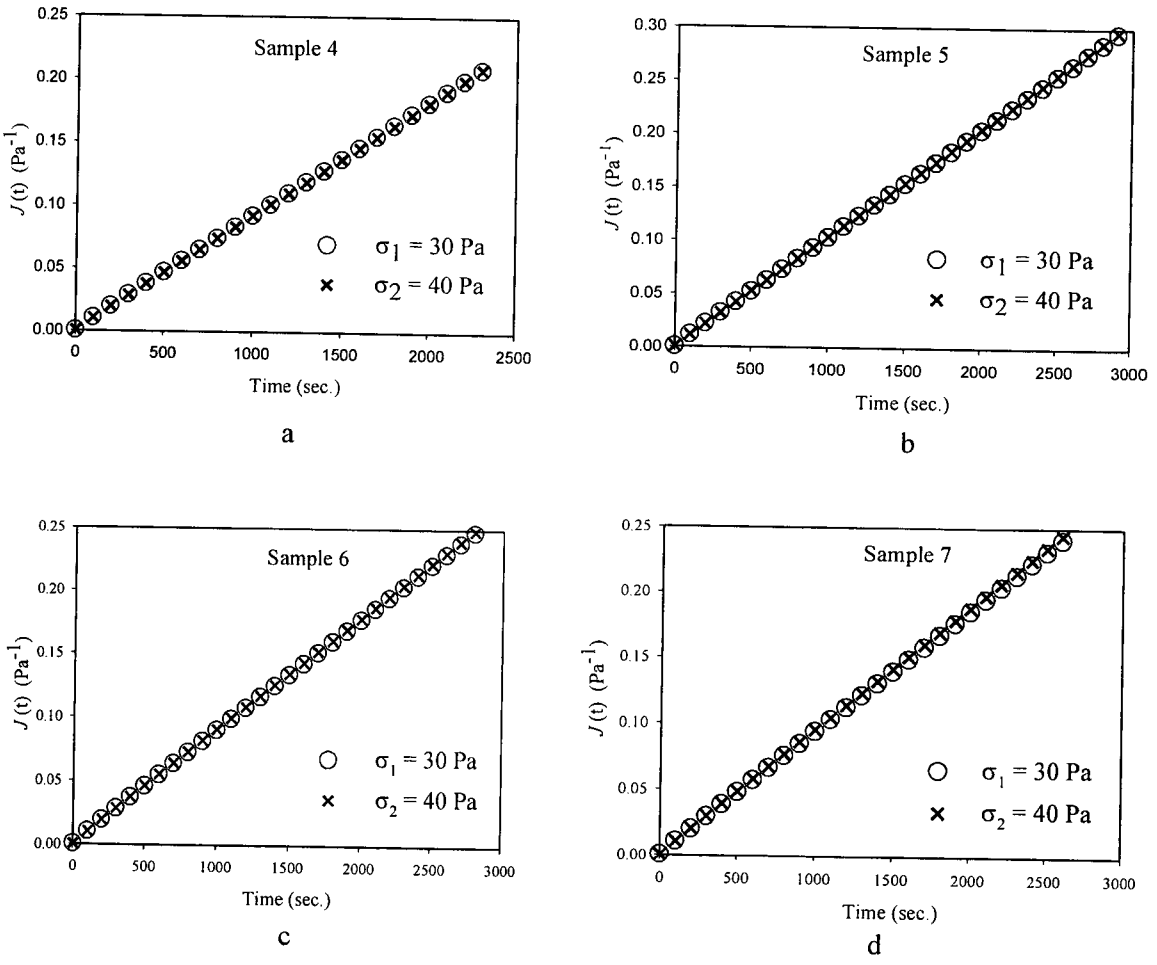

Figure 4.24: Successive incomplete creep followed by recovery experiments on *the same sample,* for PP/PS(90/10)+SEBS at 200° C, a) Creep: 1400 sec., recovery: 1000 sec, b) Creep: 500 sec, recovery: 2500 sec, c) Creep: 200 sec, recovery: 2800 sec, d) Creep: 100 sec, recovery: 2900 sec

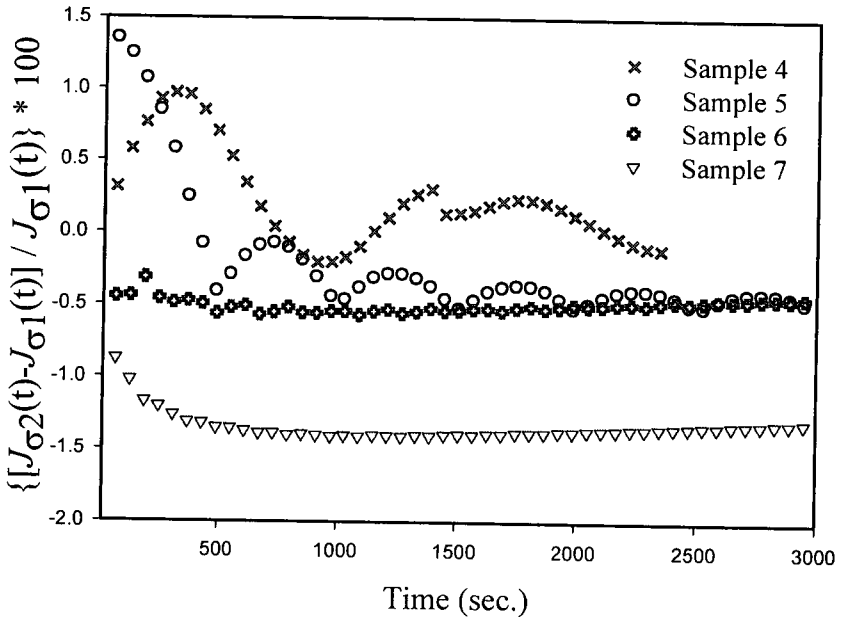

Figure 4.25: % variation of creep compliance in successive incomplete creep followed by recovery experiments on *the same sample,* for PP/PS(90/10)+SEBS at 200° C

Five incomplete creep experiments followed by recovery were then carried out on five samples of PP/PS(90/10)+SEBS. The creep portion was run at 30 Pa for 200 seconds followed by 2800 seconds recovery. The strain values obtained from recovery were then used to calculate the values of creep strain and extend the creep compliance curve up to 3000 seconds as shown in Figure 4.26.

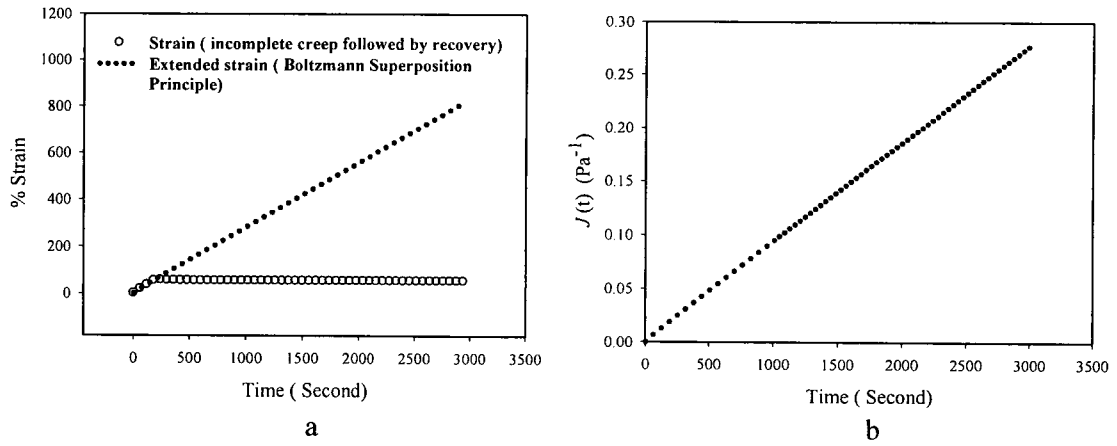

Figure 4.26: a) Extension of strain by using Boltzmann Superposition Principle, PP/PS(90/10)+SEBS (σ = 30 Pa, Creep: 200 sec., recovery: 2800 sec) at 200° C, b) Creep compliance vs. time, PP/PS(90/10)+SEBS (σ = 30 Pa) at 200° C

Similarly, the stress level to keep PP/PS(70/30)+ SEBS blends in the linear viscoelastic region was determined. Successive creep experiments were performed *on the same sample* for 200 seconds with appropriate relaxation time between each test. In addition, a longer creep test was also done on *the same sample* to make sure that the last experiment did not take the sample into nonlinear viscoelasticity within a difference of 0.5 % and 1.5 % for samples 1 and 2 respectively. A stress of σ = 15 Pa was chosen to perform the creep portion for 200 seconds and followed by 3800 seconds of recovery. Five creep/recovery experiments were done on five different samples and the average value was taken to be representative of the overall behaviour of PP/PS(70/30)+SEBS. Figure 4.27 shows the linear viscoelastic regime determination as well as the final creep compliance of compatibilized PP/PS(70/30) for 4000 seconds.

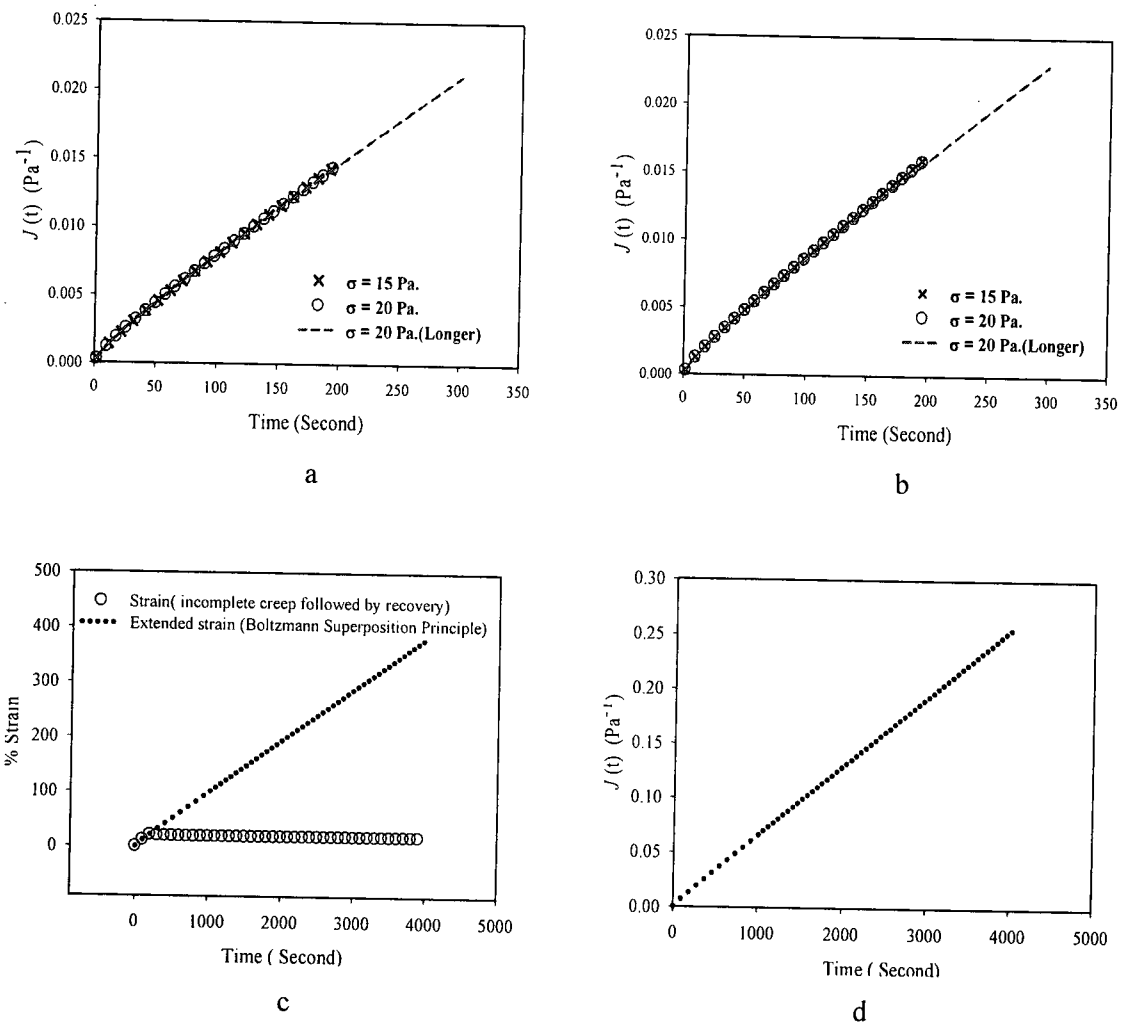

Figure 4.27: LVE determination and creep results for PP/PS(70/30)+SEBS at 200° C, a) LVE determination on *the same sample* (Specimen 1), b) LVE determination *on the same sample* (Specimen 2), c) Extension of strain by using B.S.P (σ = 15 Pa, Creep: 200 sec, recovery: 2800 sec), d) Creep compliance vs. time (σ = 15 Pa)

The same method was also employed for uncompatibilized PP/PS (90/10) and PP/PS (70/30) and the results are shown in Figures 4.28 to 4.30.

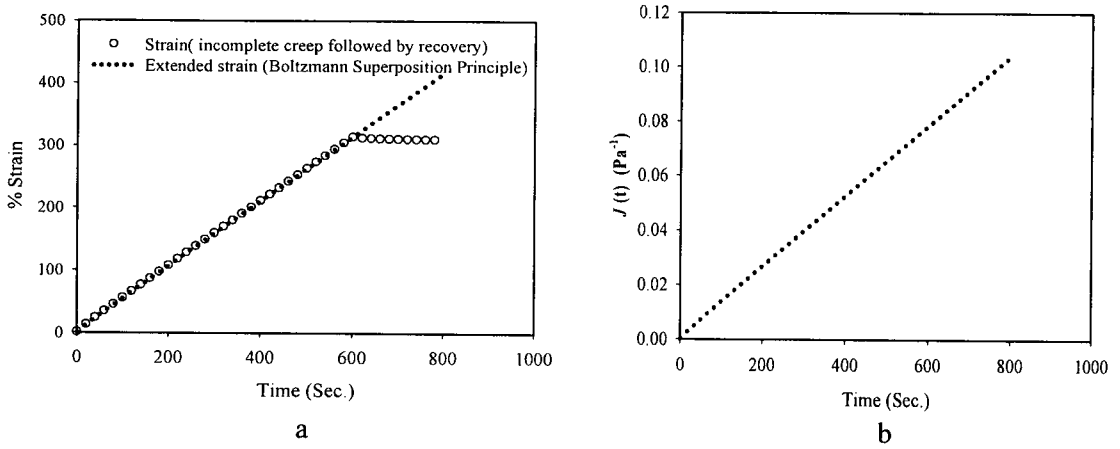

Figure 4.28: a) Extension of strain by using Boltzmann Superposition Principle, PP/PS(90/10) [σ = 40 Pa, Creep: 600 sec, recovery: 200 sec] at 200° C, b) Creep compliance vs. time, PP/PS(90/10) [σ = 40 Pa] at 200° C

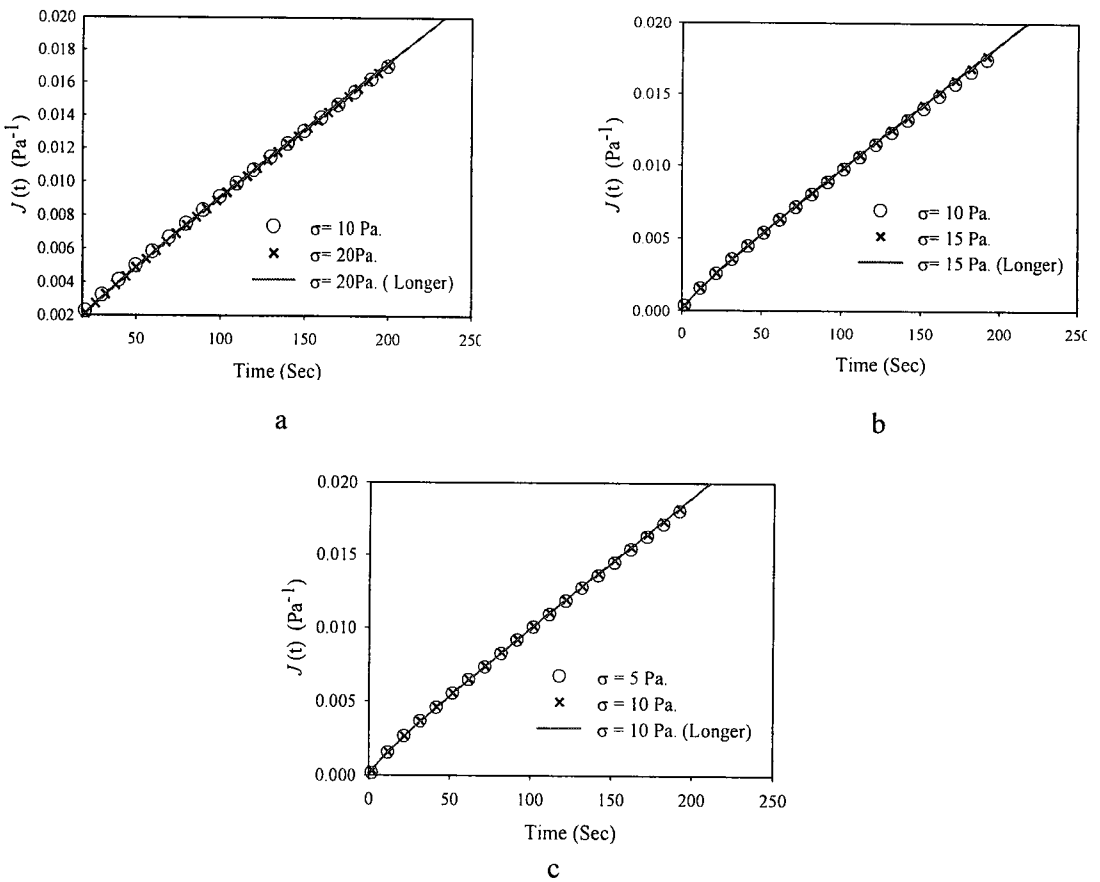

Figure 4.29: LVE determination for PP/PS(70/30) at 200° C, a) LVE determination on *the same sample*, (Specimen 1), b) LVE determination *on the same sample* (Specimen 2), c) LVE determination *on the same sample* (Specimen 3)

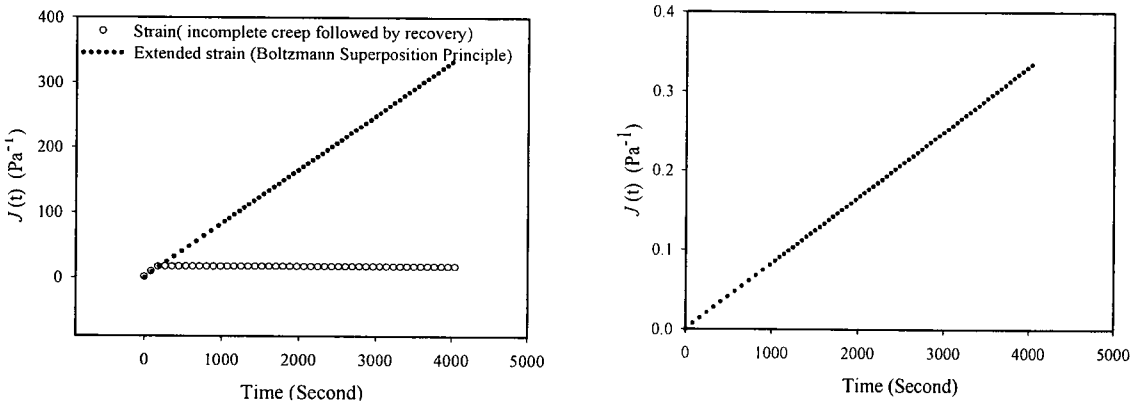

Figure 4.30: a) Extension of strain by using Boltzmann Superposition Principle, PP/PS(70/30) [σ = 10 Pa, Creep: 200 sec., recovery: 2800 sec] at 200° C, b) Creep compliance vs. time, PP/PS(70/30) [σ = 10 Pa] at 200° C

4.2.3. Morphological Investigations

As mentioned before, all samples were pre-heated for 10 minutes before running each experiment.[18,21,60,72]. During thermal annealing, coalescence occurs even at static conditions before oscillation or shearing. This thermal coalescence should be considered in the model. In other words, all dynamic and steady results obtained from the rheometer are related to the blend equilibrium morphology after being annealed sufficiently long enough at elevated temperature since the initial morphology before each experiment is very important. Lacroix *et al.*[72] showed that the droplet size in blends of polyethylene terephthalate glycol/polyester-ethylene vinylacetate rapidly increased at high temperature and reached its equilibrium size after 5 minutes. They emphasized that there is a certain time of annealing, depending on the temperature and blend composition, beyond which no significant morphological changes happen. Martin *et al.*[21] pre-heated the blends of

80/20 PS/HDPE between rheometer parallel plates for 10 minutes at 200° C. Thermal coalescence is even more crucial in steady experiments to make sure that any observed morphological modifications are due to shearing. Three samples of each blend, before and after annealing, were freeze broken (as explained in Section 3.3), then best images, representing the actual sample morphology, were analyzed and the volume average radius of each blend was calculated within experimental errors. Figure 4.31 and 4.32 show the morphology of the blends of PP/PS, before and after pre-heating.

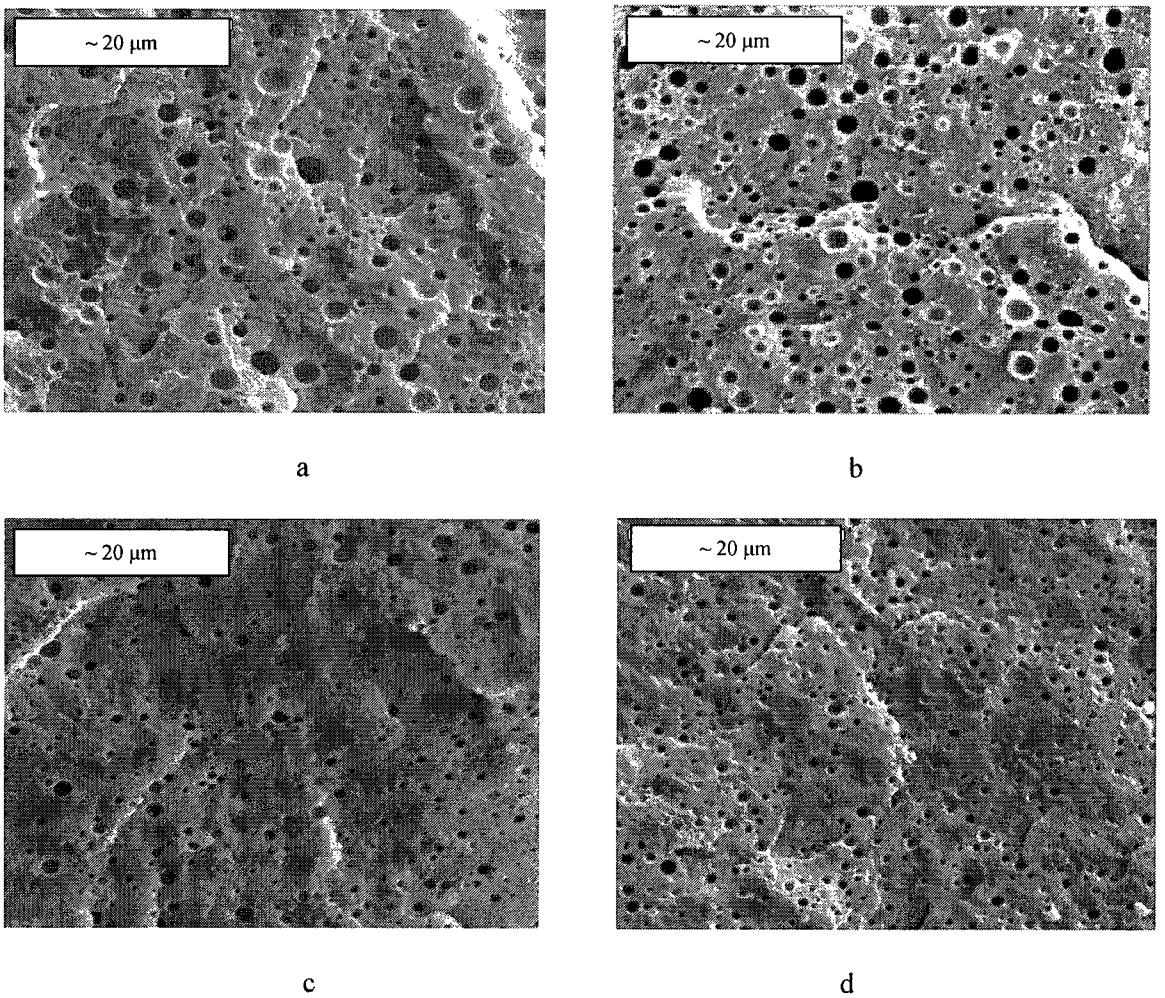

Figure 4.31: a) PP/PS(90/10), moulded b) PP/PS(90/10), pre-heated for 10 minutes at 200° C c) PP/PS(90/10)+ SEBS, moulded d) PP/PS(90/10)+SEBS, pre-heated for 10 minutes at 200° C

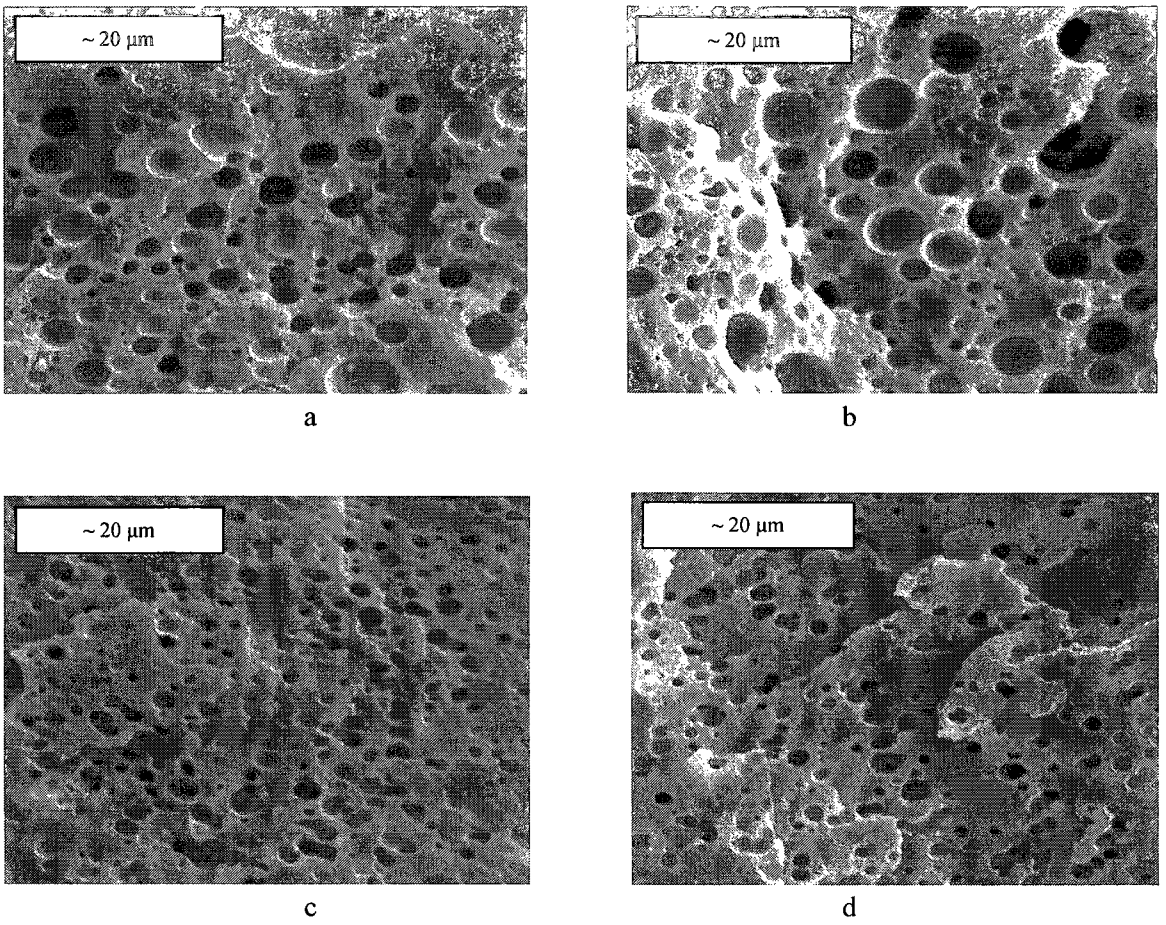

Figure 4.32: a) PP/PS(70/30), just moulded, b) PP/PS(70/30), pre-heated for 10 minutes at 200° C, c) PP/PS(70/30)+SEBS, just moulded d) PP/PS(70/30)+SEBS, pre-heated for 10 minutes at 200° C

With no doubt, the droplet size was smaller in the compatibilized blends regardless of the blend's composition, yet it seems that the effect of compatibilizer, at the same percentage of added copolymer, was more significant with the PP/PS (90/10) samples than with the 70/30 samples. In addition, the morphology changes during annealing were more significant in uncompatibilized PP/PS(70/30) in terms of a significant increase in the coalescence of droplets[68,74]. Table 4.1 shows the volume average diameter of the 70/30 blends before and after annealing.

Table 4.1: Morphological changes during annealing in 70/30 blends

Blend	$\bar{R}_v$ (μm) (Before annealing)	$\bar{R}_v$ (μm) (After annealing)
PP/PS(70/30)	3.34 ± 1	6.38 ± 0.8
PP/PS(70/30)+SEBS	2.9 ± 0.8	2.3 ± 0.8

Two mechanisms are considered for coalescence of the blends:

a) the probability of droplets to collide

b) the ability of the blend to drain the matrix layer between two drops until the coalescence occur. The collision probability depends upon the size of droplets and is higher at blends with larger droplet size.[73,75] The volume average diameter was changed from 3.34 to 6.38 μm for the uncompatibilized PP/PS(70/30) due to thermal coalescence before shearing. In the case of compatibilized PP/PS(70/30), no significant coalescence happened due to the compatibilized small droplets which inhibited the coalescence.

It is worth mentioning that the smaller $\bar{R}_v$ which is reported for the compatibilized PP/PS(70/30) after annealing in Table 4.1 is due to a considerably inhomogeneity of the morphology in the blends. Because of this variability, it was likely to have clusters of small or large droplets in one image. Despite this fact, the effect of this inhomogeneity was completely negligible whenever there was coalescence as in the annealing of the PP/PS(70/30) or the effect of shearing which will be explained at the end of Section 4.2.5.

4.2.4. Relaxation Spectra and Modeling in Blends

4.2.4.1. Relaxation Spectra from SAOS and Palierne Model

Graebling *et al.*[32] introduced the use of Cole-Cole diagrams (η''vs. η') to estimate the number of expected relaxation peaks from SAOS experiments. Figure 4.33 shows the Cole-Cole diagrams for the blends.

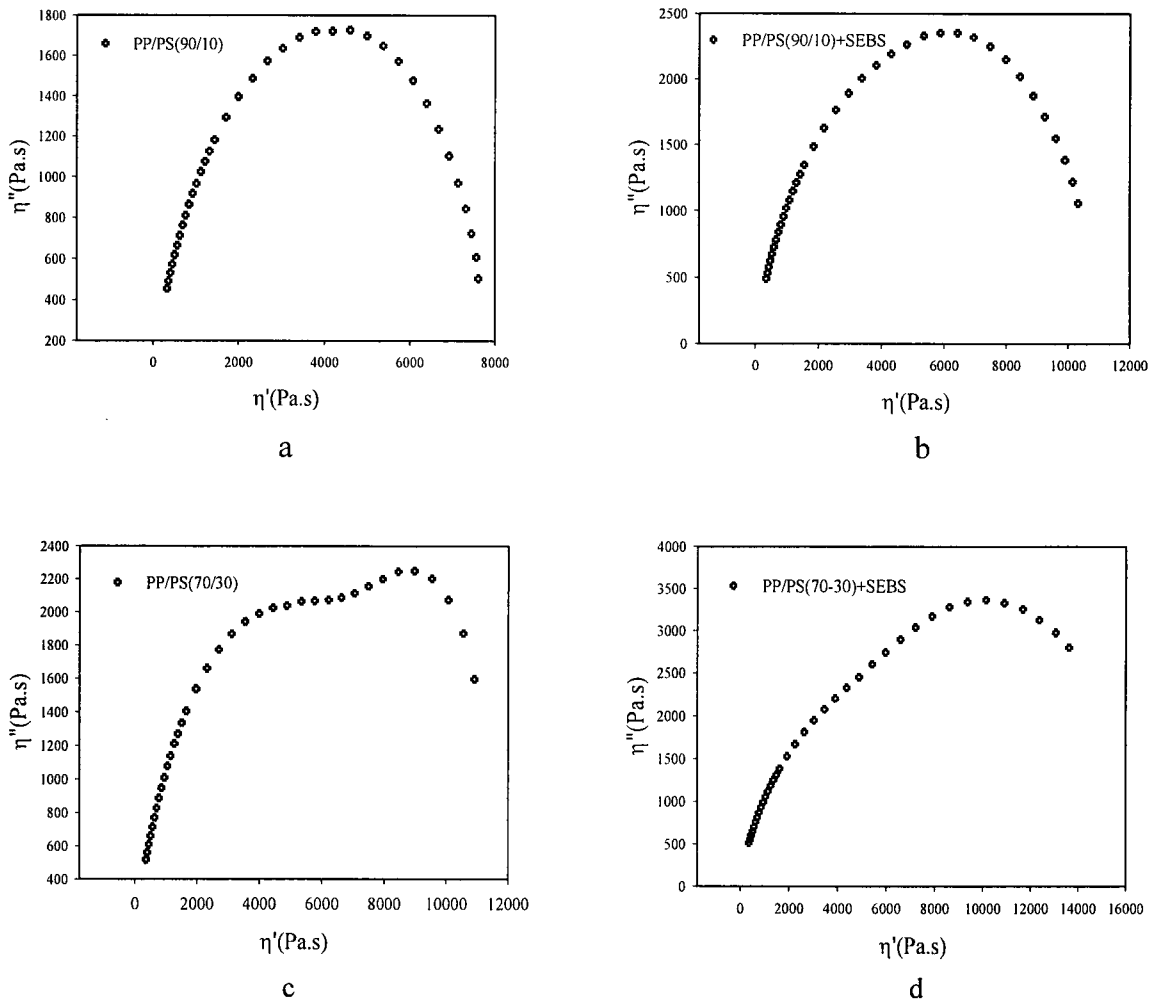

Figure 4.33: Colo-Cole diagrams: a) PP/PS(90/10), b) PP/PS(90/10)+SEBS, c) PP/PS(70/30), d) PP/PS(70/30)+SEBS

The diagrams of the blends with 10% of the second phase only predict one relaxation peak in their weighted relaxation spectra. It means that the interface relaxation time might be merged with those of pure components or at least show itself only as a shoulder. The Cole-Cole diagram predicts two separate peaks for PP/PS(70/30) blend, while it shows a shoulder for PP/PS(70/30)+SEBS.

The dynamic data obtained from small-amplitude oscillatory shear experiments were used to construct the relaxation spectrum utilizing the NLREG program. Figure 4.34 shows the weighted relaxation spectra of the four blends used in this study compared to the spectra of the pure components.

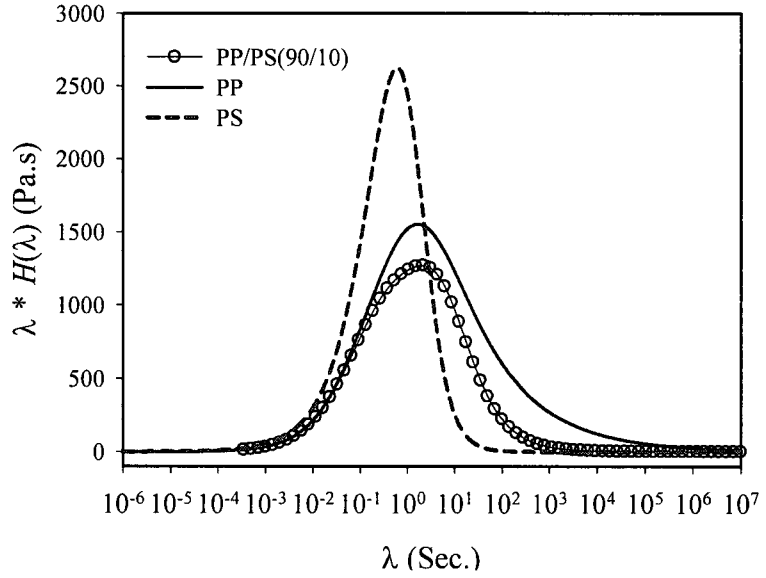
PP/PS(90/10)
PP
PS
λ * H(λ) (Pa.s)
3000
2500
2000
1500
1000
500
0
10-6 10-5 10-4 10-3 10-2 10-1 10^0 10^1 10^2 10^3 10^4 10^5 10^6 10^7
λ (Sec.)

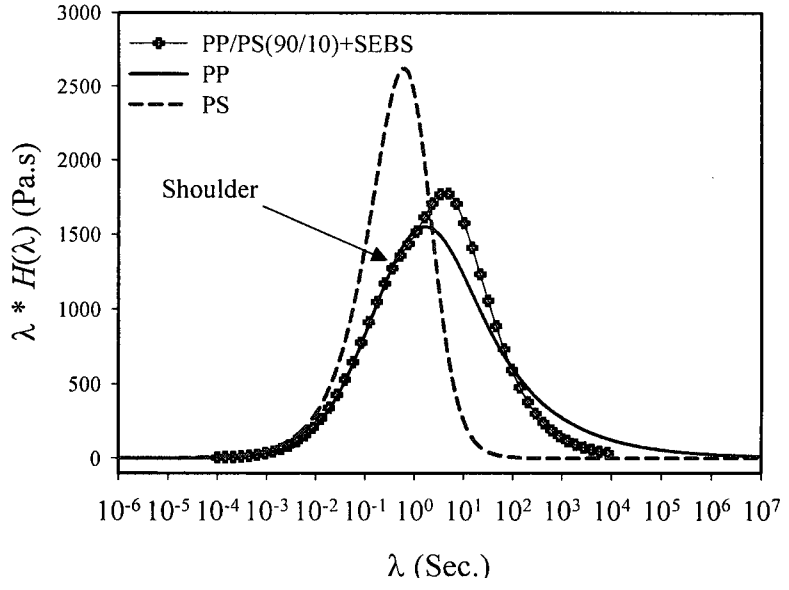
PP/PS(90/10)+SEBS
PP
PS
Shoulder
λ * H(λ) (Pa.s)
3000
2500
2000
1500
1000
500
0
10-6 10-5 10-4 10-3 10-2 10-1 10^0 10^1 10^2 10^3 10^4 10^5 10^6 10^7
λ (Sec.)

continued

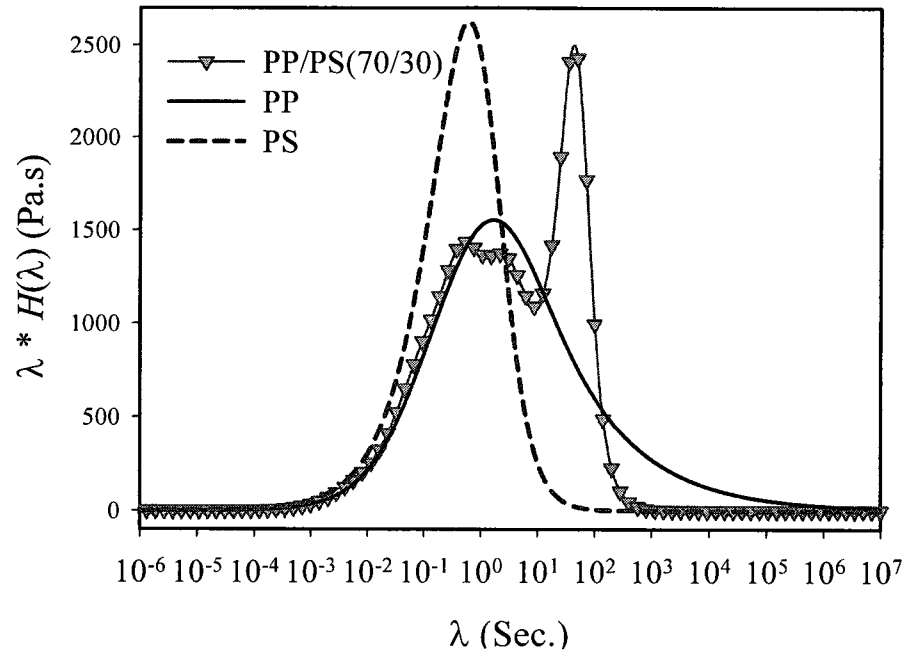

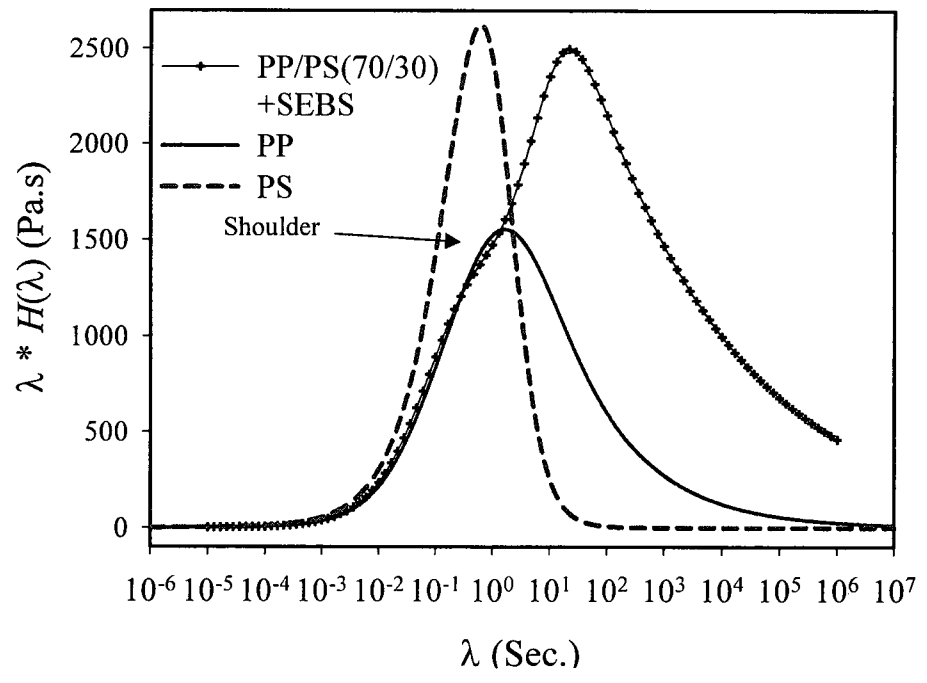

Figure 4.34: Weighted relaxation spectra for the blends of PP/PS at 200° C

The PP/PS(90/10) shows only one relaxation peak. It means that the peaks related to pure components as well as the interface relaxation peak are merged. Based on Equation (39), λ_D is proportional to R/α. In the PP/PS(90/10), the droplets' size is small, and in fact, there is small interface area between phases at this concentration and therefore the interface relaxes quickly. In the case of the compatibilized PP/PS(90/10), one separate peak is related to the interface relaxation and the relaxation peaks of the components are merged and show a shoulder at slightly shorter time. In this system, a competition between the droplet size and interfacial tension will determine the interface relaxation time. Although the interfacial tension is reduced, but the droplets' size is significantly reduced and thus the interfacial area is increased in the compatibilized PP/PS(90/10).

Three well separated maxima are seen in the relaxation spectrum of the PP/PS(70/30). Considering the times of the maxima, the first and second peaks which happen at shorter times are related to the PS and PP respectively and the last one is due to the relaxation of the interface. According to Equation (39), the interface relaxes at longer times when the droplets are bigger.

The compatibilized PP/PS(70/30) shows a shoulder related to the relaxation of its pure components and a relaxation peak due to the interface similar to the compatibilized PP/PS(90/10).

Figure 4.35 shows the effect of concentration on the relaxation time of the interface. The higher concentration which results in bigger and more droplets and thus larger interface area shifts the relaxation time of the interface to the longer times in both compatibilized and uncompatibilized blends.

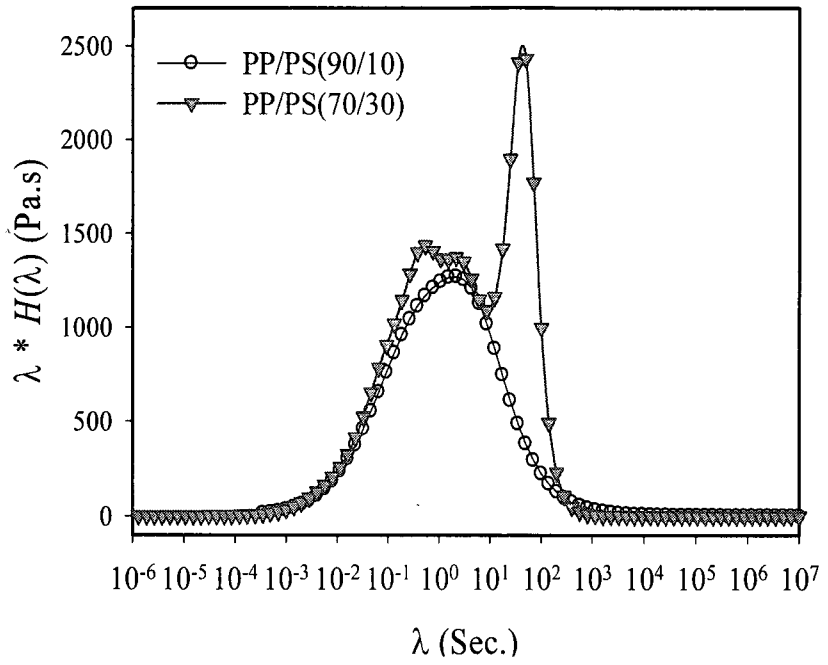

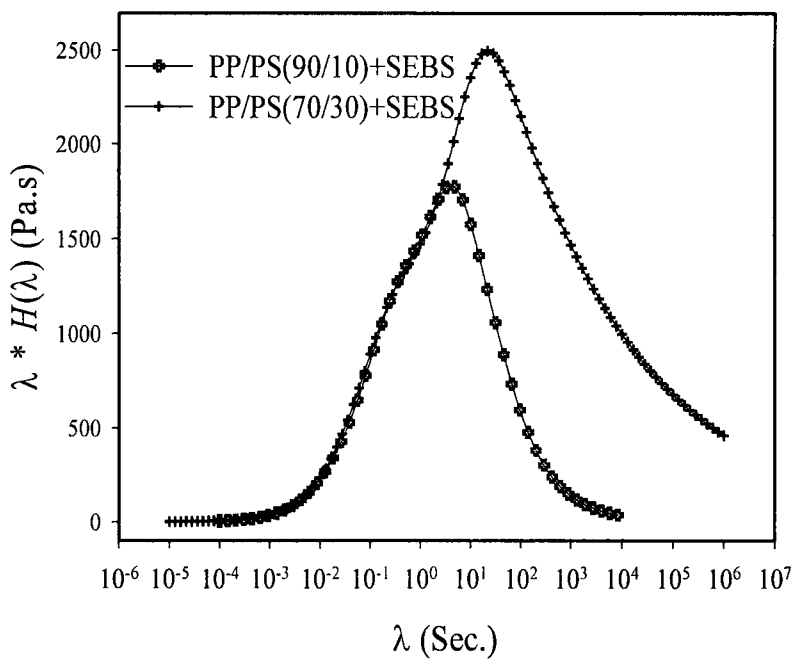

Figure 4.35 Effect of the concentration on the relaxation time of the interface

Figure 4.36 shows the effect of the compatibilizer on the relaxation time of the interface.

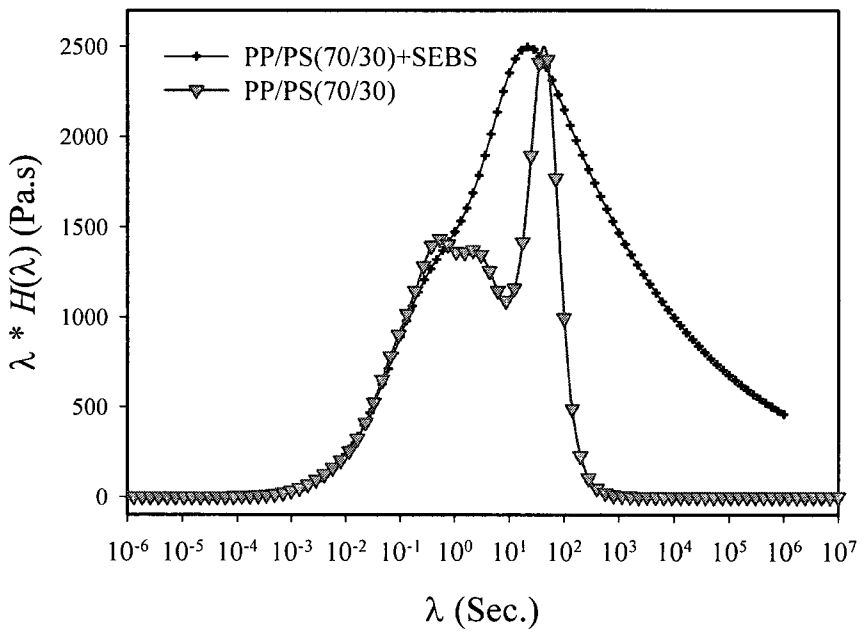

Figure 4.36: Effect of compatibilization on the relaxation time of the interface

When the blend is compatibilized, the droplets become smaller. Although the interfacial area and the elasticity of the system increase, the relaxation of small droplets is faster and the interface relaxation peak occurs at a shorter time. (As a small droplet has less deformation to retain its equilibrium shape and relax). This can be verified by Palierne model which shows the system with higher elasticity relaxes sooner [Equations (39) and (40)]. (Note should be taken that for two droplets at the same radius, the one with less interfacial tension relaxes later, because it would have less elasticity (retraction force) when sheared and so its driving force to spring back is less).

The Palierne model was used to calculate the interfacial tension and estimates the relaxation time of the interface of each blend. This model is based on the assumption that the morphology of the blend is monodisperse. Table 4.2 shows the ratio of volume average radius over number average radius of each blend after annealing without shearing.

Table 4.2: Polydispersity of the morphology of the blends, determination from images in Figures 4.31 and 4.32

Blend	PP/PS(90/10)	PP/PS(70/30)	PP/PS(90/10)+SEBS	PP/PS(70/30)+SEBS
$\frac{\bar{R}_v}{\bar{R}_n}$	1.625546	2.471575	1.598628	1.861778

Both uncompatibilized blends could not be fitted by the Palierne model. As mentioned before, the dynamic moduli of the PP/PS(90/10) did not agree with its matrix. Also, the polydispersity of the PP/PS(70/30) was more than 2. In addition, a possible coalescence in oscillatory experiments might be the reason that the results in the PP/PS(70/30) did not fit the Palierne model. Such coalescence in blends with large dispersed phase in SAOS tests has been reported by Calvao *et al.*[73]

By fitting the storage moduli of the compatibilized PP/PS(90/10) and compatibilized PP/PS(70/30), the value of $\frac{\alpha}{R}$ of each blend was calculated. Once the interfacial tension between the phases was determined, the relaxation time of the interface could be readily calculated using Equation (39). Figure 4.37 shows the fit of Palierne model for the compatibilized blends.

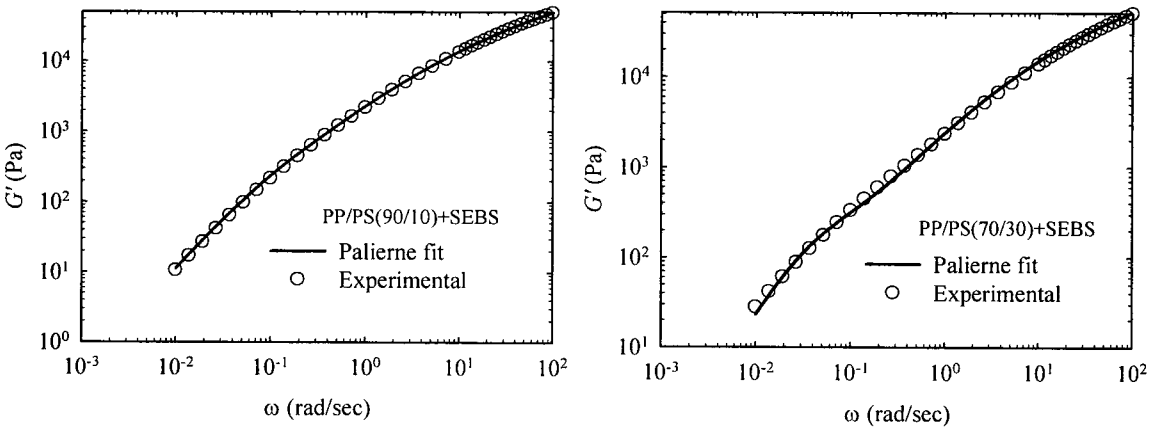

Figure 4.37: Palierne model for the compatibilized PP/PS(90/10) and compatibilized PP/PS(70/30)

Table 4.3 shows the volume average radii determined from the SEM images, the values for $\frac{\alpha}{R}$, the interfacial tension as well as the interface relaxation time obtained by fitting the experimental results of the compatibilized blends to the Palierne model.

Table 4.3: Palierne model prediction for compatibilized PP/PS(90/10) and (70/30)

Blend	$\bar{R}_v$ (μm)	$\frac{\alpha}{R}(\frac{mN}{m^2})$	α $(\frac{mN}{m})$	λ_D (sec) [Palierne model]
PP/PS(90/10)+SEBS	0.448575	33.89	1.5	7.4
PP/PS(70/30)+SEBS	1.1375	11.218	1.3	25.7

4.2.4.2. Relaxation Spectra from Creep

The creep results were converted to weighted relaxation spectrum using the NLREG software. As mentioned before, the creep experiment is more precise at longer times; consequently, the relaxation spectra obtained from creep experiments are more accurate at the times longer than the validity limit of the SAOS method. Figure 4.38 compares the weighted relaxation spectra obtained from both methods for all blends.

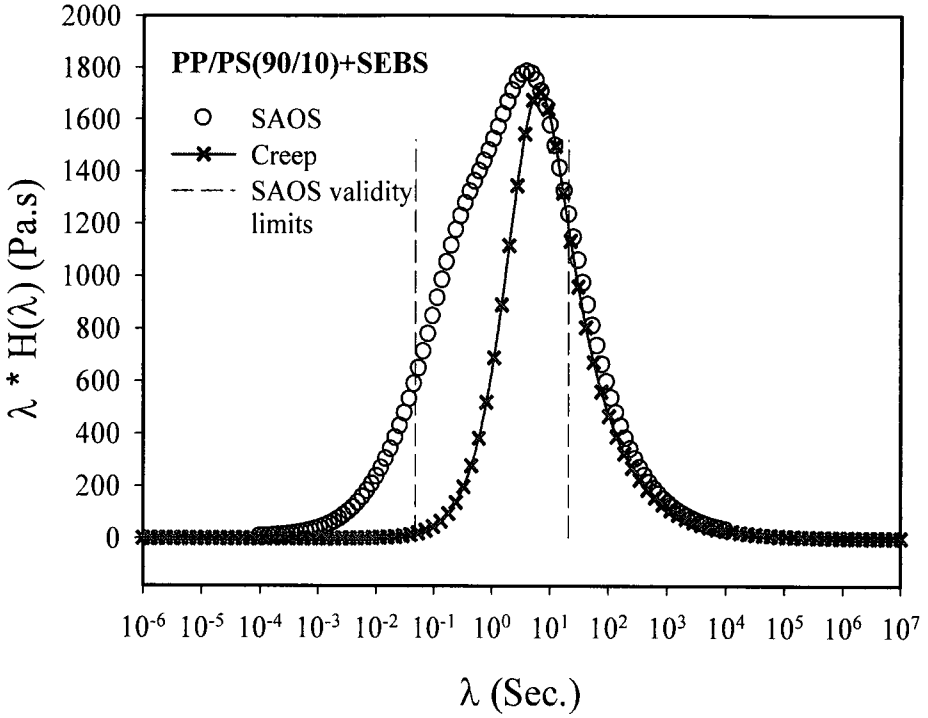
PP/PS(90/10)+SEBS
SAOS
Creep
SAOS validity limits
λ * H(λ) (Pa.s)
λ (Sec.)

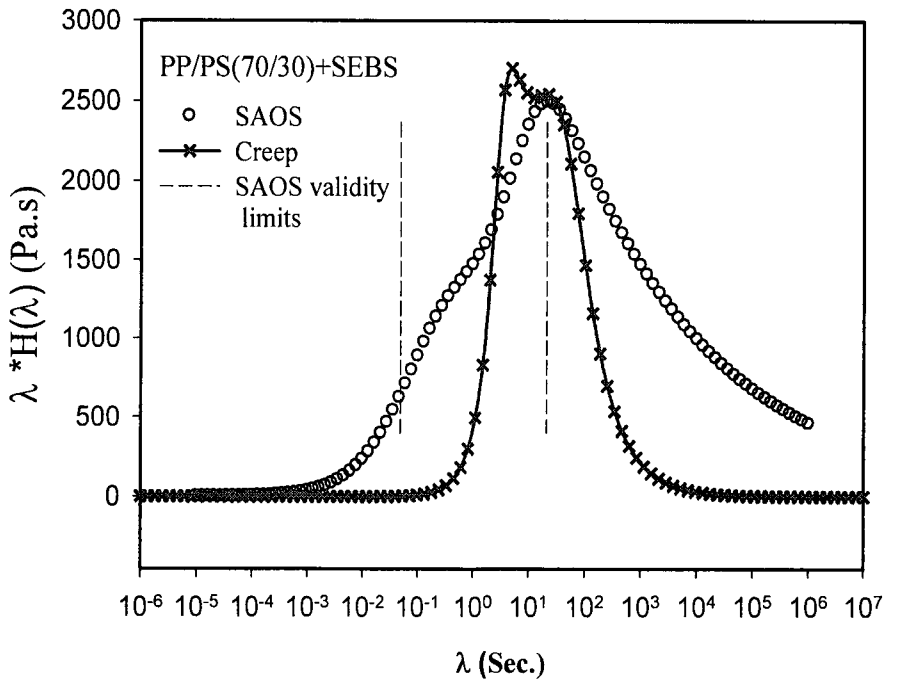
PP/PS(70/30)+SEBS
SAOS
Creep
SAOS validity limits
λ *H(λ) (Pa.s)
λ (Sec.)

continued

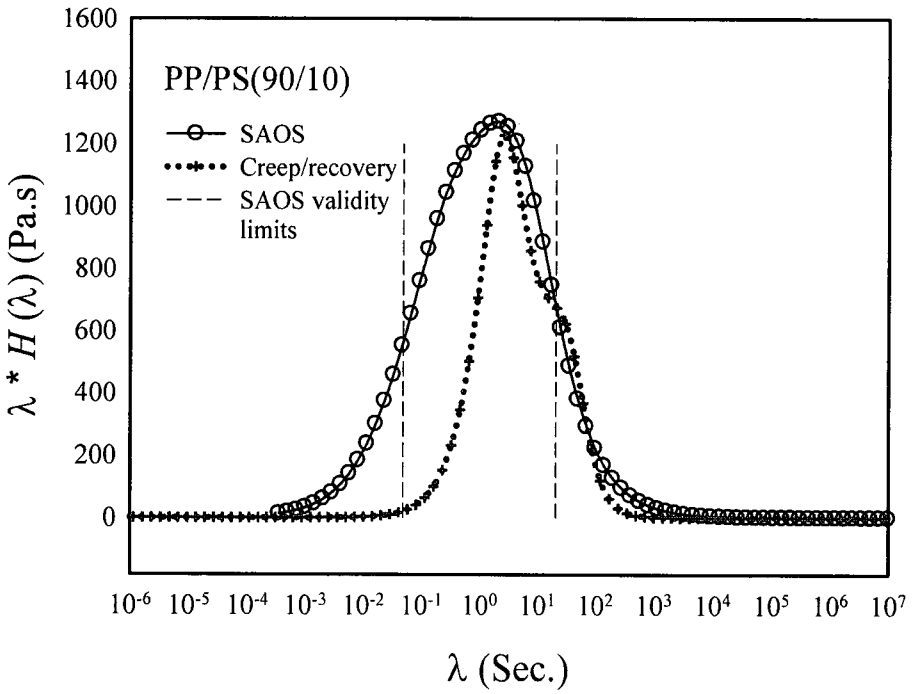

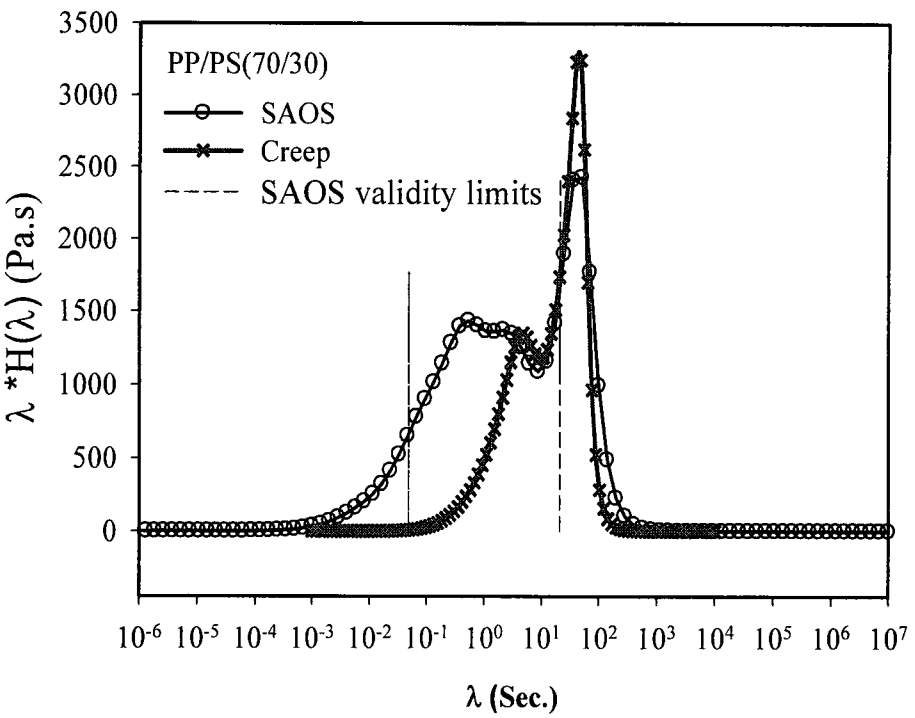

Figure 4.38: Weighted relaxation spectra of the blends from SAOS and creep experiments

The spectra from SAOS and creep both indicate qualitatively the same interface relaxation time. In the compatibilized PP/PS(90/10), the creep method cannot elucidate the shoulder for the pure components, but the long time portion of relaxation spectra from both methods are almost the same.

The importance of the creep experiment for relaxation spectrum is more obvious in the blends of compatibilized and uncompatibilized PP/PS(70/30), in which the interface relaxation phenomena occur at relatively long times. In the compatibilized PP/PS(70/30), the SAOS prediction for the times after the interface relaxation, which is longer than the validity limit of the SAOS, is wrong. Furthermore, the interface relaxation happens at 21.5 second which is longer than the upper validity limit of the SAOS. While the creep experiment cannot elucidate the relaxation shoulder of the pure components, it perfectly modifies the relaxation spectrum at times longer than the SAOS validity limit. In the PP/PS(70/30), the interface relaxation time is longer than the upper validity limit of the SAOS. In this blend, the creep measurements well predict the interface relaxation time and long-time parts of the spectrum.

In the PP/PS(90/10) system, a shoulder at around 10 second is inferred from the creep measurements. The validity of this shoulders is questionable though, because it was not found with the SAOS measurements. On the other hand, this shoulder occurs close to the upper validity limit of the SAOS, so it might be possible to accept it in experimental window. Although the interface relaxation time of this blend could not be obtained, yet with a comparison to the compatibilized PP/PS(90/10), an interfacial relaxation time in this order is logical.

4.2.5. Combination of Dynamic and Steady Results, Composite Spectra

The combination of small-amplitude oscillatory shear data with the results of creep experiment to extend the retardation spectrum window was discussed in Section 2.3. Figure 4.39 shows the retardation spectra inferred from the SAOS and incomplete creep/recovery methods and the composite retardation spectrum for the compatibilized PP/PS(70/30) determined using the combining method discussed in Section 4.1.3.

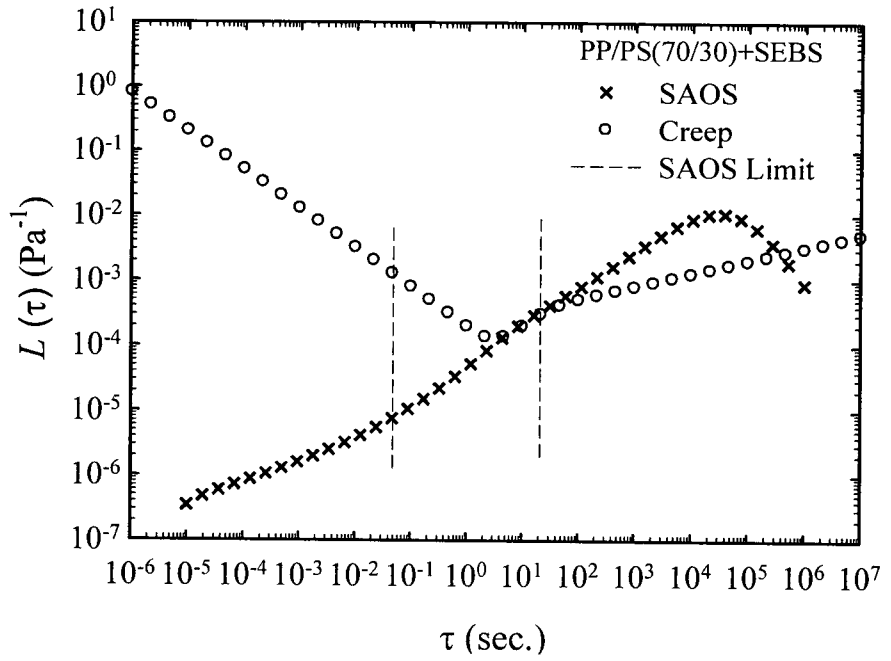

a

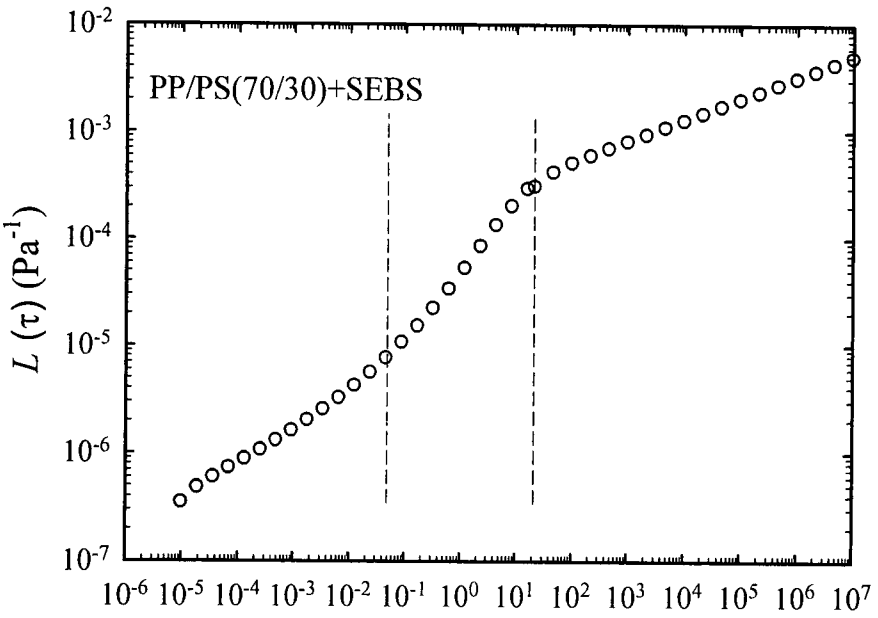

b

Figure 4.39: a) Retardation spectra from the SAOS and creep compliance for PP/PS(70/30)+SEBS at 200° C

b) Composite retardation spectrum for PP/PS(70/30)+SEBS at 200° C

There is an agreement between two retardation spectra over a considerable time interval; therefore a composite retardation spectrum was constructed from short-time part of the retardation spectrum from the SAOS experiment that smoothly switches to the long-time portion obtained from creep compliance. The extended retardation spectrum then can be used to calculate other material functions as well as a composite relaxation spectrum which is extended over a time longer than the SAOS experiment. Figures 4.40 and 4.41 show the recalculation for dynamic moduli and the extended relaxation spectrum for the compatibilized PP/PS(70/30) respectively.

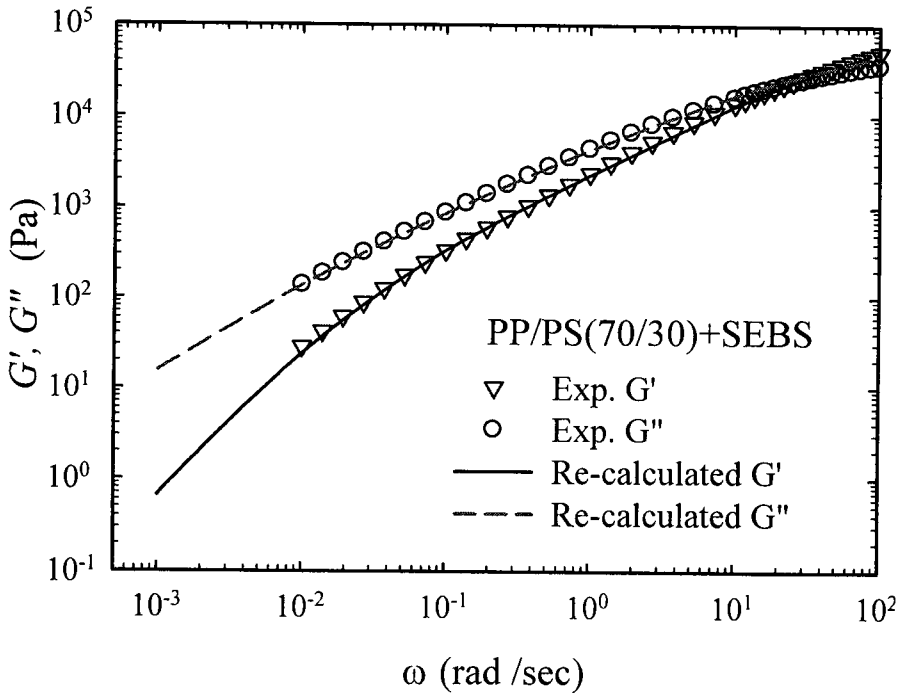

Figure 4.40: Recalculation of G' and G'' for the PP/PS(70/30)+SEBS at 200° C

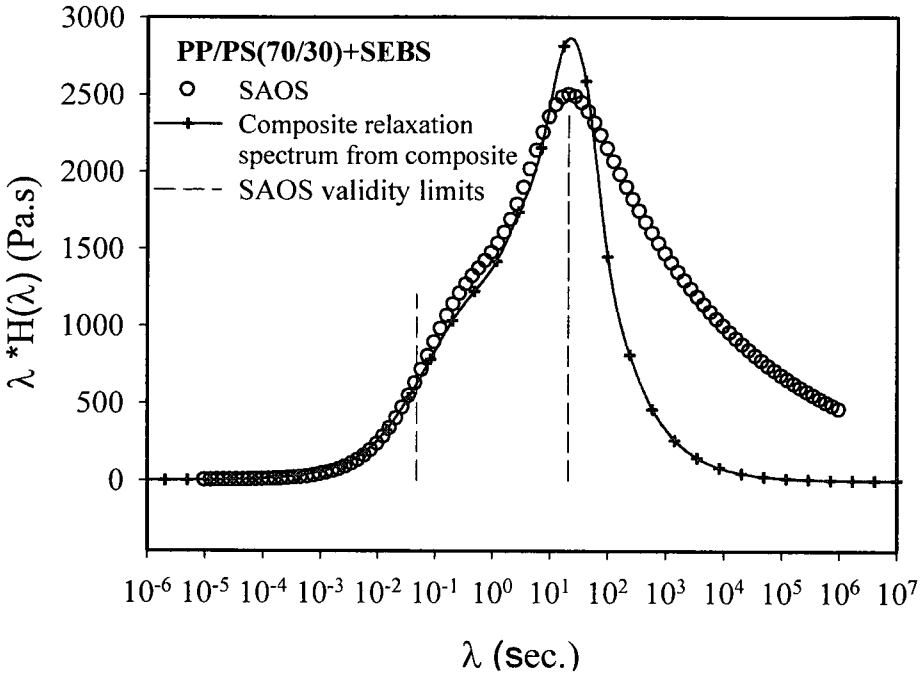

Figure 4.41 Composite relaxation spectrum for PP/PS(70/30)+SEBS at 200° C

The obtained composite spectrum is valid over a broader frequency range and includes the information of both relaxation spectra from the SAOS experiments and creep tests.

This method was successfully applied on three more blends. Figures 4.42 to 4.47 show the combining step for retardation spectra from the SAOS and creep experiments, obtained composite spectra, recalculated material functions and the composite relaxation spectra calculated from extended retardation spectra for the compatibilzed PP/PS(90/10), PP/PS(70/30), and PP/PS(90/10).

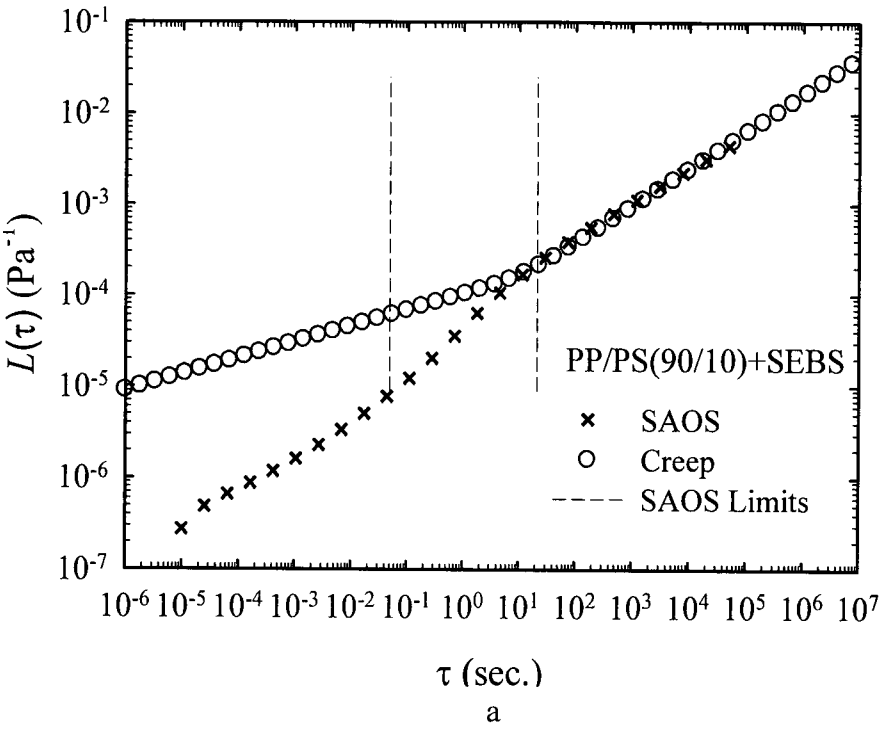

a

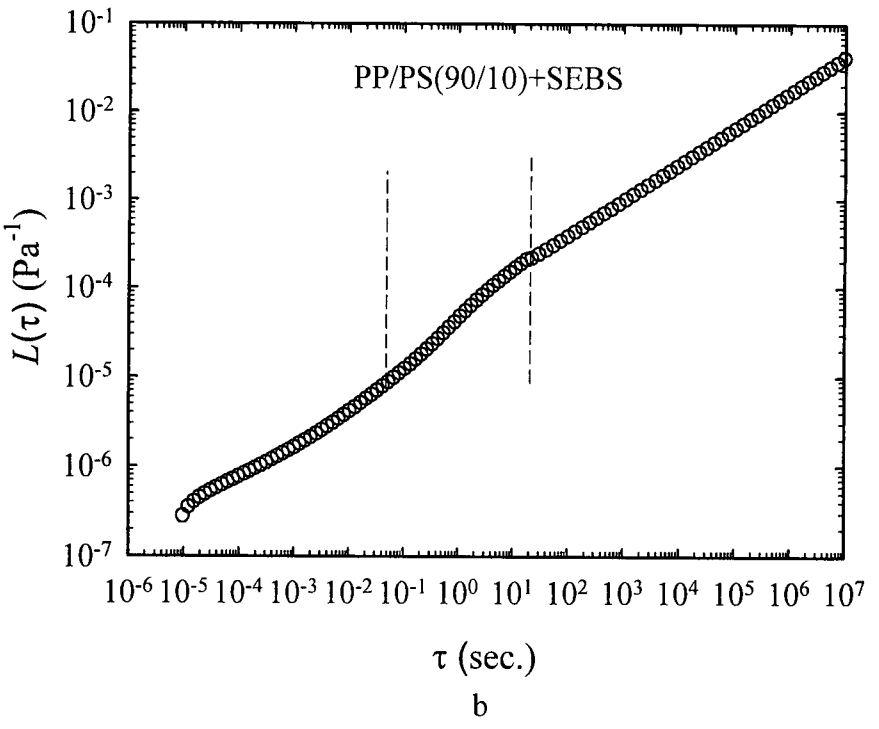

b

Figure 4.42 a) Retardation spectra from the SAOS and creep compliance for PP/PS(90/10)+SEBS at 200° C

b) Composite retardation spectrum for PP/PS(90/10)+SEBS at 200° C

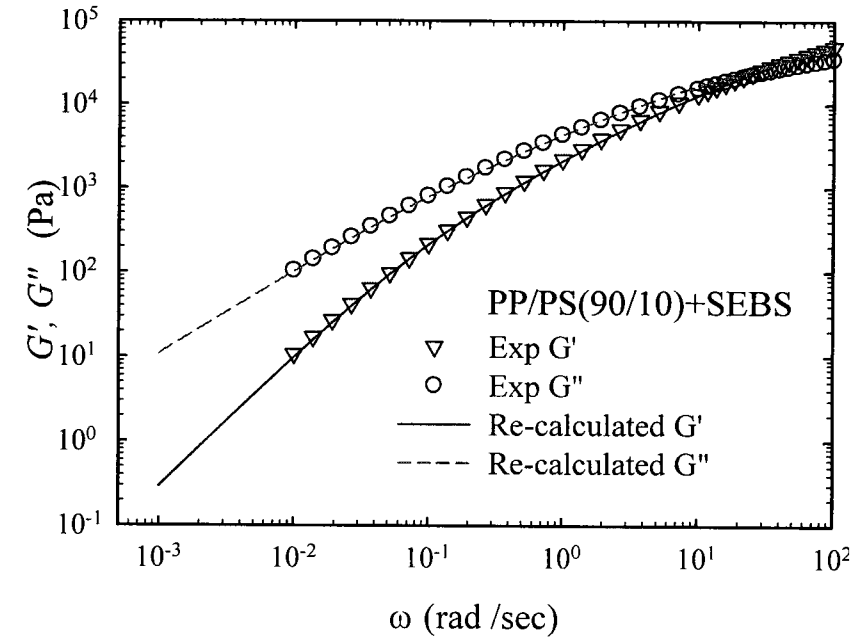

a

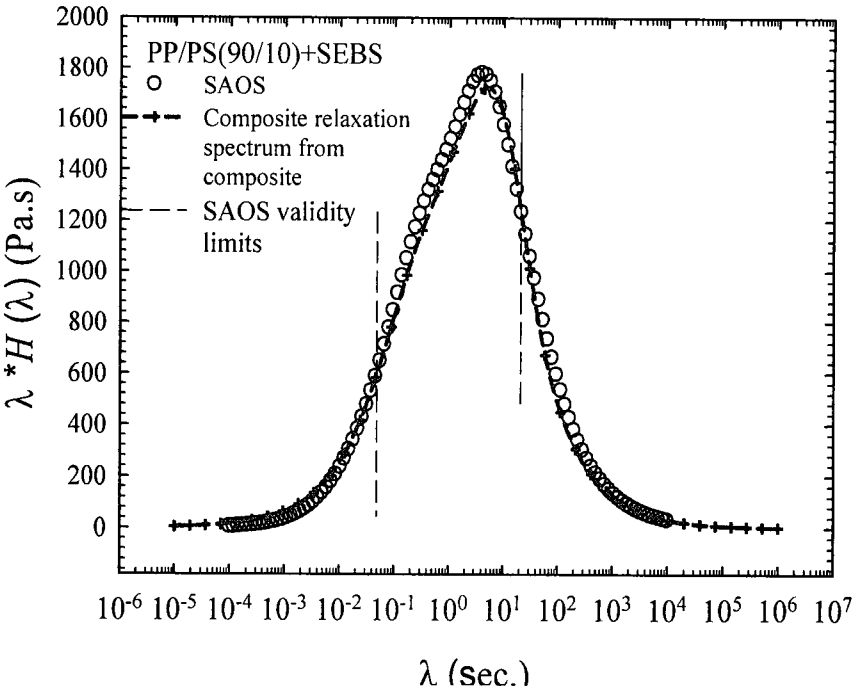

b

Figure 4.43: a) Recalculation of G' and G'' for the PP/PS(90/10)+SEBS at 200° C, b) Composite relaxation spectrum for PP/PS(90/10)+SEBS at 200° C

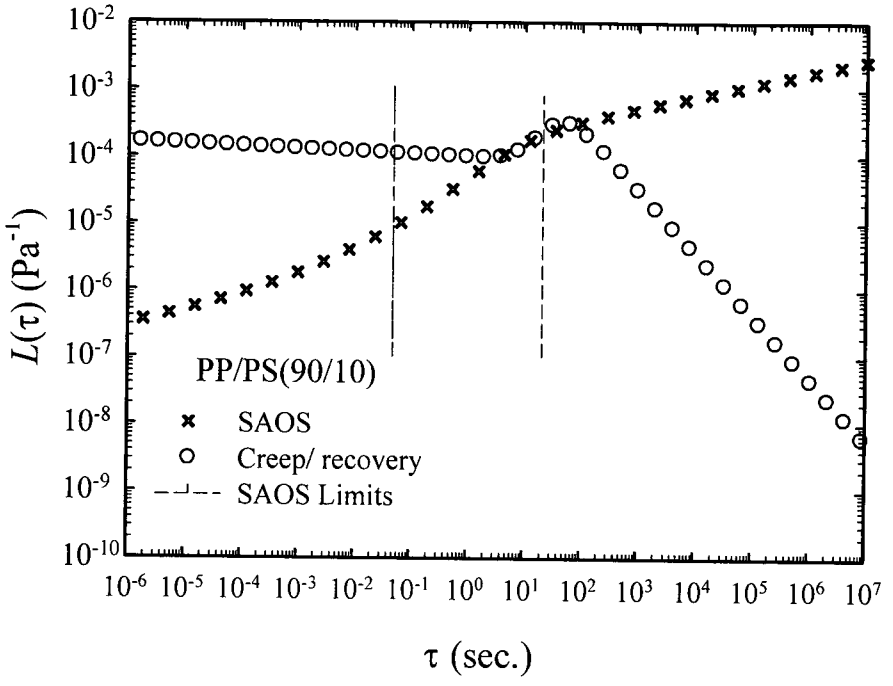

a

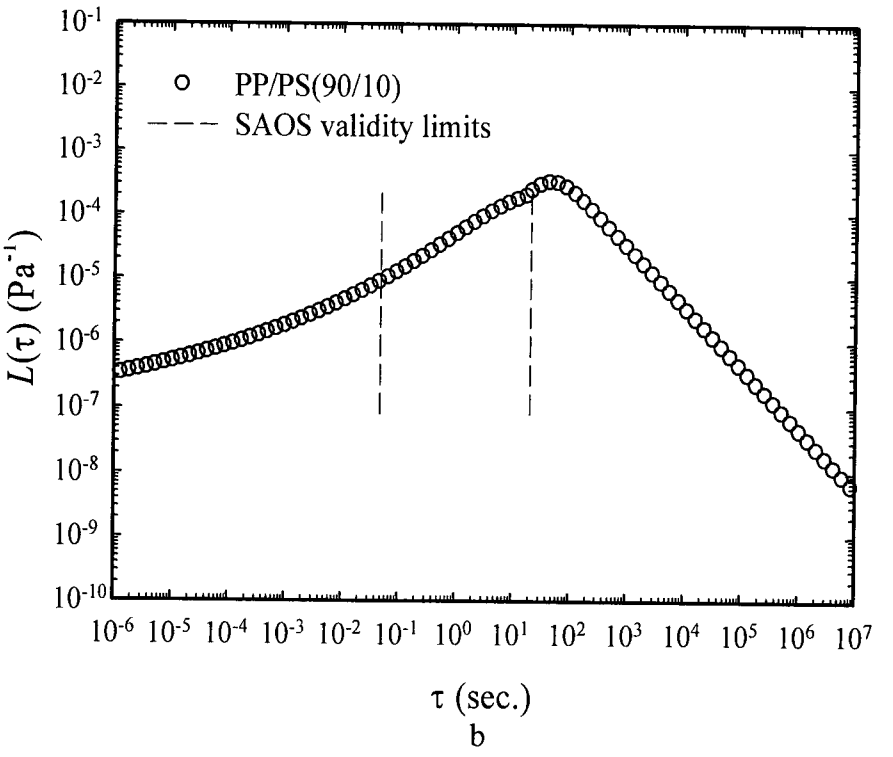

b

Figure 4.44: a) Retardation spectra from the SAOS and creep compliance for PP/PS(90/10) at 200° C b) Composite retardation spectrum for PP/PS(90/10) at 200° C

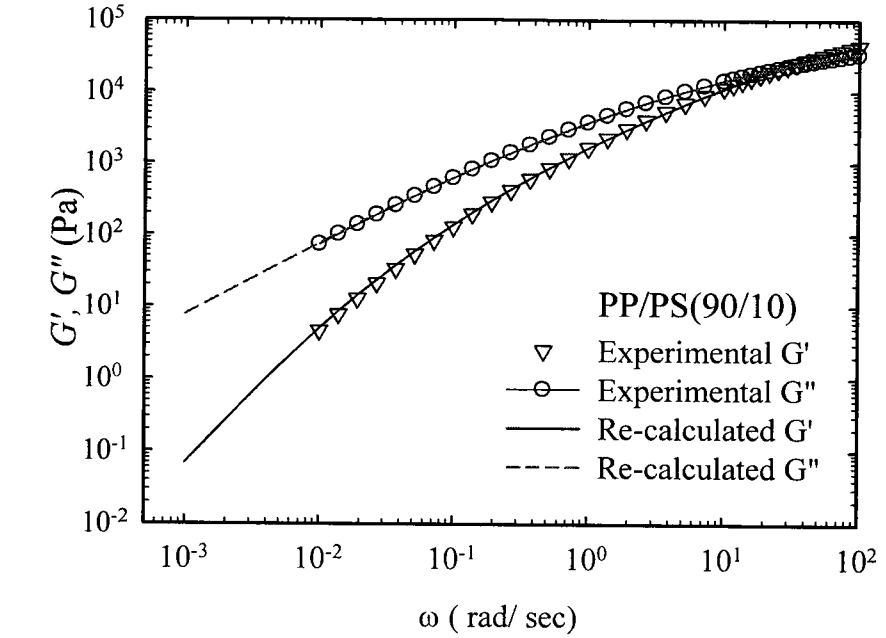

a

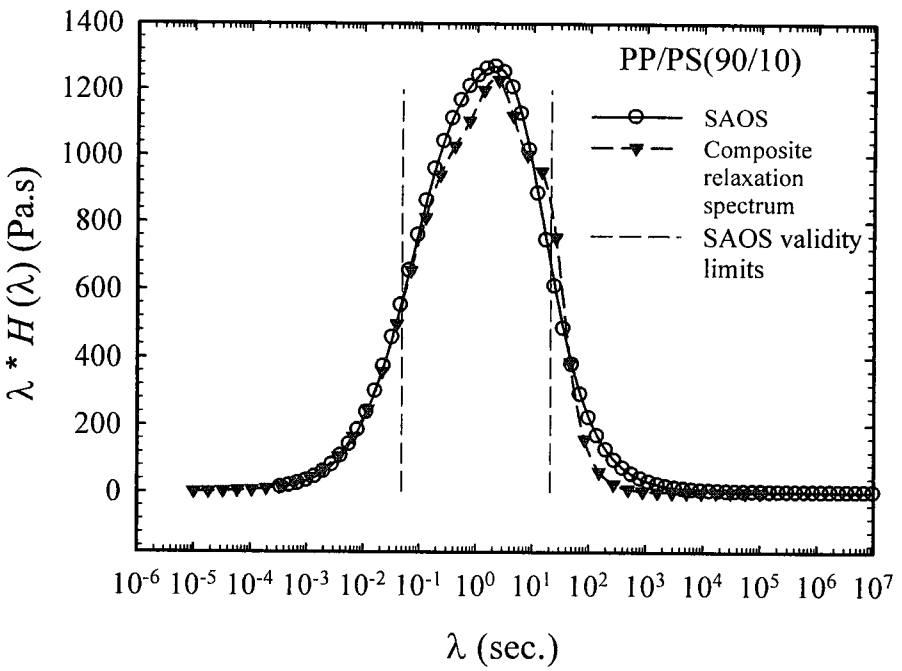

b

Figure 4.45: a) Recalculation of G' and G'' for the PP/PS(90/10) at 200° C, b) Composite relaxation spectrum for PP/PS(90/10) at 200° C

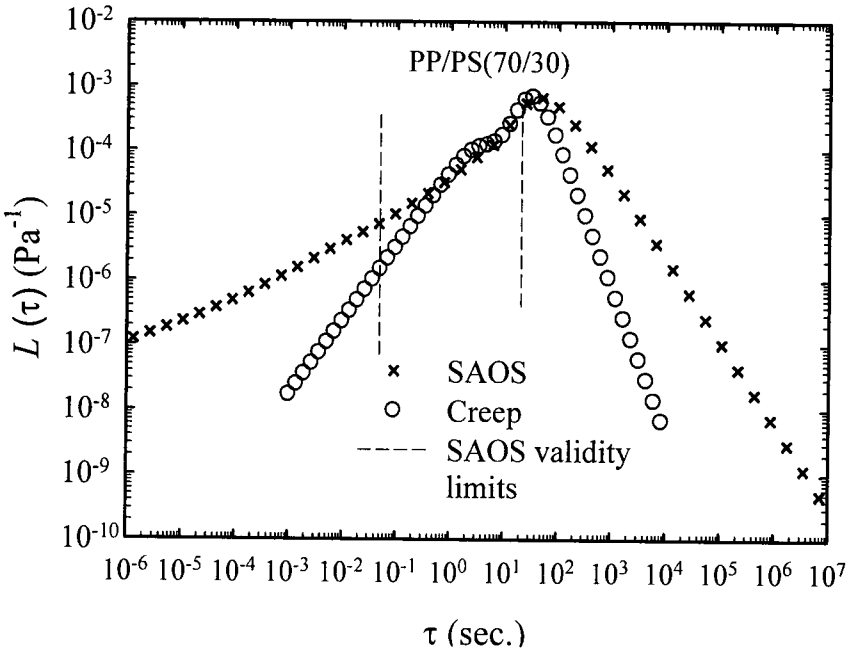

a

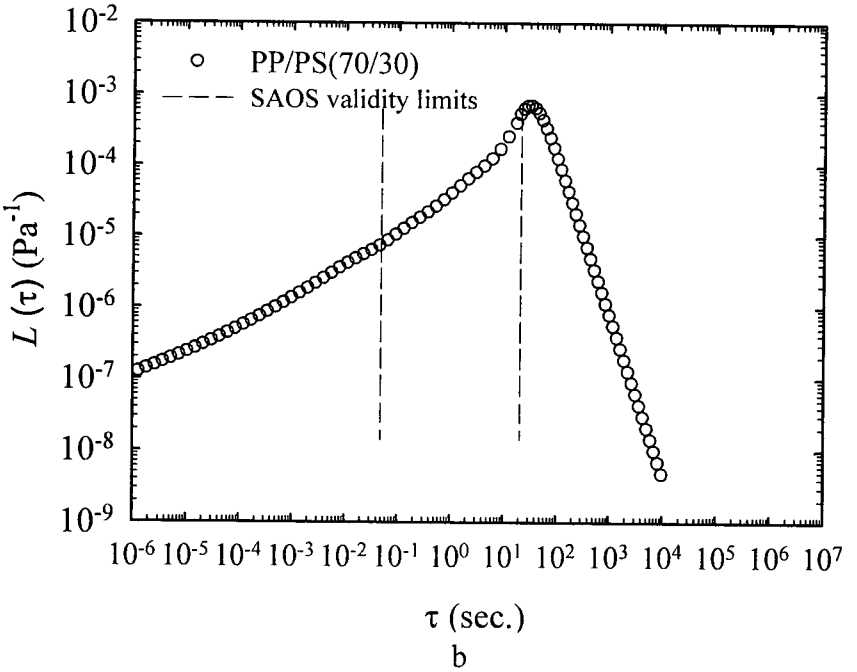

b

Figure 4.46: a) Retardation spectra from the SAOS and creep compliance for PP/PS(70/30) at 200° C b) Composite retardation spectrum for PP/PS(70/30) at 200° C

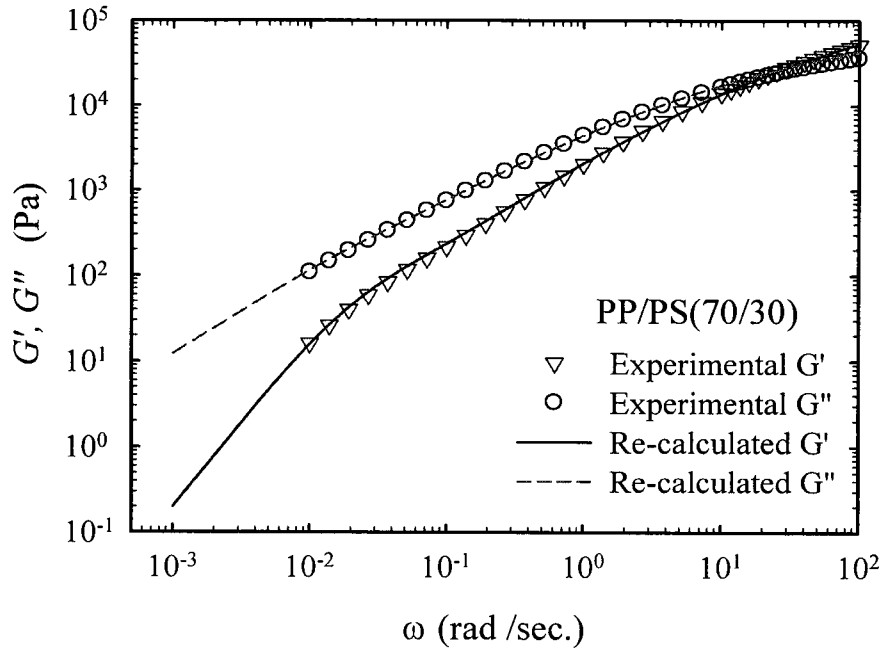

a

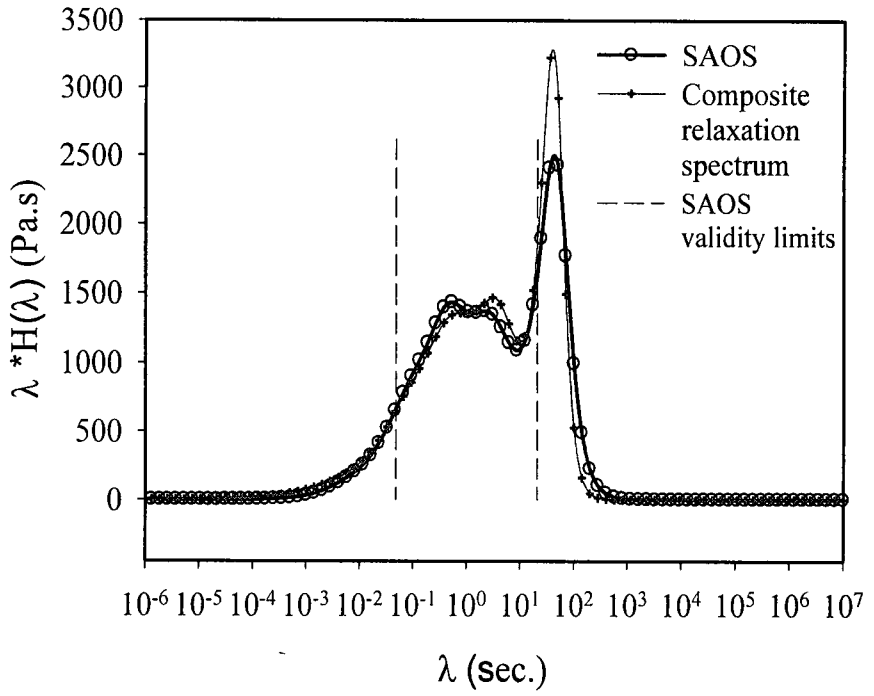

b

Figure 4.47: a) Recalculation of G' and G" for the PP/PS(70/30) at 200° C, b) Composite relaxation spectrum for PP/PS(70/30) at 200° C

The applicability of the *combining* method and the fact that the retardation spectrum obtained from creep method superpose in reasonable time interval to that from the SAOS experiments indicate that the creep experiments performed on the immiscible blends were kept in the *linear viscoelastic* regime, meaning that the morphological modifications were minimized enough to have the blends in linear viscoelastic behaviour. The key procedure was the application of incomplete creep experiment followed by recovery and the use of Boltzmann superposition principle in extending the creep compliance which kept the sample in linear viscoelastic limit and avoided any morphological changes. Morphological analysis in the compatibilized PP/PS(70/30) showed that by the application of this method, the volume average radius was only changed from 2.275 to 2.303 μm. The combination method to extend the spectrum (the LVE window of the blend behaviour) is applicable on any immiscible blend as long as a superposition over considerable time interval between the two (retardation) spectra, obtained from SAOS and creep experiments, exists. The upper validity limit of the dynamic measurements is determined by the minimum frequency (ω_{min}) used in the frequency sweep test. Therefore the viscosity of the polymer melt should be high enough such that it is possible to reach low enough frequencies for the two spectra to overlap on the time scale. This can be considered as the only limitation for this technique regarding the blend selection.

To show the importance of the application of the incomplete creep/recovery, a creep experiment was done on the PP/PS(70/30) for 2000 seconds. Figure 4.48 shows the retardation spectra obtained from the direct creep experiment and the SAOS experiment.

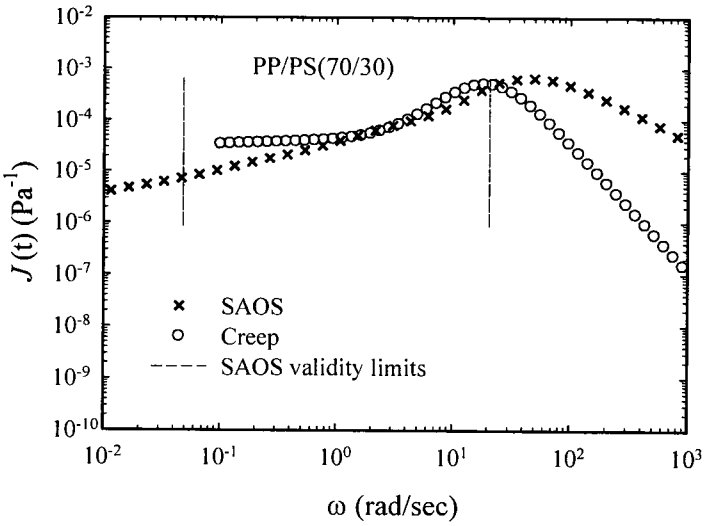

Figure 4.48: Retardation spectra from the SAOS and the direct creep experiment for PP/PS(70/30) at 200° C

It can be seen that there only a 3 second agreement between two spectra and they lose the agreement well before the upper limit of validity of the SAOS experiment; hence the retardation obtained from only creep experiment does not predict the LVE behaviour of the blend. The reason is due to the considerable coalescence that occurred during the direct creep experiment. Table 4.4 shows the changes in the volume average radius after incomplete creep/recovery experiment for the compatibilized and uncompatibilized PP/PS(70/30) as well as the direct creep experiment for the uncompatibilized PP/PS(70/30).

Table 4.4: The change in the volume average radius after incomplete creep/recovery and direct creep experiments

Blend	Experiment	Initial $\bar{R}_v(\mu m)$	Final $\bar{R}_v(\mu m)$
PP/PS(70/30)+SEBS	Incomplete creep/recovery	2.27 ± 0.7	2.3 ± 0.7
PP/PS(70/30)	Incomplete creep/recovery	6.3 ± 0.62	4.6 ± 0.62
PP/PS(70/30)	Direct creep	6.3 ± 1	11.94 ± 1

From Table 4.4, there was an 89% increase in the volume average radius of the dispersed phase for the uncompatibilized PP/PS(70/30) due to 2000 seconds of creeping. Although the stress level and the creep time were already determined by the successive experiments *on the same sample* method and the LVE condition was verified, but the large coalescence that happened changed the overall rheological behaviour of the blend. It can be seen that the change in the volume average radius was negligible for the compatibilized PP/PS(70/30) in the incomplete creep/recovery experiments. The reduction in the volume average radius for the uncompatibilizes PP/PS(70/30) in incomplete creep/recovery experiments was due to the inhomogeneity in the blend morphology that already explained in Section 4.2.3, and showed that the coalescence was negligible.

Chapter 5: Conclusion

1. Determination of the appropriate stress level for creep experiments is possible by the proposed method of successive creep tests on *the same sample*.

2. The developed creep method minimizes the morphological modifications, keeps the blends in the limit of LVE regime and can be used to study long time behaviour of immiscible blends in LVE region.

3. The comparison between the weighted relaxation spectra obtained from the SAOS and creep measurements showed that while the one calculated from dynamic measurements is accurate at shorter times, the creep prediction is more accurate at the times longer than the SAOS validity limit.

4. The SAOS results of compatibilized blend were fitted to the emulsion Palierne model and the interface relaxation time as well as interfacial tension between two phases were calculated.

5. The uncompatibilized PP/PS(70/30) could not be fitted to the emulsion model due to the coalescence during the SAOS measurements and the droplet polydispersity higher than 2.

6. It is possible to combine the SAOS results with the creep measurements to extend the window of the LVE behaviour of immiscible blends.

7. The continuous retardation spectra of the SAOS and the creep experiments were calculated using NLREG program and used to combine both sets of data from the SAOS and creep experiments to construct a composite retardation spectrum.

8. The composite retardation spectrum can then be used to recalculate other material functions as well as a composite relaxation spectrum which are extended over broader frequency range.

9. The extended composite relaxation spectrum can be used to analyze the relaxation processes of the interface in the immiscible blends.

References

[1] N. G. McCrum,C. P. Buckley, C.B. Bucknall, "Principals of Polymer Engineering", Oxford University Press, 1997

[2] L. H. Sperling, "Introduction to Physical Polymer Science", John Wiley and Sons, INC. Publivations, 2006

[3] F. A. Morrison, " Understanding Rheology ", Oxford University Press, 2001

[4] J. M. Dealy, Ronld G. Larson, "Structure and Rheology of Molten Polymers", Hanser Publisher, Munich

[5] J. D. Ferry, "Viscoelastic Properties of Polymers" , John Wiley & Sons, INC. 3th edition, 1980

[6] D. J. Plazek, I. Echeverria, " Don't cry for me Charlie Brown, or with compliance comes comprehension", J. Rheol., 44(4) (2000)

[7] J. Honerkamp and J. Weese, " A nonlinear regularization method for the calculation of relaxation spectra", Rheol Acta 32:65-73 (1993)

[8] J. Honerkamp and J. Weese, "Determination of the Relaxation Spectrum by a Regularization Method", Macro-molecules, 22:4372-4377, (1989)

[9] J. Honerkamp, Ill-posed problems in rheology, Rheol Acta 28:363-371 (1989)

[10] C. Elster, J. Honerkamp and J. Weese, "Using regularization methods for the determination of relaxation and retardation spectra of polymeric liquids", Rheol Acta 30:161-174 (1991)

[11] C. Elster and J. Honerkamp, "Modified Maximum Entropy Method and Its Application to Creep Data" *Macromolecules*,24, 310-314 (1991)

[12] J. Honerkamp and J. Weese, "Tikhonovs regularization method for ill-posed problems. A comparison of different methods for the determination of the regularization parameter", Continuum Mech. Thermodyn. 2 ,17-30 (1990)

[13] S. Hansen, "Estimation of the relaxation spectrum from dynamic experiments using Bayesian analysis and a new regularization constraint", Rheol Acta 47:169–178 (2008)

[14] A.R. Davis, R.S. Anderssen, " Sampling localization in determining the relaxation spectrum", J. Non-Newtonian Fluid Mech., 73, 163-179 (1997)

[15] C. He, P. Wood-Adams, J. M Dealy, " Broad frequency range characterization of molten polymers", J. Rheol. 48(4), 711-724 July/August (2004)

[16] M. Kraft, J. Meissner, and J. Kaschta, " Linear viscoelastic characterization of polymer melts with long relaxation times", Macromolecules, 32, 751-757 (1999)

[17] A. Eckstein, J. Suhm, C. Friedrich, R.-D. Maier, J. Sassmannshausen, M. Bochmann, and R. Mul lhaupt, Determination of Plateau Moduli and Entanglement Molecular Weights of Isotactic, Syndiotactic, and Atactic Polypropylenes Synthesized with Metallocene Catalysts, Macromolecules *31,* 1335-1340 (1998)

[18] J. Meissner, "Experimental problems and recent results in polymer melt rheology", Makromol. Chem., Macromol. Symp. 56, 25-42, (1992)

[19] J. Kaschta and E R. Schwarzl, "Calculation of discrete retardation spectra from creep data - I. Method", Rheol Acta 33:517-529 (1994)

[20] J. Kaschta and E R. Schwarzl, "Calculation of discrete retardation spectra from creep data - II. Analysis of measured creep curves", Rheol Acta 33:530-541 (1994)

[21] P.Martin, P.J. Carreau, B.D. Favis, R. Jerome, "Investigating the morphology/rheology interrelationships in immiscible polymer blends", J.Rheol.44, 569-583 (2000)

[22] I. Vinckeier, P. Moldenaer, J. Mewis, "Relationship between rheology and morphology of model blends in steady shear flow", J. Rheol, 40, 613- 631 (1996)

[23] B.D. Favis and J. P. Chalifoux, " Influence of composition on the morphology of polypropylene/polycarbonate blends", Polymer, Vol. 29, pp. 1761-1767 (1988)

[24] B.D Favis and J.M. Willis, " Phase size/Composition dependence in immiscible blends: Experimental and theoretical considerations", Journal of polymer science: Part B: Polymer science, Vol. 28, 2259-2269 (1990)
[25] B.D. Favis and J. P. Chalifoux, " the effect of viscosity ratio on the morphology of polypropylene/polycarbonate blends during processing", Polymer engineering and science, Vol. 27, No. 20, (1987)
[26] B.D. Favis, and D. Therrien, " Factors influencing structure formation and phase size in as immiscible polymer blend of polycarbonate and polypropylene prepared by twin-screw extrusion", Polymer, Vol. 32, No. 8 (1991)
[27] J.M. Willis, V. Caldas, B.D. Favis, " Processing-morphology relationship of compatibilized polyolefin/polyamide blends, Part 2: the emulsifying effect of an ionomer compatibilizer as a function of blend and viscosity ratio", Journal of materials science, 26, 4742-4750 (1991)
[28] P. G. Ghodgaonkar and U. Sundararaj, " Prediction of dispersed phase drop diameter in polymer blends: The effect of elasticity", Polymer engineering and science, Vol. 36, No. 12, (1996)
[29] R. G. Larson " The structure and rheology of complex fluids", Oxford University Press, P. 399-402 (1999)
[30] H. P. Grace," Dispersion phenomena in high viscosity immiscible fluid systems and application of static mixers as dispersion in such systems", Chem. Eng. Commun. Vol. 14,pp 225-277(1982)
[31] S. Velankar, P. Van Puyvelde, J. Mewis, and P. Moldenaers, " Effect of compatibilization on the breakup of polymeric drops in shear flow", J. Rheol, 45(4) (2001)
[32] D. Graebling, R. Muller, and J.F. Palierne, "Linear viscoelastic behaviour of some incompatible polymer blends in the melt. Interpretation of data with a model of emulsion of viscoelastic liquids", Macromolecules, 26,320-329 (1993)
[33] D. Graebling, R. Muller, and J.F. Palierne, " Linear viscoelasticity of incompatible polymer blends in the melt in relation with interfacial properties", Journal de physique IV, colloque C7, supplement au Journal de physique III, Vol. 3, 1525-1534 (1993)
[34] R. Cavallo, S. Guido, M. Simeone, " Drop deformation under small-amplitide oscillatory shear flow", Rheol Acta 42: 1-9 (2003)
[35] P. H.P. Macaubas, N. R. Demarquette, "Interfacial tension, morphology and linear viscoelasticity behaviour of PP/PS blends", Polimeros, ciencia e tecnologia, 71-77 (1999)
[36] D. Graebling and R. Muller, " Determination of interfacial tension of polymer melts by dynamic shear measurements", Colloids and Surfaces, 55, 89-103 (1991)
[37] D. Graebling and R. Muller, "Rheological behaviour of polydimethylsiloxane/polyoxyethylene blends in the melt. Emulsion model of two viscoelastic liquids", J Rheol 34:193-205 (1990)
[38] S. Velankar, P. Van Puyvelde, J. Mewis, and P. Moldenaers, "Steady-shear rheological properties of model compatibilized blend", J. Rheol. 48(4), 725-744 (2004)
[39] M. Doi and T. Ohta, "Dynamics and rheology of complex interfaces. I" , J. Chem. Phys. 95 (2), 15 July (1991)
[40] H. Mok Lee and O Ok Park," Rheology and dynamics of immiscible polymer blends", J. Rheol. 38(5) (1994)
[41] C. Lacroix, M. Aressy, P. J. Carreau, " Linear viscoelastic behaviour of molten blends: A comparative study of the Palierne and Lee and Park models", Rheol Acta 36: 416-428 (1997)
[42] J.F. Palierne, " Linear rheology of viscoelastic emulsions with interfacial tension", Rheol Acta, 29:204-214 (1990)
[43] M. Bousmina, " Rheology of polymer blends: linear model for viscoelastic emulsions", Rheol Acta 38: 73-83 (1999)
[44] J.F. Palierne, " Correction", Rheol Acta, 30:497 (1991)

[45] D. Graebling, A. Benkira, Y. Gallt and R. Muller, " Dynamic viscoelastic behaviour of polymer blends in the melt-Experimental results fpr PDMS/POE-DO, PS/PMMA and PS/PEMA blends", Eur. Polym. J. Vol. 30, No. 3, pp. 301-308 (1994)
[46] A.M.C. Souza, N.R. Demarquette," Influence of composition on the linear viscoelastic behaviour and morphology of PP/HDPE blends", Polymer 43, 1313-1321 (2002)
[47] A.M.C. Souza, N.R. Demarquette, "Influence of coalescence and interfacial tension on the morphology of PP/HDPE compatibilized blends", Polymer 43, 3959-3967 (2002)
[48] H. Gramespacher, and J. Meissner, " Interfacial tension between polymer melts measured by shear oscillations of their blends", J. Rheol. 36, 1127-1141 (1992)
[49] P.H.P. Macau´bas, N.R. Demarquette, "Morphologies and interfacial tensions of immiscible polypropylene/polystyrene blends modified with triblock copolymers", Polymer 42, 2543–2554 (2001)
[50] R.E Riemann, H. J. Cantow, and Chr. Friedrich, " Interpretation of a new Interface-governed relaxation process in compatibilized polymer blends", Macromolecules, 30, 5476-5484 (1997)
[51] M. Iza, M. Bousmina, R. Jerome, " Rheology of compatibilied immiscible viscoelastic polymer blends", Rheol Acta, 40: 10-22 (2001)
[52] J.M. Willis, and B.D. Favis, "Processing-Morphology relationships of compatibilized Polyolefin/Polyamide blends. Part 1: The effect of an Ionomer compatibilizer on blend morphology", Polymer engineering and science, Vol. 28, No. 21, (1988)
[53] J. Huitric, M. Moan, P. J. Carreau, N. Dufaure, "Effect of reactive compatibilization on droplet coalescence in shear flow", J. Non-Newtonian Fluid Mech. 145, 139-149 (2007)
[54] B.D.Favis, " Phase size/interface relationship in polymer blends: the emulsification curve", Polymer, Vol. 35, No. 7 (1994)
[55] M. Yee, P. S. Calvao, N. R. Demarquette, " Rheological behaviour of poly(methyl methacrylate)/polystyrene (PMMA/PS) blends with the addition of PMMA-ran-PS", Rheol Acta, 46: 653-664 (2007)
[56] Y. T. Hu, " Drop deformation, breakup, and coalescence with compatibilizer", Physics of Fluids, Vol. 12, No. 3 (2000)
[57] S. Lyu, T. D. Jones, F. S. Bates, and C. W. Macosko, " Role of block copolymers on suppression of droplet coalescence", Macromolecules, 35, 7845-7855 (2002)
[58] P. Van Puyvelde, S. Velankar, P. Moldenaers, "Rheology and morphology of compatibilized polymer blends", Elsevier, Current Opinion in Colloid & Interface Science 6, 457-463 (2001)
[59] M. Matos and B.D Favis and P. Lomellini, " Interfacial modification of polymer blends- the emulsification curve:1. Influence of molecular weight and chemical composition of the interfacial modifier", Polymer, Vol. 36, No. 20, pp3899-3907 (1995)
[60] N. Mekhilef, B. D. Favis, and P. J. Carreau, " Morphological stability, Interfacial tension, and Dual-Phase continuity in polystyrene-polyethylene blends", J. Of Polymer Science: Part B: Polymer Physics, Vol 35, 293-308 (1997)
[61] J.C. Lepers and B. D. Favis, " Interfacial tension reduction and coalescence in compatibilized polymer blends", AIChE Journal, Vol. 45, No. 4 (1999)
[62] R.E. Riemann, H.J. Cantow, C. Friedrich, "Rheological investigation of form relaxation and interface relaxation processes in polymer blends", Polymer Bulletin 36, 637-643 (1996)
[63] U. Jacobs, M. Fahrlander, J. Winterhalter, and Chr. Friedrich, " Analysis of Palierne's emulsion model in the case of viscoelastic interfacial properties", J. Rhol. 43(6), (1999)
[64] J. Wang, S. Velankar, "Strain recovery of model immiscible blends: effects of added compatibilizer, Rheol Acta 45: 741–753 (2006)
[65] E. Van Hemelrijck and P. Van Puyvelde, "Interfacial elasticity and coalescence supperession in compatibilized polymer blends", J. Rheol. 48(1) 143-158 (2004)

[66] P. Van Puyvelde, S. Velankar, J. Mewis, and P. Moldenaers, " Effect of Marangoni stress on the deformation and coalescence in compatibilized immiscible polymer blends", Polymer engineering and science, Vol. 42, No. 10 (2002)

[67] S. Velankar, H. Zhou, H. Kyoung Jeon, and C. W. Macosko,: CFD evaluation of drop retraction method for the measurements of interfacial tension of surfactant-laden drops", Journal of colloid and interface science 272, 172-185 (2004)

[68] U. Sundararaj, and C. W. Macosko, " Drop breakup and coalescence in polymer blends: the effect of concentration and compatibilization", Macromolecules 28: 2647-2657 (1995)

[69] J. Huitric, P. Mederic, M. Moan and J. Jarrin, " Influence of composition and morphology on rheological properties of polyethylene/polyamide blends", Polymer, Vol. 39, No. 20, pp. 4849-4856 (1998)

[70] S. Lyu, F. S. Bates, and C. W. Macosko, "Coalescence in polymer blends during shearing", AIChE Journal, Vol. 46, No. 2 (2000)

[71] I. Vinclier and P. Moldenaers, A.M. Terracciano and N. Grizzuti, " Droplet size evolution during coalescence in semiconcentrated model blends", ALChE Journal, Vol. 44, No. 4, (1998)

[72] C. Lacroix, M. Bousmina, P.J. Carreau, B. D. Favis, and A. Michel, " Properties of PETG/EVA blends: viscoelastic, morphological and interfacial properties, Part I,", Polymer, 37, 2939-2947 (1996)

[73] P. S. Calvao, M. Yee, N. R. Demarquette, "Effect of composition on the linear viscoelastic behavior and morphology of PMMA/PS and PMMA/PP blends" Polymer 46: 2610–2620 (2005)

[74] K. Wallheinke, P. Potschke, C. W. Makosco, H. Stutz "Coalescence in Blends of Thermoplastic Polyurethane With Polyolefins", Polymer engineering and science , Vol. 39, No. 6 (1999)

[75] J. C. Lepers, B. D. Favis, C. Lacroix," The Influence of Partial Emulsification on Coalescence Suppression and Interfacial Tension Reduction in PP/PET Blends", Journal of Polymer Science: Part B: Polymer Physics, Vol. 37, 939–951 (1999)